Estimating the return times of great Himalayan earthquakes in eastern Nepal: Evidence from the Patu and Bardibas strands of the Main Frontal Thrust

Laurent Bollinger, Soma Nath Sapkota, P. Tapponnier, Yann Klinger, Magali Rizza, Jerome van Der Woerd, D. R. Tiwari, R Pandey, Adnand Bitri, Séverine Bès de Berc

AGU PUBLICATIONS

JGR

Journal of Geophysical Research: Solid Earth

RESEARCH ARTICLE
10.1002/2014JB010970

Key Points:
- Six great earthquakes since mid-Holocene
- Coseismic slip of 12 to 17.5 m
- Return times of 700–900 years

Correspondence to:
L. Bollinger,
laurent.bollinger@cea.fr

Citation:
Bollinger, L., S. N. Sapkota, P. Tapponnier, Y. Klinger, M. Rizza, J. Van der Woerd, D. R. Tiwari, R. Pandey, A. Bitri, and S. Bes de Berc (2014), Estimating the return times of great Himalayan earthquakes in eastern Nepal: Evidence from the Patu and Bardibas strands of the Main Frontal Thrust, *J. Geophys. Res. Solid Earth*, *119*, 7123–7163, doi:10.1002/2014JB010970.

Received 21 JAN 2014
Accepted 3 AUG 2014
Accepted article online 7 AUG 2014
Published online 15 SEP 2014

Estimating the return times of great Himalayan earthquakes in eastern Nepal: Evidence from the Patu and Bardibas strands of the Main Frontal Thrust

L. Bollinger[1], S. N. Sapkota[2], P. Tapponnier[3], Y. Klinger[4], M. Rizza[3], J. Van der Woerd[5], D. R. Tiwari[2], R. Pandey[2], A. Bitri[6], and S. Bes de Berc[6]

[1]CEA, DAM, DIF, Arpajon, Arpajon, France, [2]Department of Mines and Geology, National Seismological Center, Kathmandu, Nepal, [3]Earth Observatory of Singapore, Nanyang Technological University, Singapore, Singapore, [4]Institut de Physique du Globe de Paris, Sorbonne Paris Cité, Université Paris Diderot, UMR 7154 CNRS, Paris, France, [5]Institut de physique du Globe de Strasbourg, UMR CNRS/UdS, Strasbourg, France, [6]BRGM, Orléans, France

Abstract The return times of large Himalayan earthquakes are poorly constrained. Despite historical devastation of cities along the mountain range, definitive links between events and specific segments of the Main Frontal Thrust (MFT) are not established, and paleoseismological records have not documented the occurrence of several similar events at the same location. In east central Nepal, however, recently discovered primary surface ruptures of that megathrust in the A.D. 1255 and 1934 earthquakes are associated with flights of tectonically uplifted terraces. We present here a refined, longer slip history of the MFT's two overlapping strands (Patu and Bardibas Thrusts) in that region, based on updated geomorphic/neotectonic mapping of active faulting, two 1.3 km long shallow seismic profiles, and logging of two river-cut cliffs, three paleoseismological trenches, and several pits, with constraints from 74 detrital charcoals and 14 cosmogenic nuclide ages. The amount of hanging wall uplift on the Patu thrust since 3650 ± 450 years requires three more events than the two aforementioned. The uplift rate (8.5 ± 1.5 mm/yr), thrust dip (25° ± 5°N), and apparent characteristic behavior imply 12–17.5 m of slip per event. On the Bardibas thrust, discrete pulses of colluvial deposition resulting from the coseismic growth of a flexural fold scarp suggest the occurrence of six or seven paleo-earthquakes in the last 4500 ± 50 years. The coeval rupture of both strands during great Himalayan earthquakes implies that in eastern Nepal, the late Holocene return times of such earthquakes probably ranged between 750 ± 140 and 870 ± 350 years.

1. Introduction

Although constraining the source parameters of large earthquakes along the Himalayan arc is of paramount socioeconomic importance, it has remained a particularly challenging scientific issue. The Main Himalayan/Frontal Thrust (MHT/MFT), the largest and fastest-slipping continental megathrust, poses one of the greatest menaces to the northern Indian subcontinent, threatening tens of millions of people in the Himalayan foothills and Ganges plain. But serious obstacles have stood in the way of assessing seismic hazard in Northern India and Nepal.

First, great twentieth century earthquakes ($M \geq 8$), particularly the 1905 (Kangra) and 1934 (Bihar-Nepal) events (Figure 1a) have long been categorized as blind events. Therefore, opinions differ, still, on whether they ruptured the MHT [e.g., *Molnar and Pandey*, 1989; *Bilham et al*., 2001], the basement sediment interface beneath the Ganges foreland basin [e.g., *Seeber and Armbruster*, 1981], or a fault within the Indian plate [e.g., *Kayal*, 2010; *Srivastava et al*., 2013], among various scenarios (Figure 1b). While perpetuating an ambiguous view of source potency, such conflicting interpretations also raise the question of whether the surface ruptures of earthquakes as large as the 1905 and 1934 events might have been missed, both at the time of occurrence and later on in trenches.

Second, along most segments of the MFT, trenches excavated across visible surface scarps (Figure 1c) have generally exposed only one event in the last 1000 years at any single site [e.g., *Lavé et al*., 2005; *Kumar et al*., 2006, 2010; *Malik et al*., 2010]. The lack of sizeable paleoseismological time series has thus precluded a reliable determination of the average return times of great earthquakes.

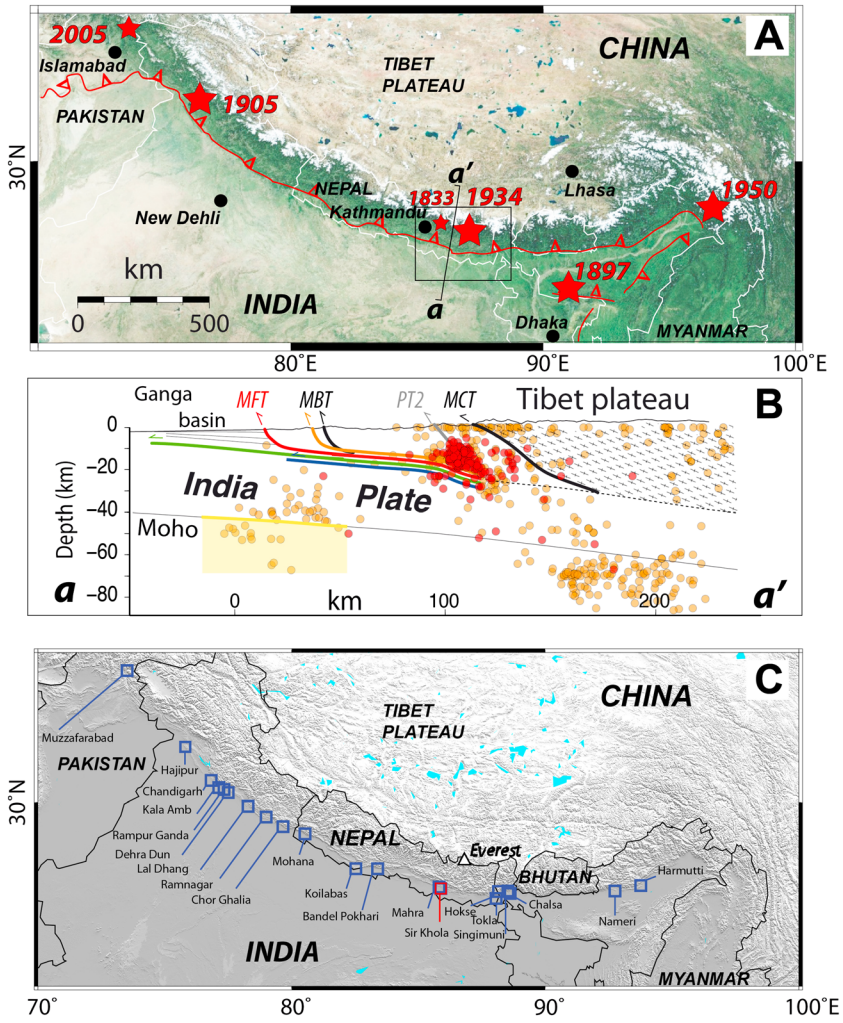

Figure 1. (a) Map of great and large earthquakes along Main Himalayan Thrust, since 1830. Box is frame of Figure 2, including most of cross section in Figure 1b. (b) Schematic section a-a′: colored lines show fault rupture scenarios and source sizes proposed for different events, mostly of thrust type. Small red and orange circles are recently recorded instrumental earthquakes ($1 < ML < 5$) under Kathmandu klippe [*Cattin and Avouac*, 2000] and in eastern Nepal [*Monsalve et al.*, 2006] respectively, with most prominent cluster on midcrustal thrust ramp. (c) Paleoseismological sites investigated by different research groups along the Himalayan front [*Kondo et al.*, 2008; *Kumar et al.*, 2001, 2006, 2010; Kumahara in *Sapkota*, 2011; *Lavé et al.*, 2005; *Malik et al.*, 2010; *Mugnier et al.*, 2011; *Sapkota et al.*, 2013; *Upreti et al.*, 2000; *Yule et al.*, 2006a, 2006b].

Third, taken together, the absence of twentieth century surface ruptures and firm recurrence time constraints have left open the possibility that earthquakes much greater (up to $M \sim 9$?) than hitherto recorded might occur on a multimillennial timescale [e.g., *Lavé et al.*, 2005; *Feldl and Bilham*, 2006]. This inference is thought to be corroborated by the postulated rupture lengths (>800 km?) of certain medieval earthquakes [e.g., *Kumar et al.*, 2010] and by GPS-based interseismic slip deficit balancing the shortening rate across the MFT derived from geomorphological studies (e.g., *Ader et al.* [2012], in Nepal). Taken at face value, both might imply infrequent events with magnitudes > 8.5 and return periods > 1000 years, which might further suggest variable slip rates and very irregular return times [*Mugnier et al.*, 2013]. Hence, mostly because of lack of evidence or speculative interpretation of insufficient data, the maximum magnitude and return period of great Himalayan earthquakes remains a subject of hot debate [e.g., *Ader et al.*, 2012; *Kumahara and Jayangondaperumal*, 2013; *Mugnier et al.*, 2013; *Srivastava et al.*, 2013; *Schiffman et al.*, 2013].

In an effort to move that debate forward, we started new fieldwork in the regions of Nepal struck by the most recent large earthquakes (1833 and 1934) [*Campbell*, 1833a, 1833b; *Bilham*, 1995; *Rana*, 1935; *Dunn et al.*, 1939] (Figure 1a). We targeted the area of the Himalayan front most severely shaken by these events, in the

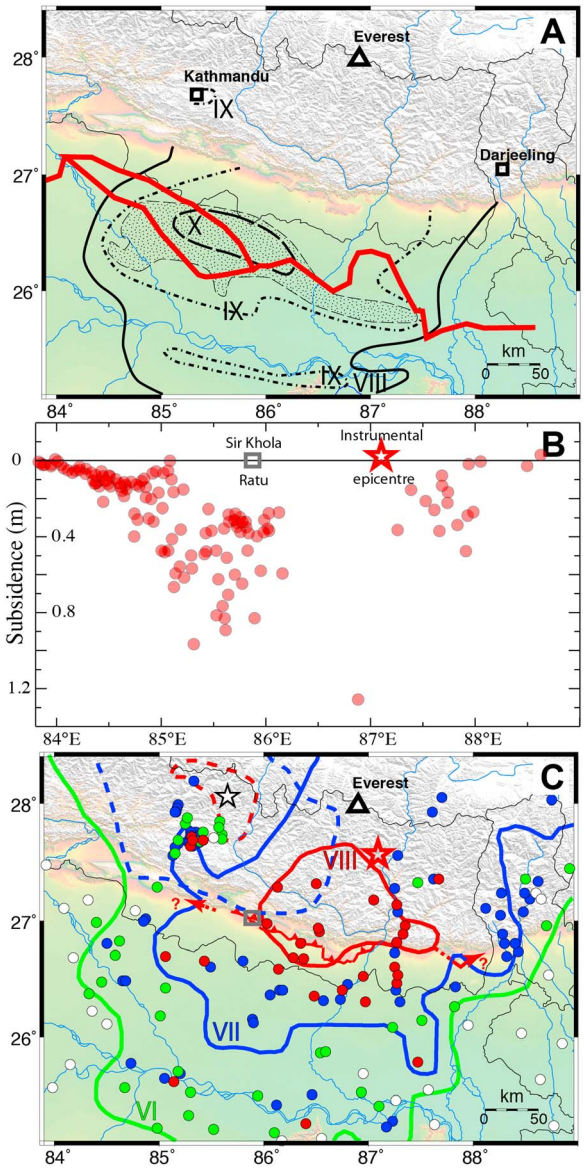

Figure 2. (a) Macroseismic isoseist map of 1934 earthquake (MMI, black contours, solid or dashed, from *Dunn et al.* [1939]). Thick red lines are profiles leveled in 1920 and 1935 along slump belt (stippled area), from which measured elevation changes are plottted in Figure 2b [*Bomford*, 1937; *Bilham et al.*, 1998]. (b) Elevation changes derived from comparison of benchmark leveling measurements on profiles in Figure 2a [*Bomford*, 1937; *Bilham et al.*, 1998]. c) Macroseismic intensities (colored dots) and isoseist map of 1934 earthquake (MSK1964, after *Ambraseys and Douglas* [2004], corrected for liquefaction effects). Continuous and dashed colored lines with roman numbers, and red and white stars, are macroseismic isoseismals (MSK1964), and instrumental and macroseismic epicenters, of 1934 and 1833 earthquakes, respectively. Thin black lines are borders. Small grey box: location of Figure 3. Red teethed polyline marks minimum stretch of 1934 MFT surface rupture, from *Sapkota et al.* [2013]. Red arrows with question marks point to possible maximum rupture extent.

easternmost part of the country (Figure 2). An initial, rapid survey of the Quaternary geology and geomorphology of the MFT between 84.5°E and 88.5°E was performed, over a distance of ~ 400 km (Figures 1 and 2). The principal goals of this broad reconnaissance were to visit and compare active faulting sites documented by previous groups [e.g., *Nakata*, 1989; *Upreti et al.*, 2000; *Lavé et al.*, 2005], to obtain a synoptic view of the present tectonics of the Himalayan front and to search for scarps or exposures showing evidence for very young thrust movement. In the region near Bardibas (Figure 3), we found particularly clear evidence of modern surface deformation and rupture on one of two strands of the Main Frontal Thrust (MFT) where it crossed the Sir Khola river valley [*Sapkota et al.*, 2013]. Our paleoseismological logging of a river-cut cliff and of trench walls, constrained by ^{14}C dating of several sedimentary units unambiguously suggested that the last and penultimate surface ruptures on that strand (Patu thrust) should be attributed respectively to the 1934 earthquake, and to the great A.D. 1255 event chronicled to have killed the king and one third of the Kathmandu valley population [*Sapkota et al.*, 2013].

This paper documents in much greater detail our neotectonic and paleoseismological findings at that initial site. It places them into a more robust regional framework by adding evidence from three additional geomorphological/paleoseismological sites. Dating sedimentary records in the footwall and hanging wall of the overlapping Patu and Bardibas strands of the MFT with 74 detrital charcoal ages and 14 cosmogenic ^{10}Be and ^{26}Al exposure ages, elucidates their seismic history much further back than was previously feasible, into the middle Holocene. We also provide the first images of the near-surface geometry of both thrust strands on two 1.3 km long profiles acquired during a dedicated shallow seismic survey. Finally, we propose first-order estimates of the mean return period and average coseismic slip of great earthquakes along this stretch of the Himalayan front.

2. Methodology

Our mapping of the tectonic geomorphology and landscape evolution was based on the comparative study of more than 400 aerial photographs—acquired in the past 50 years at scales of 1/12,000 and 1/50,000—submetric

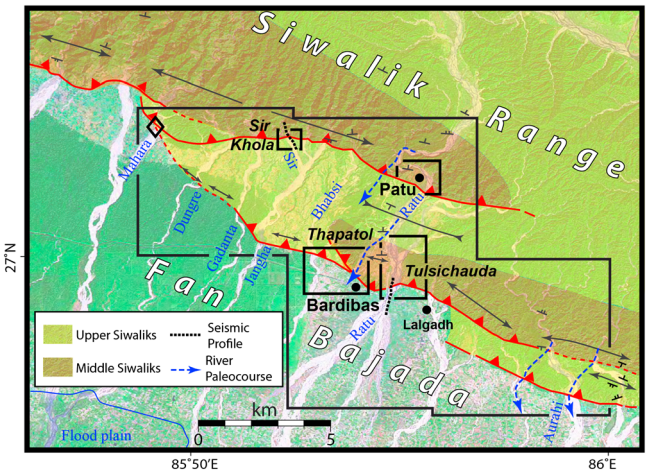

Figure 3. Map of study area, superimposed on Landsat thematic mapper image, showing right-stepping MFT strands between Mahara and Aurahi Rivers. Dashed blue lines with arrows are channels abandoned by rivers. Double arrowed lines, anticline/syncline axes. Small Ts: dips. Large box is frame of morphotectonic map in Figure 5. Smaller boxes locate four sites documented in detail in text and on Figures 7, 15a, 15b, and 17.

resolution Ikonos and Geoeye-1 satellite images, and photographs taken during a dedicated helicopter survey. The results were reported on recent, 1/25,000 scale, topographic base maps. In the field, we used Total-Station leveling and Terrestrial Lidar Scanning (TLS; Riegl VZ 400), with three-dimensional precisions of 30 and 2 cm, respectively, to survey the local tectonic/fluvial geomorphology and log the structure of newly excavated or refreshed exposures.

We identified and correlated fluvial terraces according to their relative heights, absolute elevations, lithologic consolidation, and degree of incision and lateritization. They were labeled upward from the most local base level, i.e., the present-day river flood plains, T0. Terrace abandonment generally results from climatic or/and tectonic events that lead to changes in hydrology and river base level. Where possible, we searched for horizons of similar lithology and age on either side of scarps. Such horizons, as well as most accessible fluvial conglomerates, were systematically inspected and sampled for detrital charcoals. The sampling strategy was dedicated to dating terrace abandonment. For that purpose, we sampled both the uppermost high-energy levels—pebbles and gravel deposited in the main stream channels—and overlying overbank deposits.

We dated 74 of the charcoal samples collected. The charcoal fragments were prepared and analyzed by accelerator mass spectrometry at the Scottish Universities Environmental Research Centre (SUERC) radiocarbon dating laboratory in Glasgow, at Commissariat à l'Eénergie Atomique (CEA)/Artemis in France and at Beta Analytics in the USA. The results, with associated uncertainties, are listed in Tables 1 and 3. The total time span of the stratigraphic record sampled, calibrated with IntCal09 [*Reimer et al*., 2009], extends roughly from 7000 B.C. to the present. In order to better constrain the date of the events, given the uncertainties associated with the dating of earthquake horizons, the chronological sequences were further refined by introducing a priori information from stratigraphic relationships, using the Bayesian analysis approach of Oxcal 4.1 [*Bronk Ramsey*, 2008]. This approach was also used in order to test the consistency between historical earthquakes and stratigraphic records.

As no charcoals were found in some crucially located terrace deposits, we sampled quartz-rich cobbles for cosmogenic isotope dating. The seven samples dated were processed following standard chemical procedure [*Kohl and Nishiizumi*, 1992] at the cosmogenic isotope laboratory at the University of Strasbourg, France. Accelerator mass spectrometry was performed at Accélérateur pour les Sciences de la Terre, Environnement, Risques - Accelerator for Earth Sciences Environment and Risk (ASTER) (Centre Européen de Recherche et d'Enseignement de Géosciences de l'Environnement (CEREGE), Aix-en-Provence, France) and surface exposure ages were calculated with the CRONUS-Earth calculator v2.2 [http://hess.ess.washington.edu/; *Balco et al*., 2008] using the *Lal* [1991] and *Stone* [2000] scaling factor, a constant production rate of 4.49 ± 0.39 atoms/g of SiO2, and a Be half-life of 1.387 ± 0.012 Ma [*Chmeleff et al*., 2010; *Korschinek et al*., 2010].

While on average the $^{26}Al/^{10}Be$ ratio is concordant (˜0.85), the large amount of ^{27}Al (>14 mg) in half of the samples precluded accurate accelerator mass spectrometry (AMS) measurements and explains the large error bars. Because of these large uncertainties and the generally younger ^{26}Al ages, we base our interpretation on the ^{10}Be model ages only.

By confronting dating results and geomorphic/lithologic characteristics of the terraces, especially relative height, we first estimated incision or apparent uplift rates. We then determined uplift rates where structural offsets were unambiguously constrained. Such rates were finally converted into slip rates from estimates of the subsurface attitudes of the faults.

Table 1. AMS Radiocarbon (^{14}C) Dates From Detrital Charcoals Collected From Sir River Cut/Trench and Terraces, Patu and Tulsichauda Terraces

Unit[a]	Sample Number	SUERC Laboratory Code[b]	Measured Radiocarbon Age (Years B.P.)[c]	$\delta^{13}C$ Value[d]	Calibrated Ages (Calendric, 2σ)[e]
			Sir River Cut		
U0	SIR08-03	25771	Modern (postbomb)	−27.9	A.D. 1958 or 1985
$U1_{aF3}$	SK10-07	34605	150 ± 30	−30.7	A.D. 1660–1960
$U1_{aF3}$	SK10-05	34598	195 ± 30	−27.5	A.D. 1640–1960
$U1_{H}$	SIR09-17	28375	415 ± 40	−24.6	A.D. 1420–1640
$U3_{H}$	SIR09-13	28373	145 ± 40	(−25.0)	A.D. 1660–1960
$U3_{F}$	SIR08-26	23691	150 ± 35	−25.6	A.D. 1660–1960
$U3_{H}$	SIR08-11	23683	185 ± 35	−29.1	A.D. 1640–1960
$U3_{H}$	SIR08-12	23960	245 ± 45	−25.0	A.D. 1490–1960
$U5_{F}$	SIR09-03	27999	3015 ± 30	(−25.0)	B.C. 1390–1130
$U5_{F}$	SIR09-15	28374	3095 ±40	(−25.0)	B.C. 1450–1260
$U5_{F}$	SIR09-01	27998	3100 ± 30	−27.8	B.C. 1440–1290
$U5_{F}$	SIR09-04	28371	3335 ± 45	−26.3	B.C. 1740–1510
U_{uF4}	SIR08-25	23690	3430 ± 35	−25.5	A.D. 1880–1630
$U5_{F}$	SIR09-11	28372	3830 ± 40	−26.7	B.C. 2460–2140
$U5_{F}$	SIR09-11	28372	3830 ± 40	−26.7	B.C. 2460–2140
			Sir Trench		
U1t	SIR08-2P	23694	165 ± 35	−24.4	A.D. 1660–1960
U1t	SIR08-3P	23695	245 ± 35	−27.1	A.D. 1520–1960
U3t	SIR08-27	25778	340 ± 35	−27.9	A.D. 1460–1650
U3t	SIR08-30	25779	365 ± 35	(−25.0)	A.D. 1440–1640
U3t	SIR08-16	25772	625 ± 35	−27.4	A.D. 1280–1400
U5t	SIR08-22	23961	955 ± 45	−25.0	A.D. 990–1190
U6t	SIR08-04	23680	600 ± 35	−27.6	A.D. 1290–1410
U6t	SIR08-20	25773	695 ± 35	−27.6	A.D. 1250–1390
U6t	SIR08-18	23684	875 ± 35	−26.3	A.D. 1040–1260
U6t	SIR08-19	23685	795 ± 35	−27.1	A.D. 1170–1280
U7t	SIR08-05	23681	645 ± 35	−25.8	A.D. 1280–1400
U7t	SIR08-39	23938	955 ± 40	−25.0	A.D. 990–1180
U11t	SIR08-21	25777	1415 ± 35	−25.8	A.D. 570–665
U11tEW	SIR08-06	23682	3020 ± 35	−25.5	B.C. 1400–1130
U6tEW	SIR08-24	23689	455 ± 35	−26.3	A.D. 1400–1490
U4tEW	SIR08-31	23692	465 ± 35	−25.1	A.D. 1405–1485
U6tEW	SIR08-33	23693	670 ± 35	−24.5	A.D. 1270–1400
U3tEW	SIR08-34	23937	745 ± 40	−25.0	A.D. 1210–1380
			Sir Paleochannel		
Th3	SIR08-45	25782	195 ± 35	−24.3	A.D. 1645–1955
Th3	SIR08-46	25945	795 ± 50	Online	A.D. 1050–1290
Th3	SIRT1	24125	165 ± 30	−25.0	A.D. 1662–1954
Th3	SIRT2	24124	Modern (postbomb)	−25.0	
			Patu Terraces		
ThP5	PIT2-01	48709	3346 ± 27	−27.3	B.C. 1732–1531
ThP5	PIT2-02	45793	3444 ± 34	−29.7	B.C. 1882–1682
ThP5	PIT2-03	48708	5792 ± 26	−29.2	B.C. 4712–4554
ThP5	PIT2-04	45794	1207 ± 34	−31.6	A.D. 690–934
ThP3′	PIT4-01	45798	341 ± 34	−26.2	A.D. 1467–1641
ThP3′	PIT4-07	45799	129 ± 34	−28.0	A.D. 1672–1942
ThP3′	PIT4-08	45800	943 ± 34	−26.5	A.D. 1021–1166
			Tulshichauda Terrace		
Th3	RC02	45789	1255 ± 34	−25.6	A.D. 670–870 D100 cm
Th3overbk	PIT1-01	45781	420 ± 34	−26.7	A.D. 1421–1621 D54 cm
Th3overbk	PIT1-02	45782	373 ± 34	−27.0	A.D. 1445–1634 D50 cm
Th3overbk	PIT1-04	45783	966 ± 34	−25.4	A.D. 1015–1160 D67 cm
Th3overbk	PIT1-05	45784	363 ± 34	−27.8	A.D. 1449–1635 D63 cm
Th3overbk	PIT1-08	45788	722 ± 34	−26.5	A.D. 1225–1382 D48 cm

[a] See river cut and trench logs for stratigraphic unit designations.
[b] Samples have been dated by accelerator mass spectrometry (AMS) measured at the Scottish Universities Environmental Research Centre (SUERC) AMS facility. Each number corresponds to the laboratory code for each sample.
[c] Conventional Radiocarbon years B.P. relative to 1950 A.D. (with 1σ confidence level including counting statistics as well as reference standard, blank, and random machine errors).
[d] Parentheses denote samples for which values are unavailable and assumed to be −25.0.
[e] Pre-bomb calendric dates were calibrated using the atmostpheric calibration curve IntCal09 for the Northern Hemisphere [*Reimer et al.*, 2009]. Post-bomb sample SIR08-03 was calibrated using [*Hua and Barbetti*, 2004].

Although the deep geometry of structures along the Himalayan front is documented on a large scale by seismic lines acquired by the Petroleum Exploration and Promotion project of the Department of Mines and Geology [e.g., *Bashyal et al.*, 1998], such lines are insufficient to provide constraints on the shallow dips of the MFT strands and hence assess shortening rates based on local uplift rates deduced from terrace elevation and dating. Therefore, we shot two shallow, 1.3 km long, seismic reflection profiles along the Sir and Ratu river valleys, which cross at high angle the Patu and Bardibas thrusts, respectively (Figure 3). Dynamite rods (100 g), buried at shallow depth ($<$2 m) within unconsolidated river gravel, were fired every 10 m. The blasts were recorded by 40 Hz geophones spaced 5 m apart (2 s. recording time; 48 traces; 12 nominal fold; 270 m maximum offset). Standard seismic processing included amplitude correction, geometry spreading compensation, random noise attenuation, band-pass filtering (30 Hz–95 Hz), high-precision stacking, and 2-D FX poststack time and depth migration. The seismic profiles were interpreted by integrating surface geological observations. The geometry of the thrusts at depth was then used to convert incremental amounts and rates of uplift into coseismic fault slip and slip rates.

Two complementary methods were used to determine the return times of great earthquakes. In the first, an average recurrence interval was derived from a number of events over a period of time covering the entire age span of the terraces, based on our finding that terraces abandonments were locally consecutive to great earthquakes. We also used an alternative approach taking into account the minimum, maximum, and median intervals between events as deduced from the observations at a given site, as well as from the combination of observations at all sites. The return times and associated uncertainties were then estimated from the distribution of these interseismic intervals.

Throughout our study, geomorphic/paleoseismological observations and interpretations were always compared to the regional historical earthquake catalog and to all observations, including macroseismic or geodetic evidence, documented during these past earthquakes. In the next section, we start by summarizing this historical data, which is essential to assess the size of these earthquakes.

3. Large Historical Events in Central and Eastern Nepal

According to historical accounts going back to the thirteenth century A.D., central and eastern Nepal have been shaken by about 10 destructive events [*Pant*, 2002], most likely sourced within the Himalayas, because they are not documented to have caused maximal damage elsewhere. Much of the information concerning these earthquakes comes from destruction described in Kathmandu and adjacent areas. We review here the evidence that concerns the largest events, based on published studies [e.g., *Pandey and Molnar*, 1988; *Bilham*, 1995] and in the light of more recently translated historical accounts [*Pant*, 2002; *Rana*, 1935].

The first historical event to stand out is the major earthquake of 7 June 1255 A.D. Although it was preceded by another large earthquake on 24 December 1223, very little is known about that earlier shock because the relevant manuscript was damaged. A lot more information survived for the 1255 event [*Pant*, 2002]. The destruction was extreme throughout the Kathmandu valley, with one third of the population killed. Mortally wounded, King Abhaya Malladeva died 8 days after the earthquake. Perceptible aftershocks ensued for 4 months. By comparison with twentieth century events in the Himalayas, the 1255 A.D. earthquake should thus be ranked a great earthquake.

Another very large event occurred on 14 September 1344, causing also major destruction in Kathmandu and again the death of the King, this time the next day. No information, however, is available on aftershock occurrence or the total number of casualties.

The next major event to cause significant destruction in the Kathmandu valley occurred more than 575 years later, on 26 August 1833. It followed a smaller shock on 4 June 1808 that destroyed houses in Bhaktapur (Kathmandu valley) though little more is known about that earthquake [*Pant*, 2002]. The 1833 event struck at night (11 h, 55 min P.M. Calcutta time) and was preceded by two strong foreshocks, 5.5 h and 25 min earlier [*Campbell*, 1833a, 1833b; *Bilham*, 1995]. The main shock lasted for about 1 min and caused ample swing of the trees, with undulatory, NE-SW oriented vibrations and noises perceived as coming from the east or northeast. In Kathmandu, many houses fell or were leveled to the ground, and many temples were destroyed [*Campbell*, 1833a, 1833b]. The total number of fatalities in the valley, though uncertain, appears to have been about 500 and was probably minimized by the occurrence of the two big foreshocks. There were six

strong aftershocks in the next hour and 20 more the next day. Aftershocks continued to be felt during 3 months, up to 26 November 1833. The effects of the earthquake reached far from the Kathmandu valley, with significant damage to houses at Monghyr (Bihar state—India) and other cities in the Ganges plain, as well as in the Gyirong area to the North. The Kamala River was reportedly dammed for 4 days by a rock slide. According to *Ambraseys and Douglas* [2004], based on 61 macroseismic MSK64 intensity data points, the surface area within isoseist VIII (MSK64) was 2300 ± 880 km^2, a value reassessed at 2500 ± 1600 km^2 by [*Sapkota*, 2011]. The estimated $M_{w\_macroseismic}$ magnitude—deduced from the macroseismic data available—for this event is thus 7.7 ± 0.2 [*Bilham and Wallace*, 2005], somewhat greater than the value (7.6) assessed by *Ambraseys and Douglas* [2004]. The contoured isoseismal VIII region lies entirely between 85.2°E and 86°E and between the city of Kathmandu and southernmost Tibet, implying an epicenter located N-NE of Kathmandu (Figure 2). Although the magnitude was recently lowered to 7.3 ± 0.1 by *Szeliga et al*. [2010] and the epicenter inferred to have been 80 km S-SE of Kathmandu, this latter location is not in agreement with the extent of destruction north of Kathmandu into South Tibet and with the NE provenance and polarization of the oscillations felt during the main shock [*Campbell*, 1833a, 1833b].

Another large earthquake occurred 33 years later, on 23 May 1866, around 15 h, 35 min Calcutta time. While a significant portion of Kathmandu was reportedly destroyed and this shock was felt in the Gangetic plain as well as in Darjeeling [*Oldham*, 1883], with one house collapse at Monghyr (Bihar state—India) [*Martin and Szeliga*, 2010], it was clearly smaller than the 1833 earthquake. The M_{w_macro} magnitude estimated by *Szeliga et al*. [2010] is 7.2 ± 0.2.

Since then, the last and only major earthquake that affected Kathmandu is the great, 15 January 1934 event, the unique instrumental entry of the catalogue. Its effects were extensively documented in India and Nepal, generating abundant reports (e.g., in *Roy* [1939] and *Rana* [1935]). This earthquake is described in the dedicated section below.

4. The Great 1934 Earthquake

The great 1934 Bihar-Nepal earthquake occurred at 2:24 P.M. Nepal time on 15 January. Many accurate and deeply moving details of the people's reactions during the shaking were reported by Bhrama Shumsher Rana, a military officer responsible for the rescue operation and reconstruction, in his book "Mahabukampa"—the great earthquake—[*Rana*, 1935], see Appendix A.

Following the shaking, major destruction was reported in Kathmandu as well as in the valley, with the cities of Bhaktapur, Patan, and Lubhu being nearly leveled to ground while the Nagarjun royal palace was destroyed. But the damage went far beyond the Kathmandu valley. B. S. Rana collected many testimonies of devastation in eastern Nepal. Among them, the major destruction in villages of the Bhojpur district is particularly representative of the violence of the main shock there. The ground in this area, as pulled and compressed, was torn by innumerable cracks. In addition, landslides affected all surrounding mountains. The large amounts of dust spread in the air were so dense that witnesses could not see anything around during half an hour. When the dust dissipated, Bhojpur bazaar was reduced to a desert heap of ruins. Catastrophic landslides and rockslides triggered by the earthquake were not restricted to the Bhojpur area but extended along much of the east Nepal Himalayan front, particularly between Udayapur and Dharan (Figure 2). Moreover, the devastation was not restricted to the eastern Nepal hills and mountains. Widespread geological effects of the earthquake were spectacularly documented in the Terai plain and in Northern India [e.g., *Dunn et al*., 1939]. A 300 km long region of Bihar, dubbed the "slump belt," was strongly impacted by liquefaction and slumping. This, combined with elastic strain during the event, resulted in tens of centimeters of regional subsidence (locally up to a meter), measured by leveling shortly after the earthquake [*Bomford*, 1937; *Bilham et al*., 1998], (Figures 2a and 2b). Although the slump belt was long thought to reflect faulting beneath the Gangetic foreland, either on a blind, shallow-dipping decollement [e.g., *Seeber and Armbruster*, 1981], or on a deeper, steep basement fault [e.g., *Kayal*, 2010], (Figure 1b), it has been recently interpreted as the result of focusing of the *SmS* wave phases [*Hough and Bilham*, 2008]. This latter interpretation, together with the subsidence in the foreland, is in keeping with a scenario in which the causative fault of the 1934 Bihar-Nepal earthquake was in Nepal, as pioneered early on by *Rana* [1935], and then gradually constrained to be the Main Himalayan Frontal Thrust [*Pandey and Molnar*, 1988; *Bilham et al*., 2001; *Avouac et al*., 2001; *Sapkota et al*., 2013].

Overall, landslides and the collapse of buildings were fatal to more than 15,000 people. More than 8000 victims were identified in Nepal, including two of the King's daughters and one of the prime minister's. The number of wounded is estimated at several tens of thousands [*Rana*, 1935]. More than 7000 victims were counted in Bihar. It is possible that the former number was underestimated because of missing data in remote mountainous areas. On the other hand, given the violence of the shaking and the surface area impacted, the total number of victims was probably—and fortunately—minimized by the occurrence time—2 P.M. on a festive day—when many were enjoying the outdoors [*Rana*, 1935].

Unlike the 1833 event, the 15 January 1934 earthquake had no reported foreshock. Aftershocks were widely felt throughout the epicentral area, in rapid succession for the first 2 days, then in steadily decreasing number during the first month. Additional events were still felt and reported by the population during the first 5 months and instrumentally recorded for about 20 months after the main shock, ceasing completely at the end of 1935. Although the duration of felt aftershocks was similar to that reported in 1255, the 1934 earthquake had many fewer aftershocks than either the 1905, 1950, or 1897 earthquakes, possibly because it ruptured a simpler, more mature fault.

The individual testimonies and official macroseismic questionnaires collected after the event have been translated into macroseismic intensities (MMI) [*Dunn et al*., 1939], [MSK64: *Ambraseys and Douglas*, 2004], (EMS98) [*Martin and Szeliga*, 2010]. Whatever the scale chosen, the earthquake qualifies as a very large event. The area affected by intensities I ≥ VII appears to be larger than 100,000 km^2. Local site effects notwithstanding the zone impacted by the greatest destructions and encompassed by the isoseismal I ≥ VIII, which is commonly correlated with the length of the earthquake rupture, is more debatable, given the sparse macroseismic data set available in eastern Nepal. However, the data delineate a roughly oval-shaped surface area > 10.000 km^2, extending from the foot of the High Himalayas to the Terai plain and crossing the MFT near Bardibas and east of Dharan (86–87.6°E and 26.6–27.7°N) (Figure 2).

The macroseismic magnitude estimated by *Ambraseys and Douglas* [2004] is $M_{w\_macrosesmic} = 8.1$. But the instrumental magnitude generally assigned for the 1934 Bihar-Nepal earthquake has been 8.4, with most articles referring to C. Richter's determination of a "revised magnitude" ("*M*") [*Richter*, 1958]. This magnitude was refined (by Richter) in *Geller and Kanamori* [1977], who determined a body wave magnitude (m_b) of 7.8 and a surface wave magnitude (M_s) of 8.3, both confirmed by *Abe* [1981, 1984]. *Chen and Molnar* [1977] determined the seismic moment of the event by estimating the spectral density of the Rayleigh and Love wave at long periods. They concluded on a moment magnitude (M_w) of 8.0 before revising it at $M_w = 8.4$ [*Molnar and Qidong*, 1984].

Overall, the geological effects and seismological source parameters of the 1934 event imply that it was a great earthquake and that slip occurred on a 150–300 km long stretch of the MFT in eastern Nepal (Figure 2).

5. Regional Tectonic Geomorphology of the Siwalik Front in the Ratu Nadi Region

It has long been known [e.g., *Upreti*, 1999] that crustal shortening in the Himalayas has been principally absorbed by a south younging sequence of four main thrust systems, namely, from north to south, the Tethys Himalayan thrusts, the Main Central Thrust, the Main Boundary Thrust, and the Main Frontal Thrust (MFT), which separate, respectively, the Tethyan passive Indian margin sediments, the High Himalayan crystallines, the metasedimentary Lesser Himalayas, the Siwalik molassic sandstones—deposited in the Neogene foreland basin of the range—, and the deposits filling the present Indo-Gangetic foreland basin. These thrusts are often interpreted to merge at depth into a single decollement, the Main Himalayan Thrust [e.g., *Pandey et al*., 1995; *Cattin and Avouac*, 2000].

Only the youngest, southernmost thrust (MFT) appears to be active in central Nepal, with the basal decollement absorbing up to about half of the convergence between India and Asia. Large patches of the decollement interface, which is generally locked—as presently—from the surface to beneath the front of the High Himalayas over a distance of more than 80 km [*Ader et al*., 2012] rupture during great earthquakes that release the slip deficit accumulated during the interseismic period. The ruptures have been inferred to propagate up to the Main Frontal Thrust, given the ~ 20 mm/yr average Holocene shortening rate accommodated there [*Lavé and Avouac*, 2001].

The existence of deformed terrace surfaces and superficial faulting along the Siwalik front in the Ratu Nadi area has long been established by studies based on air photo interpretation and fieldwork [e.g., *Nakata*, 1972;

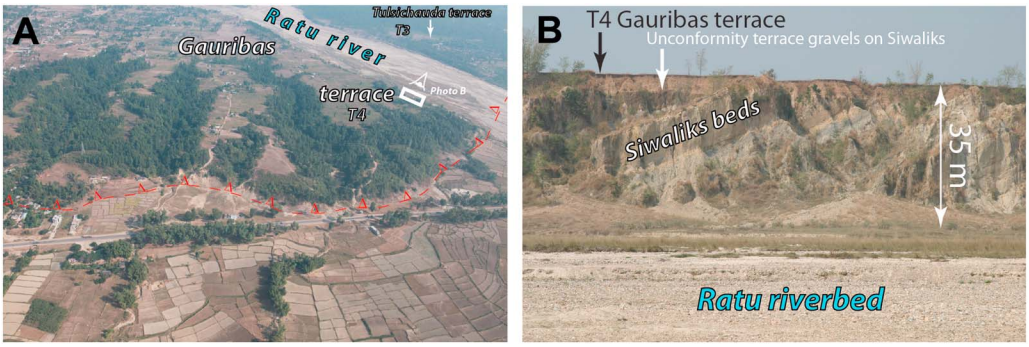

Figure 4. (a) Helicopter view (toward north) of Bardibas strand of MFT. Thrust escarpment, just north of road, sharply limits Gauribas terrace (T4), ≈ 40 m above present day Ratu riverbed. Note free-faced top of escarpment and fresh scree colluvial slope beneath. Retreating gullies in deeply incised, forested valleys deposit small fans at foot of escarpment. White box locates photograph in Figure 4b. (b) Photograph (toward west, from Ratu riverbed) of unconformable gravel of Gauribas strath terrace on 30°S dipping middle Siwaliks mudstones and conglomerates.

Hérail and Mascle, 1980; *Delcaillau*, 1992]. Specifically, these previous authors found exposures of faults cutting young fluvial deposits along several valleys. One such outcrop, first described by *Delcaillau* [1992], (diamond, Figure 3) on the Maraha river bank, in the westernmost part of the 1934 mesoseismal zone, provided a starting point for more detailed work, including lateral refreshing and trench excavation [*Lavé et al*., 2005]. The resulting paleoseismological logs were interpreted to reveal the occurrence of one great medieval event (~A.D. 1100), but to show no trace of a rupture in 1934.

Eastward, between the Maraha and Ratu Rivers, the MFT surface trace splits into two distinct strands with very sharp geomorphic expression (Figure 3). Regionally, along the Siwalik front, this is one of the areas where steep cumulative tectonic scarps and multiple, uplifted, inset terraces are most prominent and best preserved (Figures 3–5). These telltale features are clear on all remote sensing images, from Landsat Thematic mapper to High-Resolution scenes (Ikonos, Quickbird), as well as on 1964 air photo swaths and 1/25,000 topographic maps, making the area a target of choice for morphotectonic studies. We thus first focused our search on this area—mapping in detail tectonic structures, terrace surfaces, Quaternary fault scarps, and fluvial risers (Figure 5) and then quantifying further the tectonic geomorphology at three sites selected for paleoseismological investigation.

5.1. Terrace Morphology and Relative Elevations

Between the village of Bardibas and the Ratu River, the south facing cumulative escarpment of the southern strand of the MFT (Bardibas Thrust) bounds abandoned hanging wall terraces with a range of different elevations (Figures 4 and 5). Along the river, there are at least four distinct, asymmetric terrace levels just north of the thrust. The highest one, to the west, with deep, forested incisions, is the Gauribas terrace surface (T4), 40 to 45 m above the riverbed (Figures 4 and 5). On the east side, the Tulsichauda surface (T'3) stands somewhat less than half as high. Two more low-level terraces are visible in the river valley, the lowest of which (T'1) is still high enough (up to 2 m) to shrink the floodplain width by half as one crosses the thrust trace from footwall to hanging wall (Figures 4a and 5). Where best exposed just north of the thrust along the high risers of the Ratu Nadi, the hanging wall terraces are fairly flat straths, made of pebbles and gravel unconformably capping south dipping Mid-Siwalik beds of sandstones/siltstones with microconglomerate horizons (Figure 4b). Along the T4/T2 riser, the Siwalik dips increase toward the thrust from ~ 40° to ~ 70° in a distance of less than ~ 200 m (Figure 6a), implying that the hanging wall ramp anticline beneath the terraces (Figure 5) is a south vergent fault propagation fold. This inference is confirmed by the near vertical attitude of Siwalik beds beneath T'3 north of Thapatol (Figure 5). Likewise, along the Patu thrust, northern strand of the MFT, there are flights of abandoned terraces, as well as riverside exposures of north dipping thrust faults cutting shallow pebble beds and reaching close to the ground surface [*Delcaillau*, 1992].

In the field and on air photos, we could map as many as seven main regional levels of terraces in the area shown in Figure 5. The highest terrace surface (T5) stands uplifted ~ 70 m above the floodplain of the main river, the Ratu Nadi. Locally, there may be more subterrace levels, while southward on the footwall, surfaces of

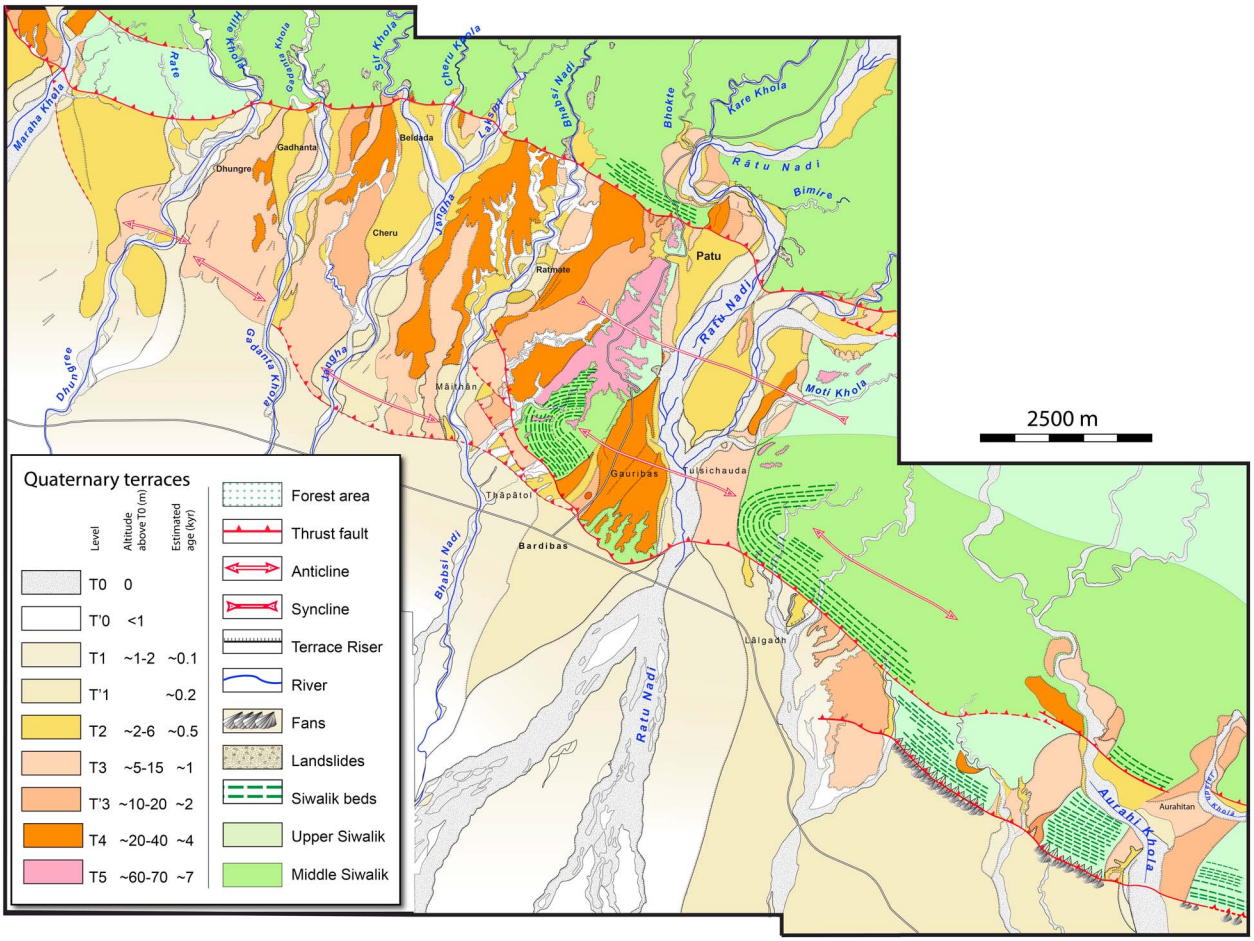

Figure 5. Geomorphic and neotectonic map of Bardibas/Dhalkebar area. See text for discussion of relative ages of Quaternary terraces, and of 3-D geometry of the thrust system.

different ages likely merge or mingle within the Terai foreland, which is a bajada of coalescent fans (Figure 3). While the relative ages of such terraces, based on height above the local riverbed, is not in doubt at the sites we visited, correlations into areas that are forested, hence difficult to inspect with air photos or high-resolution (HR) satellite images, remain tentative. Correlations upstream or downstream in the river valleys or from valley to valley are also somewhat uncertain. This is because a single terrace tread can be emplaced diachronously along one stream [e.g., *Bull*, 1991]. Besides, two terraces of identical relative heights in adjacent

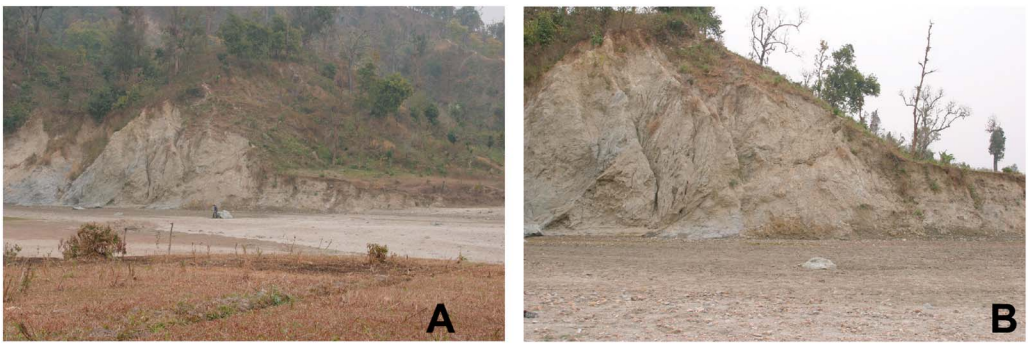

Figure 6. Photographs (toward ENE and E, respectively) of river cut and cumulative scarp of MFT Patu strand in Sir Khola valley, as initially observed in 2008. Four north dipping thrusts are visible in steep east bank cliff. See detailed mapping of refreshed exposure in Figure 8.

valleys whose rivers have different catchments may be of slightly different ages. The main inference underlying regional correlation is that the ages of local terrace emplacement and abandonment, which result chiefly from climate change and tectonically driven vertical motion—both ultimately timed by global processes—should not vary much spatially over tens to hundreds of kilometers. Conversely, terrace ages then provide key information on both processes, as shown elsewhere in the Himalayas [e.g., *Lavé and Avouac*, 2001] or in other active tectonic regions of central Asia [e.g., *Van der Woerd et al*., 1998, 2001; *Mériaux et al*., 2012, 2005; *Chevalier et al*., 2005]. Clearly, the correlative, first-order, terrace ages represented by specific colors in Figure 5 should thus be regarded only as tentative.

In the Bardibas area, the terrace emplacement and abandonment chronology was largely unknown when we started this study. However, the highest terrace between the Patu and Bardibas thrusts (T5), 70 m above the present-day river bed, had already yielded a rich macrolithic Mesolithic industry. Some of the mesolithic artifacts were found embedded in a red soil developed within the upper part of alluvial silt capping the terrace, hence probably emplaced shortly before or after terrace abandonment [*Corvinus*, 1987, 1989; *Corvinus*, 2007; *Gaillard et al*., 2011]. The silt deposition was ^{14}C dated by these authors at ~ 7 ka B.P. with charcoals sampled in this soil horizon. This provides an upper bound for the ages of all terraces, which thus span much of the late Holocene. The tentative ages indicated in the caption of Figure 5 are based on the simple inference of a constant relative uplift rate during this time span, which we discuss later in the light of the new ages we obtained with our own charcoal samples at the different sites we investigated.

5.2. Relationship With Underlying Tectonic Structures

The simplified structural map of Figure 3 combines our own observations (Figure 5) with features documented in the Geological Map of Petroleum Exploration [*Pradhan et al*., 1996] that covers much of the Frontal Himalayas in central and eastern Nepal. The overall regional structure helps understand first-order links between active faulting and fold growth along this stretch of the Siwalik Hills.

West of Bardibas, the multiple scarps that splay northwestward from the principal escarpment of the MFT's south branch (Figure 5) appear to bound the periclinal termination of the Aurahi ramp propagation anticline whose hinge is clearly outlined by Mid-Siwalik sandstone beds north of Lalgadh and Bardibas. Though active shortening along the Bardibas thrust extends past the Bhabsi Nadi, this is where the abraded Mid-Siwalik anticline apex stops, giving way westward to shallower and gentler folding of more recent upper Siwalik and Quaternary beds. The splay scarps long identified by *Nakata* [1989] may thus follow tear/transfer faults, possibly connecting the Bardibas thrust with a deeper, oblique ramp beneath the Patu thrust.

The south branch of the MFT continues to be marked westward past Thapatol by a more modest cumulative scarp that can be traced across the Jhanga Khola, where it is still 15 m high, to at least the Gadanta Khola valley (Figures 3 and 5). The associated ramp anticline similarly continues westward. Along both the Jhanga and Gadanta Rivers, high risers expose exhumed red claystones and conglomerates belonging to the Uppermost Siwalik formation, which is therefore folded, albeit less because it was probably deposited unconformably upon the Mid-Siwaliks, as observed in other places on the north side of the Siwalik range (e.g., roads from Hetauda to Amlekghanj and Muksar to Udaypur Ghari). Exhumation due to folding is still clear inside the large hairpin meander of the Dhungre Khola but stops short of the Mahara Khola River.

The presence of at least four levels of uplifted terraces (T2–T4) in the piedmont of the Siwaliks range front, between the Bhabsi Nadi and Dhungre Khola, is thus a simple consequence of the overlap between the two active, en echelon strands of the MFT. The sediments brought into the Patu thrust foreland by the south flowing rivers fill a gentle sag—a piggyback syncline—dammed farther south by anticlinal folding above the Bardibas thrust ramp. Yet these rivers, which maintain a uniform downstream profile while crossing the Bardibas thrust, continue to incise in tune with hanging wall uplift on that thrust. The fact that foreland folding and terrace uplift are not observed along the Mahra Khola valley indicates that the MFT's south strand stops before reaching that valley, perhaps on a lateral ramp that transfers shortening northwestward back to the unique frontal thrust west of the river. We infer that one of the southernmost faults visible on Mahra Khola's west bank river cut [*Lavé et al*., 2005] corresponds to the branching, off the MFT's north strand, of such a transfer ramp (Figure 5).

The detailed geometry of the stepping thrust traces in map view corroborates an architecture with branching in 3-D. East of the Mahra Khola fan, the MFT's northstrand surface trace swings 30° northeastward while

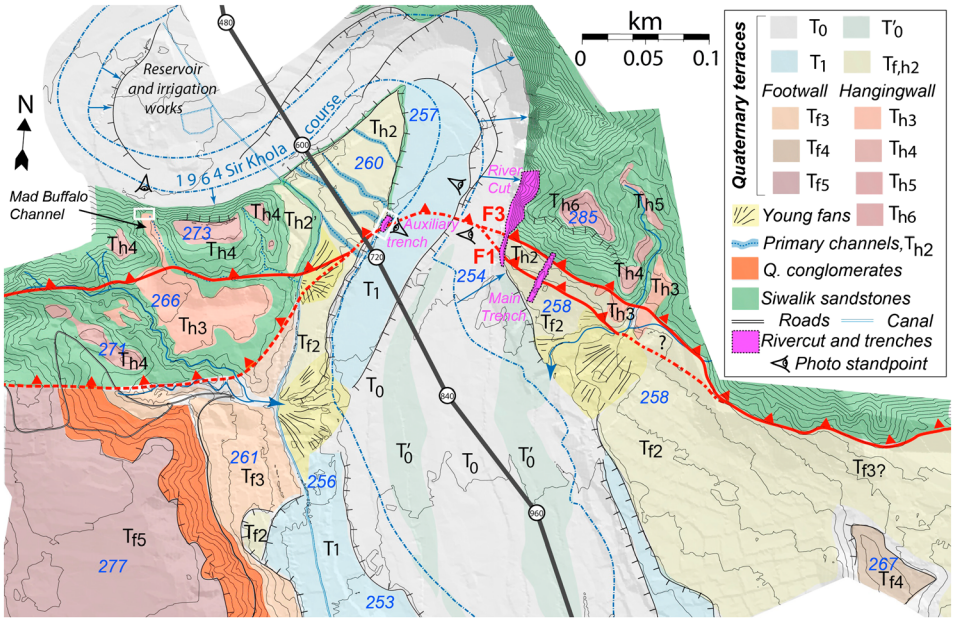

Figure 7. Map of Quaternary/active tectonics and geomorphology of Sir Khola outlet (see location in Figure 3). Black line is trace of seismic profile in Figure 10 (distance, in meters, within small circles). The two white boxes are locations, respectively from left to right, of the auxiliary trench and beheaded channel shown in Figures 13a-b and 13c-d.

stepping back northward by 2 km, as would occur if it ramped up more steeply from a shallower-dipping thrust whose updip projection emerged along the surface trace of MFT's south strand. The geometry of the next step, southeastward across the Ratu Nadi fan, is similar. The Bardibas strand of the MFT makes a sharp, 1 km dogleg toward the north, as if it receded from the westward projection of the next, Aurahi strand, located farther south (Figure 5). These geometrical relationships in plane view may be interpreted to reflect an imbricate fan structure [e.g., *Boyer and Elliott*, 1982], supporting the inference that the distinct thrust branches connect at depth. Deep, oblique thrusting with a dextral slip component would produce the right-stepping overlapping strands observed at the surface. Such deep connectivity in active thrust systems, similarly inferred elsewhere from geomorphic mapping [e.g., *Meyer et al.*, 1998], probably favors coeval rupturing of separate surface strands during large earthquakes, as observed for instance during the 2008 Wenquan [e.g., *Xu et al.*, 2009; *Liu Zeng et al.*, 2010] or the 1932 Changma events [e.g., *Peltzer et al.*, 1988]. Note that the separation between the thrust strands, here between ~ 1 and ~ 5 km, is small enough not to preclude coeval rupturing [e.g., *Wesnousky*, 2008].

Within the overlap between the Patu and Bardibas thrusts, the terrace tread heights above river generally increase east of the Mahara Khola, reaching a maximum along the Ratu Khola (Figure 5). This suggests that the partitioning of shortening between the two thrust strands varies along strike, due in part to their ages and dip angles, an inference we discuss later.

6. The Patu Strand

6.1. Sir Khola Valley Outlet

The northern, "Patu" strand of the MFT, or Patu thrust, forms the main topographic front of the Siwalik Hills west of the Ratu Nadi (Figure 3). Among the several narrow river gorges that incise the hanging wall (Figure 5), the Sir Khola valley outlet provided the most promising evidence of well-preserved modern faulting, coupled with a geomorphically spectacular, 25–30 m high cumulative thrust scarp with clear signs of ongoing uplift (Figure 6).

Four north dipping thrusts were visible in the 15–20 m high cliff cut by the river on its east bank (Figures 6, 7, and 8). Three of them offset thin, unconsolidated pebble beds by a few meters. One more thrust in sheared Siwaliks was abraded and capped by low-level terrace gravel. All thrust planes were outlined by dark, gouge-rich, shear zones. The detailed morphology of the escarpment transverse to the river was equally informative

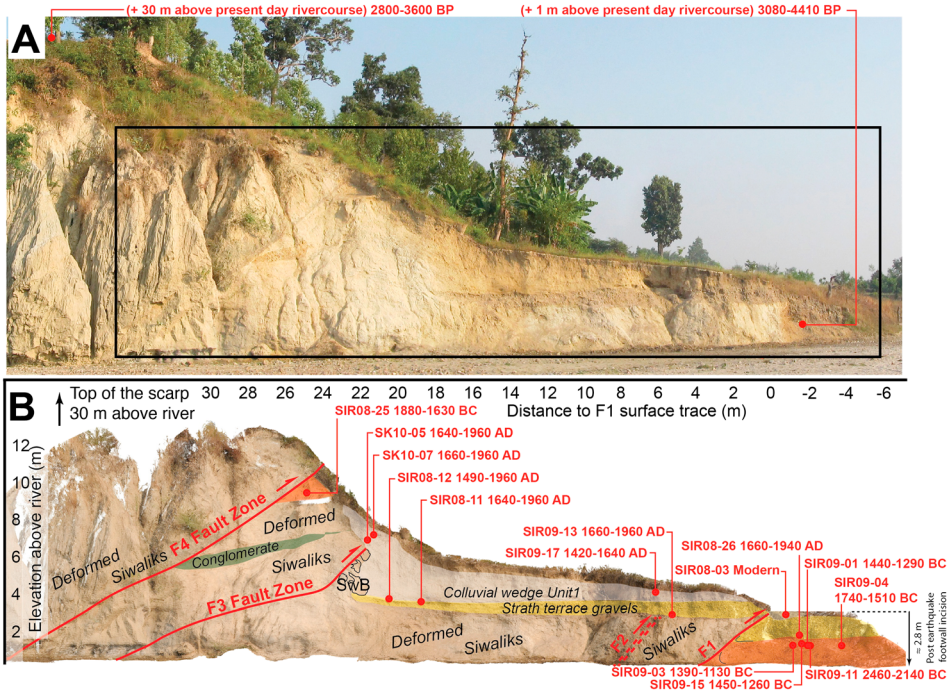

Figure 8. Refreshed, east bank river-cut cliff at Sir Khola outlet. (a) Complete photomosaic. Black box is area of high-resolution Lidar DEM, interpreted in Figure 8b. (b) Simplified interpretation of Lidar DEM of river-cut face. Red lines are young active thrusts. Red numbers: calibrated calendric ages of detrital charcoal samples. Youngest terrace: yellow shade. Older terrace: orange shade. [after *Sapkota et al.*, 2013].

(Figure 7). This main cumulative scarp showed at least two distinct bevels separated by steeper slopes, with a subtler, smoother scarp cutting across the low-level strath terrace at its base and projecting to the most frontal thrust plane uplifting this strath's gravel. This suggested the occurrence of a very recent event. Moreover, the valley of a small tributary crossing the main escarpment ~110 m east of the river stood in hanging position and was flanked by narrow terrace benches perched yet higher (Figures 7 and 9). We thus selected this site, which, to our knowledge, had never been investigated prior to our first reconnaissance, for an in depth study whose results, first discussed in [*Sapkota et al.*, 2013] and now complemented by additional surface and subsurface evidence, are presented in greater detail below.

6.1.1. Subsurface Seismic Imaging

The 1300 m long seismic profile shot in the river valley (Figures 3, 7, and 10) images fairly clearly structures in the hanging wall and footwall as well as the positions and attitudes of shallow thrusts, down to ~ 300 m depth (Figure 10). The main, shallowest thrust, which seems to ramp all the way up to the surface (near 700 m from the origin) appears to dip variably northward, from 30 to 15° deeper down. It seems to divide complexly upward into several hanging wall splays that duplicate packages of ~ 30°N dipping Siwalik beds. Beneath this main active thrust, faulting and bulk warping of footwall strata, likely Upper Siwalik beds (Figures 3 and 5), suggest the existence of a deeper thrust/decollement, emplacing the latter upon the Terai Pleistocene fanglomerates. That deeper thrust may ramp up farther south, possibly along the scarp that extends west of Thapatol to the Gadhanta River (Figure 5).

6.1.2. Morphotectonics and East Bank River-Cut Cliff

To document and quantify the relationships between thrusts and footwall/hanging wall fluvial terraces at the Sir Khola outlet, we jointly used stereo-paired, 1964 and 1997 aerial images and recent high-resolution Ikonos satellite images (Figures 9a and 9b). The precise topographic map, with a resolution of ~ 20 cm, of Figure 9c was generated from a Total Station (TS) survey covering an area of ~ 500 × 1000 m^2. It was complemented by a Riegl VZ-400 Terrestrial Lidar Scanner (TLS) survey that provided finer details on flat or steep surfaces, enabling for instance the identification of individual pebbles within strath terraces or of small braided channels in the riverbed. This helped understand deposition patterns in section and progressive shifts in map view of the flood currents that laterally cut the main meander year after year. It also helped contour the

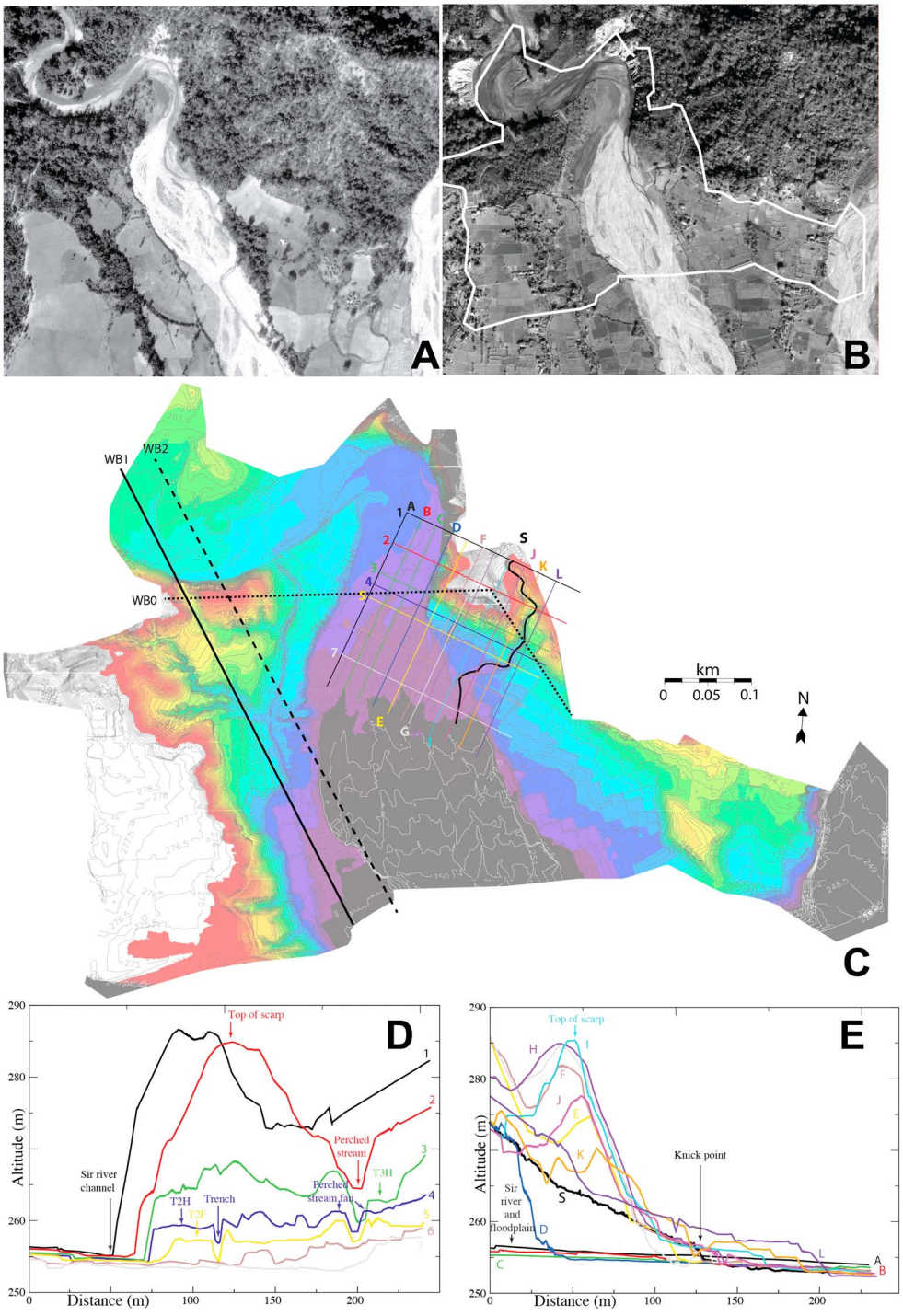

Figure 9. Coregistrated images of Sir Khola outlet: (a) aerial photo acquired on 16 January 1964 and (b) panchromatic IKONOS-2 image acquired on 20 January 2001. White polyline on Figure 9b marks contour of digital elevation model in Figure 9c. (c) Total station digital elevation model with location of (d and e) elevation profiles across the east bank of the river, oriented WNW-ESE and NNE-SSW, respectively as well as (f and g) elevation profiles across whole valley and west bank.

steepest cliff faces within less than 0.2 m. Topographic profiles were extracted from the resulting TS and TLS Digital Elevation Models to separate and measure discrete events of incision and terrace surface uplift (Figures 9d–9g). Combining all this information with systematic, outcrop-scale geological observations in the field yielded the Quaternary tectonics and geomorphic map of Figure 7.

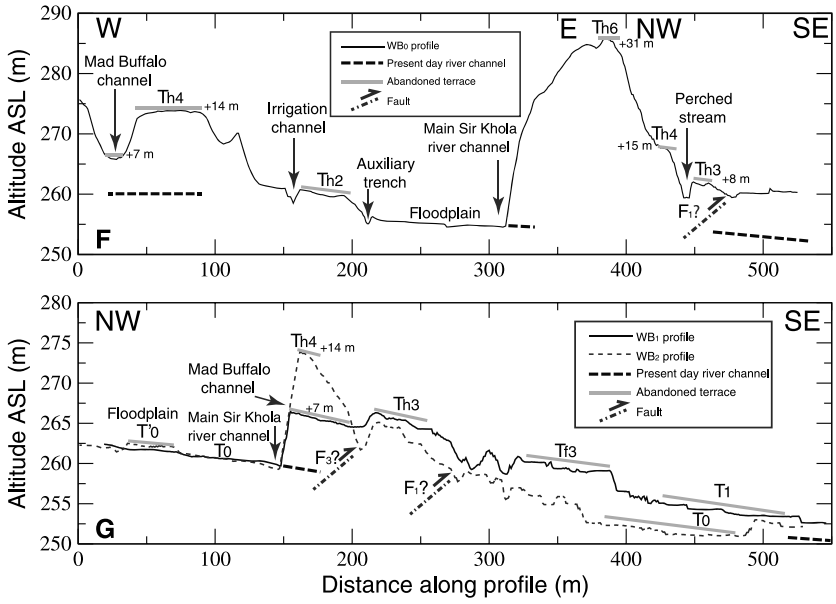

Figure 9. (continued)

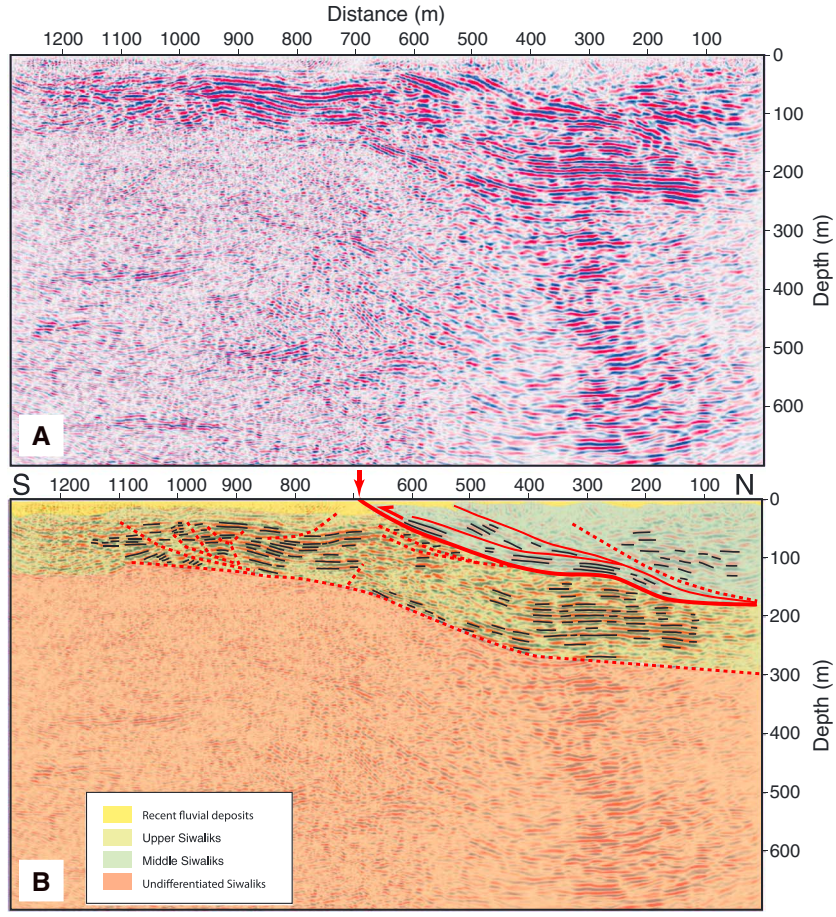

Figure 10. (a) Depth migrated seismic profile (scale 1:1) across north branch of MFT along Sir Khola valley (location in Figure 3). (b) First-order interpretation showing, on north side, north dipping, hanging wall Siwalik beds stacked up by splays of main active thrust, which dips about 30°N and surfaces around 700 m (red arrow). Blind decollement ramping up farther south is likely responsible for folding of beds in footwall. Red lines are thrusts, dashed where inferred.

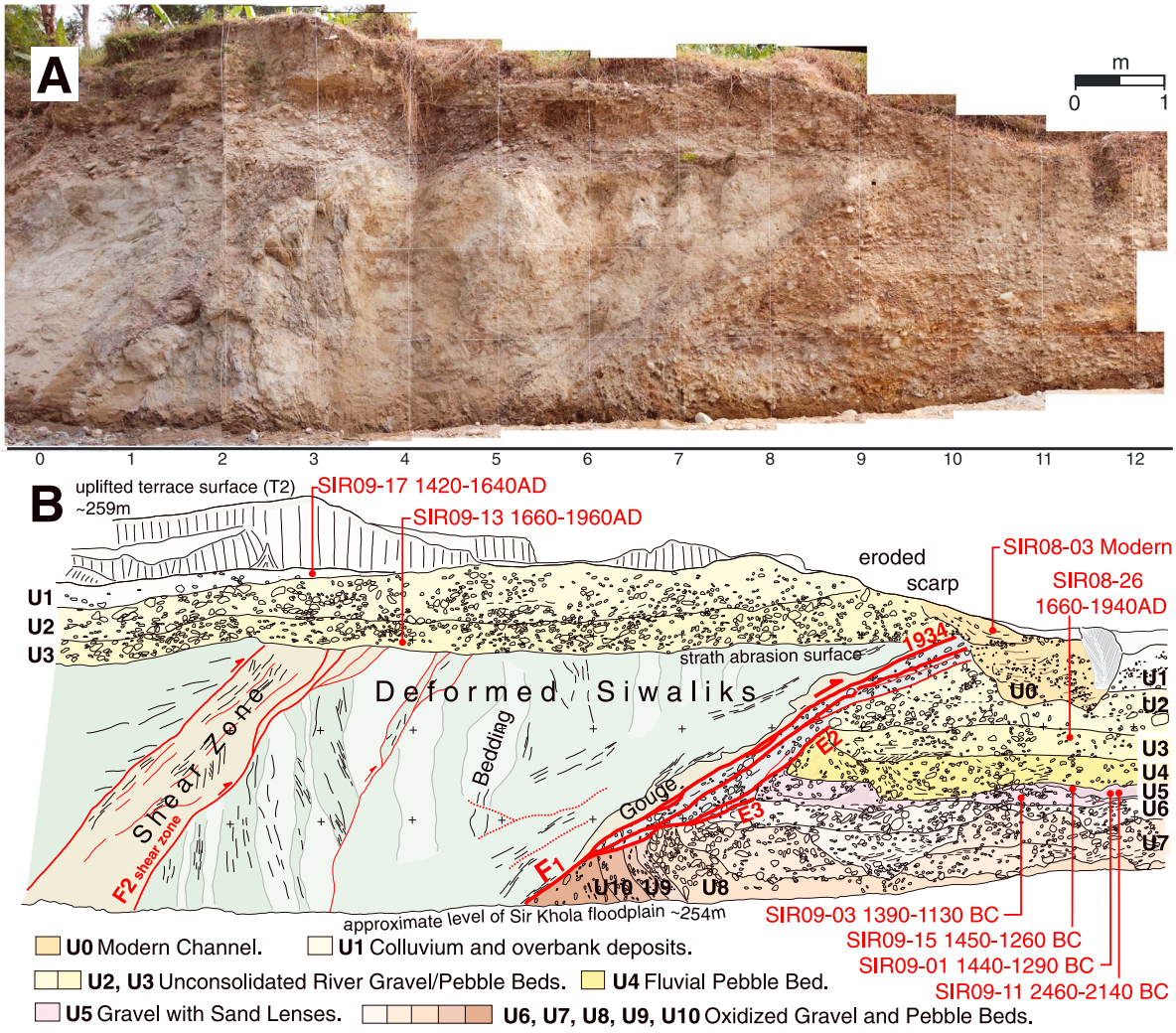

Figure 11. Frontal part of refreshed Sir Khola river-cut face. (a) Orthorectified photomosaic of gridded part of face (grid squares are 1 m on a side). (b) Simplified structural and stratigraphic log of mosaic in Figure 11a [from *Sapkota et al.*, 2013]. Faults and calibrated charcoal ages as in Figure 8.

The natural river-cut cliff along the Sir Khola's east bank was thoroughly inspected. This key outcrop is about 200 m long (Figure 7), from the couple meters of footwall gravel unearthed beneath the southernmost thrust splay (F1) to the first meander of the river, where over 50 m of hanging wall Siwaliks capped by fluvial terrace conglomerates have been incised. To the north, in the meander hairpin turn, the river dissects south vergent anticlines with recumbent/overturned limbs folding Mid-Siwaliks stata (light grey/white siltstones with intercalations of yellowish/dark grey mudstones), [*Sapkota*, 2011]. In the south, the cliff exposes monoclines of light-colored, predominant siltstones, stacked by several thrusts and intensely deformed beneath and south of the main escarpment. Our most detailed paleoseismological work targeted that frontal ~ 40 m long section, which was cleaned and refreshed several times for logging (Figures 8a, 8b, and 11).

The clearest thrusts lie beneath the cumulative escarpment (F3 and F4), and under the toe of Siwalik siltstones capped by the Th2 gravel underlying the escarpment's south tapering colluvial wedge (F1), (Figures 7, 8, and 11). Two strath terrace gravel layers, $<$ 1 m thick, have recorded multiple offsets by slip on the thrusts. The lowest abandoned strath terrace in the footwall (Tf2) was uplifted 3–4 m above the river by slip on F1, whose emergence coincides with the scarplet south of the main escarpment. Th2 is truncated again northward by thrust F3, near the base of that escarpment. The higher strath (Th3?) is preserved on a small bench, ~ 10 m above river, below the upper tip of F4 (Figure 8). It was truncated and uplifted by F4, at least up to the top edge of the river-cut cliff farther upstream, which stands at least 16 m above the riverbed, and possibly up much higher.

F1, which strikes N80°–100°E and dips 27–30°N, marks the sharpest contact between sheared, near-vertical, white Siwalik siltstones and near-horizontal, buff-colored alluvium (Figure 11). A dark, centimeter thick gouge zone forms a thrust sole at the base of the Siwaliks. Beneath are lenses of footwall conglomerates dragged upward by thrusting, separated by shallower-dipping splays. Drag is also clear from the sharp upward bending, only ~ 1 m away from the thrust, of pebble beds in the footwall (Units U7–U10 and U4–U5, Figure 11). Two splays that terminate upward at the base of different footwall units while truncating those underneath may attest to distinct seismic events (Figure 11b), as further specified below. The deepest units exposed beneath F1 (U8-10) are the most drag folded, consistent with the inference of fault motion increasing with depth. They include consolidated, clast-supported, pebble conglomerates with parallel, 10–15 cm thick beds (U10), overlain by another similar bed with a distinctive, rusty brown, oxydation color (U9). Similarly folded is the more massive, 50 cm thick conglomerate layer above (U8), with rounded cobbles and pebbles grading southward into variegated sublevels including oxidized gravel and thin yellowish silt lenses. U8 is overlain, with clear erosional contact, by a 20–50 cm thick, coarse, indurated conglomerate layer (U7) composed of poorly sorted cobbles and pebbles. Above it, Unit U6, ~ 30 cm thick, is not drag folded, though it is the shallowest unit truncated by the lowermost splay of F1. It starts with contorted sand/silt lenses including pockets of matrix-supported clasts at the base and continues upward as a clast-supported conglomerate of well-rounded cobbles and pebbles. Both U6 and U7 show inset channel substructures (Figure 11), with clearly imbricated, flat pebbles/cobbles in U6, indicative of south directed water flow. Both U8 and U6 are somewhat coarser beneath F1.

Unit U5 is markedly different. It is made of irregular, thin gravel layers interbedded with buff sand/silt lenses ($<$20 cm thick) including clusters of matrix-supported pebbles. The contrast between the light hue of the sands and the dark rust color of the oxidized, lowermost gravel provides a local stratigraphic marker. Four detrital charcoals found in the southernmost sand lens yielded ages between 1130 B.C. and 2460 B.C., with a ^{14}C age distribution suggesting deposition during or after 1390–1130 B.C. (Figure 11). The base of U5 caps the tip of the lowermost F1 splay (Figure 11), marking the horizon of one seismic event (E3), which must have occurred before 1390 B.C. In turn, Unit 5 has been strongly drag folded by motion on the next thrust splay that stops farther up, at the base of Unit U3, which thus postdates another event (E2, Figure 11). One detrital charcoal found in U3, over 1 m below the tips of the uppermost splays of F1, yielded a calibrated age of A.D. 1660–1940. This constrains the penultimate (E2) and latest earthquakes on F1 to have ruptured the surface prior to A.D. 1660 and after the seventeenth century A.D., respectively.

Units U3 to U1 in the footwall are distinctly less consolidated than those below, with loose sandy/silty matrix and lighter color. Unit 4, an unsorted gravel/pebble conglomerate with rare cobbles and a dark sandy matrix, whose base erodes U5, shows an intermediate degree of consolidation. The stratigraphy and sedimentology of U1-3 are similar to those of the fluvial conglomerates that cap the Siwaliks above F1 (see *Sapkota* [2011], for details). Hence, we correlate these footwall and hanging wall units and interpreted them to have been deposited coevally in the same former bed of the Sir River [*Sapkota et al*., 2013].

The lowest fluvial deposit on the hanging wall (U3, Figure 11) unconformably abrades and caps white Siwalik siltstones with interbedded, ~ 80° S dipping grey mudstones that are truncated by a meter-wide, north dipping shear zone (F2, Figure 11). This flat, 30–40 cm thick strath, now 3 m above the riverbed, is a buff-grey, mostly clast-supported conglomerate with a loose sandy/silty matrix, and rounded, locally imbricated pebbles/cobbles. It locally includes thin, southward dipping pebble/gravel horizons, implying progradation and/or channeling. The upper conglomerate layer (U2) is also mostly clast supported and unconsolidated, with a few larger cobbles, sand pockets, and variable thickness due to channeling. U2 is capped by a northward thickening wedge of soft, yellowish, chiefly colluvial deposits (U1, Figures 8 and 11), composed mostly of fine silts and sands with rare, small pebbles. That wedge thickens to more than 3 m at the foot of the main escarpment and becomes coarser, with mixed Siwalik blocks and recycled fluvial pebbles (Figure 8). It clearly results from degradation of the escarpment by gravity collapse and wash. A thin arable soil caps the whole hanging wall sequence.

The six detrital charcoals dated between the base of U3 and the top of U1 (Figures 8 and 11) yielded consistent ages (A.D. 1420 to 1960) (Table 1 and Figures 8 and 11) confirming the identity of U1-3 from footwall to hanging wall. Moreover, one of the youngest charcoals, dated at 1660–1940 A.D., was sampled only a few centimeters above the T2 abrasion surface. Hence, the U3 and overlying U2 deposits on the hanging wall necessarily

postdate 1660 A.D., as they do on the footwall. That both units are offset by the uppermost splays of F1 thus demonstrates the occurrence of a large earthquake on that thrust after 1660 A.D. Detailed inspection of the toe of the thrust wedge shows that the tips of the uppermost F1 splays and parts of Unit 3 on the hanging wall and of Unit 2 on the footwall have been incised, eroded away, and then capped by the fill of a modern, shallow channel transverse to the river-cut face. The rill in that channel probably collected and drained wash flowing down the main escarpment along the base of the smoothed scarplet on T2, trace of the last earthquake on F1. The deposits filling the channel (U0) are soft silts including isolated pebbles and sands with thin, concave upward, gravel beds. One small, detrital charcoal found in the uppermost sands yielded a modern, "postbomb," age spectrum (Table 1 and Figure 11). The last surface rupture on thrust F1 thus occurred between the early seventeenth and the midtwentieth centuries, likely during the greatest seismic event of that period, the 1934 Bihar-Nepal earthquake, consistent with Oxcal modeling of all the ages in U0-3 [*Sapkota et al*., 2013]. The present TLS/TS digital elevation model (DEM) elevations of the ground surfaces on the hanging walls and footwalls show that the residual height of the T2 scarplet is ~ 1.3 m, comparable to the vertical separation of the bases of Unit 3 across F1 (~1.4 m). Given the 27–30° dip, this constrains coseismic slip in 1934 to have been 2.9 ± 0.2 m. That the 1934 vertical throw is only a fraction of the height (~4 m) of Th2 above the Sir floodplain implies that the river incised ~ 2.5 m into the footwall since the earthquake. Though only ~ 6 m north of F1, the 45°N dipping thrust shear zone F2 did not slip since deposition of Unit 3 (post 1660 A.D.), hence in 1934 (Figure 11).

The next thrust northward, F3, 21 m north of F1, is a > 12 m long shear zone cutting Siwalik beds deformed beyond recognition by many small conjugate faults, reflecting strong horizontal shortening. Up section, it kinks sharply from a dip of 10–15° to 35–40°, with its upper, steepest 3 m marked by ~ 10 cm thick gouge (Figure 8). It nearly reaches the surface close to the foot of the main escarpment, about 2 m north of the basal slope break, above the thickest part of the colluvial wedge (U1). The fault tip offsets the base of that wedge, locally a complex collapse mix of unsorted pebbles/cobbles and Siwalik blocks. Hence, as on F1, the last slip event on F3 postdated deposition of Unit 2, with a throw of ~ 2 m or more, most likely in 1934 (Figure 8).

F4, most conspicuous because outlined by thin continuous gouge, dips 36°N, cutting the whole river-cut cliff face up to the escarpment slope surface, ~ 11 m above the riverbed (Figure 8). Beneath a hanging wall made of light brown siltstones with indistinct strata capped by flat fluvial conglomerates 13–16 m above river, the white Siwaliks beds in the footwall dip 17°N, parallel to a 70 cm thick, light brown indurated conglomerate horizon (Figure 8). Wedged under the tip of F4, ~ 9–10 m above river, is a meter thick layer of consolidated, oxidized pebble/gravel resting flat on abraded Siwaliks. This uplifted strath remnant, dated by one detrital charcoal at 1880–1630 B.C., correlates with Units 5 or 6–7 in the footwall of F1 (Figure 8). While slip on F4 in 1934 can neither be demonstrated nor ruled out, that thrust splay likely contributed a large fraction of the total cumulative coseismic throw on the Patu thrust strand at the Sir Khola outlet in the last 3500 years.

Overall, our logging of the river-cut cliff shows that two of the four thrusts, F1 and F3, each slipped ~ 3 m during the 1934 earthquake. The resulting, total coseismic slip amount (~6 m), however, is probably a lower bound, for lack of evidence on F4 and imprecise constraints, due to scarp collapse, at the tip of F3. Additional uplift/slip estimates are discussed in a later section.

6.1.3. Paleoseismological Trenches

To better assess the lateral locations of the faults seen on the river cut, as well as extend and complement the chronology of paleoseismic events, two trenches were excavated on either side of the river: a large (main) trench on the east bank (Figures 7 and 12) and a smaller (auxiliary) trench on the west bank (Figures 7, 13a, and 13b).

The 14 m long, 2 m deep west bank trench dug at the foot of the T1/Th2 riser (*Auxiliary trench* in Figure 7) unfortunately yielded little information on recent earthquakes. This is because, due to the proximity of the main river channel (T0/T1) and to flood abrasion on Th2, no young deposits, other than modern veneers, were found to be preserved on the hanging wall or footwall. But this "auxiliary" trench clearly exposed white Siwaliks siltstones thrust atop several units of fluvial conglomerates (Figures 13a and 13b). As F1 on the east bank river cut, the ~ N40°E striking, ~ 25°NW dipping thrust fault is a sharp contact outlined by a dark, irregular, gouge-rich, hanging wall shear sole. Beneath are sheared conglomerates dragged by thrust motion and cut by several shallower-dipping thrust splays (Figures 13a and 13b) that merge downdip with the shear sole, again as observed on F1 (Figure 11). Although there is little evidence here for tight, small-scale drag-folding, realigned pebbles are visible in the topmost units (U3, U4, and U8) beneath the thrust.

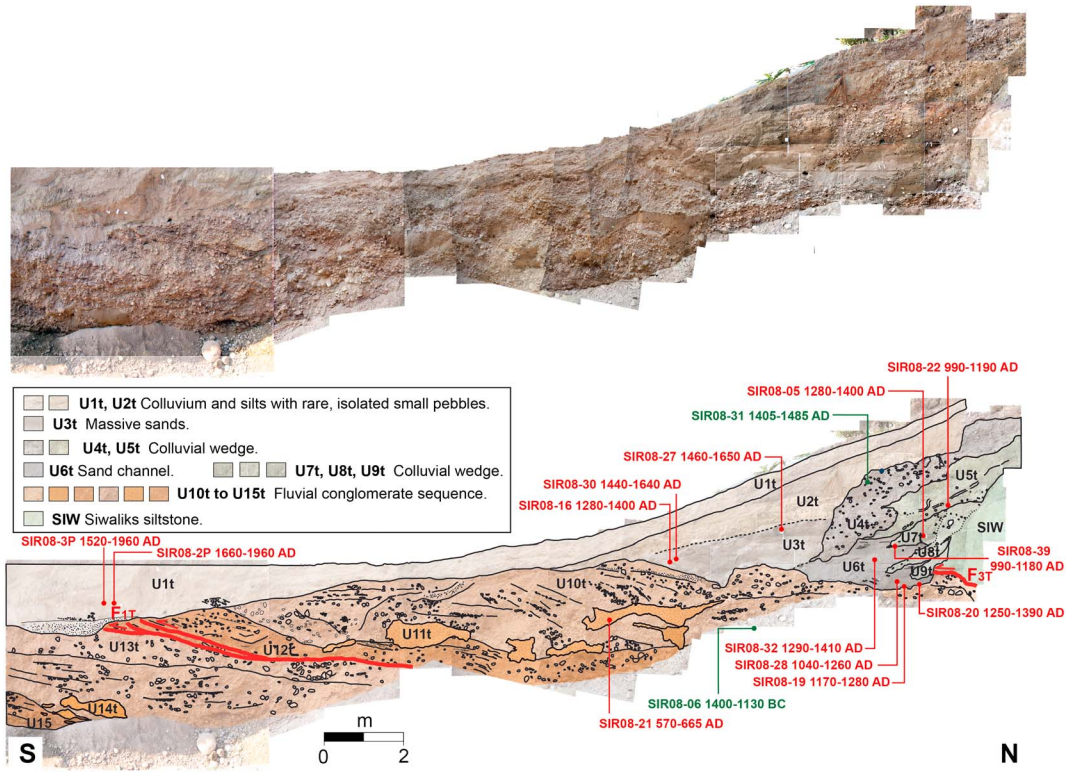

Figure 12. East bank main trench, Sir Khola outlet. (top) Photo mosaic of trench western wall. (bottom) Simplified interpretative log from *Sapkota et al.* [2013]. Faults and calibrated charcoal ages as in Figures 8 and 11. Green numbers are calibrated calendric ages of detrital charcoal samples sampled on the east wall of the trench, projected on the west wall grid.

The uppermost fluvial units incorporate brown pebbles/gravel and light grey pebble/sand layers (Figures 13a and 13b). U3 and U4 tectonically and/or unconformably overlay deeper conglomerate units (U5, U6, and U7), which all dip south by about 20°. While such dip may partly be of tectonic origin, it might also result from southward prograding deposition. U5 is a chiefly clast-supported, indurated conglomerate of oxidized, dark red pebbles and gravel. U6, also consolidated, is composed of buff-colored pebble/cobbles filling small fluvial channels. U7, a much finer, light grey unit, comprises mostly thin gravel layers and light grey sand/silt lenses, with rare cobbles. We infer these three units to be rough lateral equivalents of Units 6–8 along the river cut. That the calibrated ^{14}C age (2840–2470 B.C.) of the only detrital charcoal dated in U4 (Figure 13b and Table 1) is distinctly older than that of the oldest sample retrieved in U5 on the river cut (2460–2140 B.C., Figure 11) supports this correlation. So do the older, stratigraphically ordered, calibrated ^{14}C ages obtained in U6 (4330–4050 B.C.) and U9 (6220–6050 B.C.), the deepest unit in the trench, unconformably capped by U7, that includes brown sand lenses, pebble beds, and very large, deeply oxidized cobbles with weathered rinds (Figure 13b and Table 1). That these oldest footwall fluvial deposits now stand roughly at the level of the present river channel implies that in the last 8000 years, the Sir Khola has been able to maintain a steady profile, with negligible net average incision averaged on a millennial timescale. One important consequence of this quantitative observation is that long-term incision and tectonic uplift rates in the Patu thrust hangingwall should be approximately the same (within a few percent), at least locally. It seems likely that this should also be the case in the valleys of adjacent rivers comparable to the Sir Khola.

The main trench on the east bank of the Sir Khola was excavated at the foot of the 27 m high cumulative escarpment, penetrating ~ 10 m into it, and about 30 m east of the river-cut cliff (*Main Trench* in Figure 7). Overall, it was ~ 43 m long and 5 m deep on average, with a 2.5 m high bench in Siwalik rocks near its northern end. To the south, the excavation was stopped at groundwater level to avoid collapse of portions of the walls.

At that location, this large trench cuts through better preserved units than on the west bank. We first unraveled the structure of the northern part of the trench that exposed collapse colluvium and Siwaliks thrust over a massive fluvial sequence. The uppermost 10 m of the west and east walls were thus cleaned, gridded,

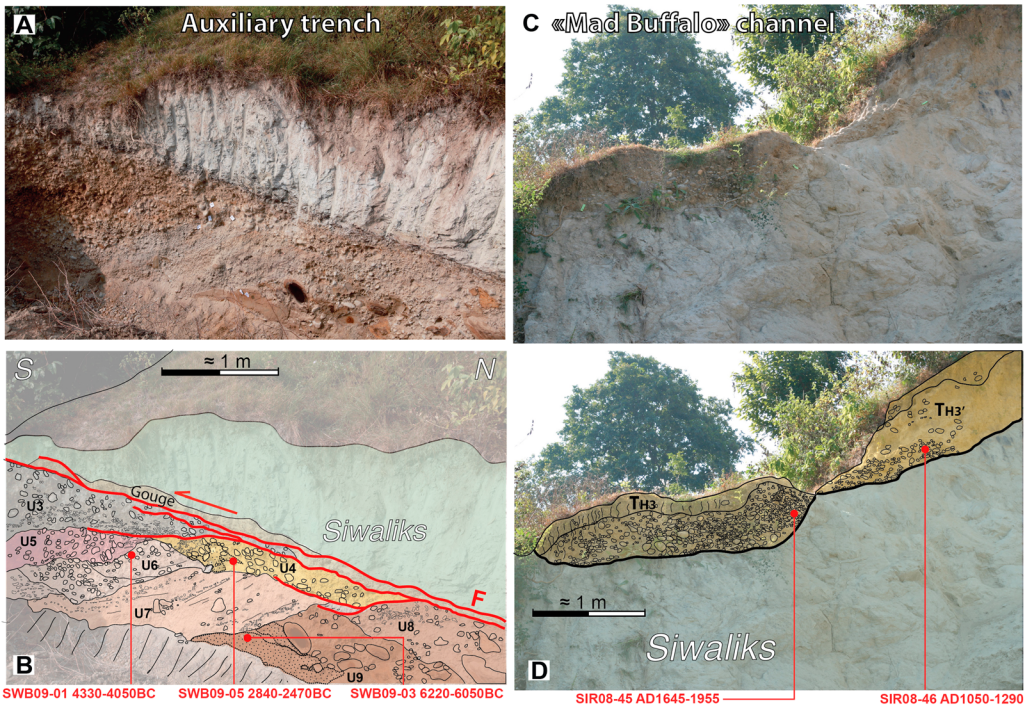

Figure 13. (a and b) Sir Khola west bank auxiliary trench (see location on Figure 7). Oblique, west looking photograph of trench west wall (Figure 13a) and simplified interpretative log (Figure 13b). Fault *F* emplaces light-colored Siwalik siltstones (beneath Th2 grass-covered strath surface) on buff-colored fanglomerate units (U3–U9). *F*, a shear zone outlined by dark gouge, is oriented N27 to 40°E and dips 24 to 27°NW. As on east bank river-cut face, splays of F1 extend into conglomerate units beneath. (c and d) Beheaded Mad Buffalo channel, inside Sir Khola's meander (see location on Figure 7). Photograph of river-cut cliff beneath west side of channel (Figure 13c). Simplified, interpreted section with positions and ages (in red) of ^{14}C samples collected 6 and 7 m above riverbed (Figure 13d).

and logged. We subsequently studied faulting across the conglomerate/sand sequence south of the main escarpment. Although both walls of the trench were inspected in detail and sampled for charcoals, we present only the log of the west wall in Figure 12. All the units identified are labeled from top to bottom and hanging wall to footwall.

The uppermost Units 1 and 2 (U1t, U2t) are fine colluvium with a thin top soil, and silty colluvium/alluvium with only rare small pebbles, respectively. Unit 1 is continuous, smoothly mantling the slopes of the escarpment and of terrace Th2/Tf2 south of it. It thins above the base of the escarpment, while Unit 2 pinches out downward roughly at the escarpment slope break (Figure 12). U2t, whose thickness varies atop an irregular base, was deposited over two radically different units. U3t, essentially clean massive sands, fills twin channels near the base of the scarp slope. U4t is a coarse, light colored, loosely consolidated collapse wedge with a steep toe, composed mostly of unsorted, well-rounded pebbles and cobbles likely derived from terrace conglomerates perched higher on the escarpment (Figure 12). Unit 5, beneath U4t, also south dipping, is a brown to yellow mixture of pebbles/cobbles and Siwalik clasts embedded in an organic-rich clay matrix with veneers of yellowish silt. It is also a collapse wedge, with more abundant Siwalik clasts at the base and larger ones at the apex (Figure 12). It must have been fed by a free-faced scarp exhuming Siwalik beds.

Both U4t and U5t appear to have fallen on a stratified sand unit (U6t), which likely filled an ~ EW trending channel along the foot of the escarpment at the time of collapse. At places, especially near the top, just beneath and north of its contact with U4t, U6t incorporates thin, finely laminated sands interbedded with organic-rich clay layers. In addition, beneath U5t, the northernmost sandy layers of U6t are distinctly interfingered with three smaller collapse wedges, only ~ 1–2 m high, that mix fluvial pebbles with large blocks of Siwaliks within a clayey matrix (U7t, U8t, and U9t) (Figure 12). The apexes of the five collapse wedges, particularly of the lowest four (U5t–U9t), rest directly upon a steep "nose" of white to light grey Siwalik siltstones whose leading edge is brecciated and cracked. The cracks are filled with red-brown clays, a material also found inside gaps between large Siwalik boulders and above them, on top of the trench north bench.

At the bottom of the north end of the trench, the Siwaliks are thrust over consolidated pebble/cobble conglomerates overlying well-sorted fluvial deposits ranging from coarse sands to gravel (Figure 12). Although the excavation was too shallow to expose deeply enough the thrust contact between the Siwaliks and the conglomerates, the relative location of that thrust implies that it is the lateral equivalent (F3t) of F3 on the river cut. Below F3t is a ~ 3 m thick, generally N dipping fluvial sequence that makes up most of the footwall beneath the surface of terrace T2, at the foot of the cumulative escarpment. The fluvial deposits are mostly discontinuous pebble/gravel layers intercalated with metric size sand bodies. Overall, they are poorly stratified due to ubiquitous channeling, but bedding strikes ~ N110 ± 20°E and dips ~ 15 ± 10°N where visible. We identified three main units (U10t, U11t, and U12t) in these deposits. The shallowest, U10t, comprises two separate channels filled with light-colored, unconsolidated gravel and loose coarse sands (Figure 12). It overlies a more consolidated, slightly oxidized conglomerate with poorly sorted pebbles and cobbles, containing large, elongated pods of massive, beige to light brown sand, especially near the base (U11t). Beneath the lowest sand bodies, U12t is an indurated, clearly stratified, gravel/pebble conglomerate, with rust-colored, more oxidized horizons.

A N117 ± 10°E striking, 19 ± 2°N dipping thrust zone (dubbed F1t), composed of parallel splays marked by oxidized, indurated gravel and by flat, aligned pebbles, crosses obliquely the entire footwall, from the cobble/pebble conglomerates at the bottom of the trench to the top of the fluvial sequence just beneath the base of U1t (Figure 12). The lowest splay heaves up, by 30–40 cm, the abraded top of U12t. Other splays in the relative hanging wall have been eroded away. On the relative footwall of F1t is a small trough filled by loose, fine sands and capped by the flat base of U1t. The footwall sequence beneath thrust F1t may also be divided into three principal units (U13t, U14t, and U15t) that closely resemble those in the hanging wall, and also dip ~ 15°N. U13t, made of light-colored, unconsolidated pebble and gravel beds, extends several meters northward beneath F1t. U14t is a less well sorted, more consolidated and slightly oxidized pebble/cobble conglomerate with metric sand bodies at the base. Deeper down, U15t is an indurated, better stratified alternance of pebble and gravel beds, with some thin, rust-colored horizons. Hence, despite the absence of clear drag folding along the F1t thrust splays, we interpret U10t-U11t-U12t and U13t-U14t-U15t to have been partly duplicated by thrust movement on F1t. The last increment of motion on this thrust must be young because it is only covered by U1t, a superficial colluvial wash unit. Unfortunately, erosion of U12t's top on the hanging wall makes it difficult to assess the vertical separation of this unit across F1t. Besides, the small difference in dip between the thrust and the conglomerate beds, and the fact that bedding in them is poorly defined, make it even harder to assess amounts of slip on that thrust.

The ^{14}C calibrated ages of 14 detrital charcoals place limits on the deposition age of certain units on the trench west wall. Because the overall structure, appearance, and depositional history are comparable on either side of the trench, additional chronological constraints are provided by five more ^{14}C ages on the east wall. Unfortunately, we found only two datable charcoals in the footwall fluvial sequence to the south. This made it difficult to confirm the correlation between Units 10t/11t/12t and 13t/14t/15t. The two dates obtained, however,—1400–1130 B.C. for SIR0806 in a pebble conglomerate exposed on the east wall in U11t and 570–665 A.D. for SIR0821 in one of the largest sand bodies on the west wall—are in correct stratigraphic order. They imply ages for U12t and U11t that are consistent with those of U5 on top of the consolidated, oxidized fluvial conglomerates on the river-cut face (Figure 11). The youngest age, possibly in a lateral equivalent of U4 or in beds eroded away on the river cut, confirms that the river was still flowing here, in an east directed channel or bend, in the seventh century A.D.

All the other ages obtained come from Units 1t to 9t. The majority of them (10) are for charcoals collected in the massive or laminated sands of Units 3t and 6t, respectively ahead or beneath the wedges that collapsed in front of F3t's tip (Figure 12). In U6t, the sample ages are in rough stratigraphic order. They range from a cluster at 1040–1390 A.D. (SIR0828, SIR0819, and SIR0820) near the base, to 1400–1490 A.D. (SIR0824), ~ 1 m above, near the top. The three mutually compatible ages of SIR0816, SIR0830, and SIR0827 in U3t (1280–1400 A.D., 1440–1640 A.D., and 1460–1650 A.D., respectively) indicate that this unit is somewhat younger than U6t, as expected from its stratigraphic position. While the U6t ages roughly cover the period from the eleventh to fifteenth centuries (~A.D. 1250 ± 250), those in U3t span the thirteenth to seventeenth centuries (~A.D. 1400 ± 200), (Figure 12). Note the comparable average deposition rate of the sands, on order of ~ 5 mm/yr, in these two channels.

The few ^{14}C calibrated ages of detrital charcoal fragments collected in the collapse wedges are compatible with the ages of U6t and U3t. SIR0839 (990–1180 A.D.) and SIR0805 (1280–1400 A.D.), picked at the toe and in the middle of U7t, respectively, imply that this wedge must have collapsed after ~ 1200 A.D., likely sometime during the final deposition span of U6t, as implied by stratigraphic position. Similarly, based on the age of one sample collected at its base (SIR0822: 990–1190 A.D.), wedge U5t, just on top of Ut7, must have collapsed after ~ 1200 A.D. That the two samples located right at the toe and base of U7t and U5t have the same age (990–1190 A.D.) might be taken to reflect the minimum age of occurrence of a collapse-triggering seismic event soon after 1200 A.D., though in this case SIR0805 would be both reworked and out of stratigraphic order. Finally, consistent with stratigraphic position, the only calibrated age in U4t (SIR0831: 1405–1485 A.D.) implies that this wedge collapsed on top of U5t and U6t after 1500 A.D., likely during deposition of U3t.

Despite the absence of a datable charcoal in U2t, U1t, the uppermost of the two shallowest units capping U3t-U4t and, in fact, the entire footwall, is very young, as shown by the calibrated ages (1660–1960 A.D. and 1520–1960 A.D.) of two samples (SIR082P and SIR083P) collected from the fine wash colluvium above the tip of F1t. The upper bound of these two ages leaves open the possibility that the last event on F1t, and perhaps also on F3t—if U3t and U2t substantially postdate the seventeenth century—, might have occurred as recently as in the first half of the twentieth century.

In summary, although the shallow stratigraphy exposed in the Sir Khola main trench (Figure 12) is different from that on the river-cut face (Figure 8), it strengthens and complements several conclusions. The two thrusts exhumed in the trench, F1t and F3t, are clear extensions of F1 and F3 on the riverbank. Their distance (~21.6 m) is similar to that measured along the river. In the trench, the hanging wall of F1t is different from the deformed Siwalik wedge observed in the hanging wall of F1 along the riverbank. But, despite the lack of datable charcoal in the footwall of F1t, it is likely that U13t-U14t and U11t-U12t are lateral equivalents of the consolidated, oxidized conglomerates of Units 6–9 in F1's footwall on the river cut, and beneath F1 in the auxiliary trench. Also, while the thick fluvial sequence on F3t's footwall is different from the thin strath Units 2–3 south of F3 on the river cut, the existence, east of the modern river course—from at least 1400–1130 B.C. to 570–665 A.D.—of a channel later abandoned (due to thrusting?) accounts well for this difference.

The last event on F1t in the trench occurred very recently, shortly before deposition of the fine, U1t wash colluvium. The modern, upper bound of the calibrated ages of the two detrital charcoals collected in this unit is compatible with the conclusion reached on the river cut that this event must be the 1934 Bihar-Nepal earthquake.

Finally, the relative stratigraphic positions and emplacement ages of the proximal wedges U5t and U7t and sand-filled channels U3t and U6t above the tip of F3t are consistent with seismically triggered collapse due to slip on that thrust during the great historical earthquake of A.D. 1255, rather than during an older event in the eleventh century, as demonstrated by Oxcal modeling in *Sapkota et al.* [2013]. It is also plausible that the collapse of the shallowest wedge (U4t) was triggered by repeated slip on F3t during the 1934 earthquake.

6.1.4. Terrace Morphology

The profiles derived from the DEMs (Figures 9c–9g) provide additional evidence for relative uplift along the Sir Khola thrust escarpment. East of the river, the surface of T2 (Figures 6 and 7) stands 4–6 m above the riverbed, sloping gently southward due to accumulation of modern colluvium, fed by wash from the escarpment, in the wedge above the flat strath gravel.

The bed of the small perched stream 110 m east of the river shows a steep, 3–4 m high, knickpoint as it crosses the eastern extension of thrust F1, about 10–12 m in front of the main escarpment (profile S on Figure 9e and 7). At least three more, subtler knickpoints disrupt the stream course farther up, with three perched terrace levels, each separated from the next by 2 to 5 m high risers (Figure 9). Given its steep profile and small catchment, the stream transports mostly cobbles and boulders. It used to aggrade on the surface of Th2 at the foot of the main escarpment, where it built a small fan, clear on the DEMs (Figures 7 and 9). Although we found no datable material in those coarse deposits, and even though sporadic incision can evidently result, in most environments, from factors other than coseismic uplift, we infer it likely that here discrete episodes of entrenchment of the stream into its fan and three upstream terraces resulted from the upward growth of the escarpment during distinct coseismic uplift events, reflecting the occurrence of at least four large earthquakes, including those in 1934 and 1255 A.D.

Correlating terrace height and incision across the Sir Khola meander (Figure 7) is not straightforward. The interior of that meander has clearly been short circuited and abraded by modern, decadal floods, as attested by shallow, NW trending channels lined with thicker grass and bushes on Th2 (Figure 7) and by differences between the 1964 aerial photo and present-day topography (Figure 9). West of the valley, one broad tread of the old regional terrace surfaces that stand 20–30 m above river between the Patu and Bardibas thrusts (T4, Figure 5; locally Tf5, Figures 7 and 9) comes to abut directly the Siwalik range front. The resulting topographic corner funnels a range front catchment into two deep tributary streams that straddle the thrust trace, incise footwall and hanging wall, and deposit distal gravel fans on the Sir Khola bank, obscuring the tectonic geomorphology. Man-made dirt paths, roads, one canal, and other constructions further disrupt the natural landscape. Nevertheless, the trace of the thrust can be mapped precisely from geological contacts between white Siwalik sandstones and various Quaternary gravel units.

Next to the river, the lowest, 20–40 cm high, thinly grass-covered terraces (T'0 and T1) show no obvious trace of the thrust even though in the riverbed itself (T0, Figure 7) the passage between hanging wall Siwaliks and modern, footwall pebble/gravel is marked by a distinct color change on the HR satellite images and air photos (Figure 9b). The variations in shape and aspect of T'0 on such images imply that it is washed and reworked by yearly floods. Across the next terrace riser westward, between T'0-T1 and T2, the thrust (F3) is clear again, as it separates white Siwalik sandstones capped by thin strath gravel from thick unconsolidated gravel. At the foot of this 2–3 m high riser, the small trench we dug (Auxiliary Trench in Figure 7) exposes the shallow north dipping contact particularly well (Figures 13a and 13b). The Th2 strath terrace tongue inside the meander rests on abraded, N115–130°E striking, steeply north dipping Siwalik beds, and stands 2 to 4 m above river. It has thus been incised/uplifted about as much as Th2 north of F1 on the east bank but, as on T'0-T1, no surface scarp is visible along the projected thrust trace. Furthermore, the height of the Th2/T'0-T1 riser decreases gently northward, from footwall to hanging wall. Given the 1.5 m downstream gradient over the same distance, we relate this peculiar morphology to a combination of flood abrasion of the hanging wall terrace top and distal fan deposition on the footwall top (Figure 7). This shows how, in Nepal, monsoon driven high-energy fluvial processes can quickly obliterate geomorphic traces of surface faulting.

None of the higher-level, albeit young, terrace surfaces preserved on the west bank of the Sir Khola are as high as the flat, abraded top of the main escarpment on the east bank (Th6, +30 m, Figures 7 and 9). The patches that remain—Th3 and Th4 (Figure 7)—, stand about 8–10 m and 14–16 m above river, respectively, on either side of two thrust strands. The northernmost Th4 patches appear to be tilted southward, possibly due to folding, and are cut and separated by two perched, abandoned, NNW trending channels (Figure 9c). These ancient channels of the Sir Khola, now beheaded to the north by the EW, actively migrating, meander cliff-face, hang 7–8 and 10–12 m above the riverbed (Figures 7 and 9). The lowest, westernmost of the two, hereafter dubbed "Mad Buffalo" channel (Figures 7, 9f, and 9g), shows two distinct, inset incisions into the Siwalik bedrock, floored by unconsolidated, matrix supported, pebble/cobble conglomerates (Figures 13c and 13d).

Constraints on the full age range of the Sir Khola high-level, hanging wall terraces come from dating both Th6 and the Mad Buffalo channel (Tables 1 and 2 and Figures 8, 13c, and 13d). On the top of Th6, we excavated two pits in silty, light brown soil above a pebble layer. Only two charcoals were found, at depths of 30 and 60 cm. Unfortunately, the deeper charcoal (SK10-SK09) turned out to be too small (less than 10–20 mg) to provide sufficient carbon for AMS dating and the most superficial one was modern (Tables 1 and 3). We also collected 11 sandstone cobbles from remnants of a thin pavement capping the very top of Th6 for cosmogenic radionuclide dating (^{10}Be and ^{26}Al). The model ages of the seven samples analyzed (Table 2, see section 2 for process description) are plotted in Figure 14, together with the stacked probability distributions including uncertainties for each sample.

The seven ^{10}Be ages range between 2.7 and 4.5 ka (mean age and standard deviation: 3.43 ± 0.65 ka). Two distinct age subclusters stand out, with ~ 2.8 and ~ 3.6 ka means highlighted by the distribution plot. While these results warrant dating of the remaining four cobbles and perhaps further surface sampling—given the ~ 20 cm thickness of the pavement, a depth profile would not be feasible—, it is possible at this stage to interpret the older age (~3.6 ka) to be that of terrace abandonment—C7 being an older outlier with some inheritance. The younger age cluster (~2.8 ka) might then result from exhumation due to regressive erosion of the perched, narrow remnant of Th6, here a plausible process [e.g., *Van der Woerd et al*., 1998;

Table 2. Cosmogenic Isotopes (^{10}Be and ^{26}Al) Exposure Ages of Sandstone Cobbles From Top Surface of Sir Khola East Bank Th6 Terrace

Sample	Quartz (g)	^{9}Be Added (mg)	^{10}Be/^{9}Be[a]	Error	^{10}Be concentration (at/g Qz)	Error[b]	Exposure Age (year)[c]	Error	^{27}Al Native (mg)[d]	^{26}Al/27Al[a]	Error	^{26}Al Concentration (at/g Qz)	Error[b]	Exposure Age (years)[c]	Error
C1	26,8332	0.2898	2,33E−14	1,86E−15	16211	1345	3755	443	15,4424	6,89E−15	3,78E−15	92579	50773	3256	1811
C2	72,2657	0.2909	5,67E−14	2,88E−15	14817	775	3461	348	0.7005[d]	1,41E−13	9,89E−15	101730	7127	3551	396
C4	36,9847	0.2913	3,25E−14	3,82E−15	16257	2012	3765	550	39,5210	5,47E−15	1,73E−15	136493	43186	4648	1529
C6	60,1789	0.2722	4,10E−14	2,21E−15	12067	670	2858	292	14,0245	1,01E−14	3,11E−15	55053	16904	1943	621
C7	72,1023	0.2833	7,82E−14	5,20E−15	19948	1368	4541	497	50,4131	5,51E−15	2,87E−15	90006	46835	3173	1677
C8	37,5076	0.3047	2,33E−14	1,87E−15	12450	1018	2947	348	4,0567	2,56E−14	3,43E−15	64567	8654	2291	366
C9	66,3070	0.3008	3,81E−14	2,40E−15	11392	729	2702	290	5,8818	2,82E−14	3,59E−15	58191	7415	2058	317

[a] AMS measurements were performed at ASTER (CEREGE, Aix-en-Provences, France). ^{10}Be/^{9}Be ratios were normalized using a NIST4325 standard with a value of 2.79 ± 0.003eE11. ^{26}Al/^{27}Al ratios were normalized using SM-Al-11 standard with a ratio of 7.401 ± 0.006E−12.
[b] Error on the concentration includes AMS, a 2% error on the standard concentration and weighing errors.
[c] Age is *Lal* [1991]/*Stone* [2000] time-dependent production model calculated using the CRONUS-Earth online calculator (http://hess.ess.washington.edu/) version 2.2 (June 2013). Error on age is the external uncertainty that includes both error on the nuclide concentration and error of model age used.
[d] Added to C2 were 1.53487 mg of ^{27}Al.

Mériaux et al., 2012]. In keeping with this inference, the equivalent calendric age of Th6 would be between 2200–1200 B.C. This would make it coeval with the pebble layer wedged beneath F4 (Figure 8) and with U5-U6 on the footwall (Figure 11), implying a total structural uplift of ~ 30 m in the last 3 to 4 kyr by cumulative thrusting on F1, F3, and F4.

The lowest, albeit perched, fluvial deposits on the hanging wall west of the river are preserved in the Mad Buffalo channel (Figures 7, 9f, 9g, and 13). Though the total width of that channel is less than 10 m, the long-traveled, well-rounded pebbles and cobbles in a sandy matrix exclude a provenance other than by transport in the main river. We dated two detrital charcoals found within the two inset, ~ 1 m thick, strath pebble layers that abrade the Siwaliks on the west side of the channel (Table 1 and Figures 13c and 13d). The youngest calibrated age (1645–1955 A.D.), of the charcoal on the edge of the inner paleochannel, attests to very recent uplift and final abandonment, likely after the 1934 earthquake. The older calendric age (1050–1290 A.D.), of the sample in the outer, higher subchannel, may, as discussed below, attest that this channel was active at the end of the thirteenth century, plausibly following breaching by the river of a seismic scarp related to the 1255 earthquake.

6.1.5. Kinematics and Return Times of Large Earthquakes

Combining the measurements and dates obtained along the river cut, in the trenches, and on the terraces throws light on hanging wall uplift rates and coseismic thrust evolution. The new dates not only confirm our observations of primary ruptures on F1 and F3 during the great 1934 and 1255 events [*Sapkota et al.*, 2013] but provide further bounds on slip per event, return times and millennial growth of the cumulative scarp.

The best constraints on the millennial uplift rate derive from the ages on the river cut, particularly that of the highest, flat, cobble-paved strath surface Th6 at the very top of the scarp, 285 m above sea level (asl), 30 ± 1 m above the riverbed (Figures 7 and 8). Given the clear correlation between footwall and hanging wall fluvial deposits, found, respectively, in U5 beneath F1 at the river level, and on Th6 at the top of the scarp (Figure 8a), the elevation difference translates into equal geomorphic and structural vertical offsets. The uplift—and comparable incision—rates consistent with the mean ages of the three dashed boxes in Figure 14 would thus be about 8.3 mm/yr, 8.8 mm/yr, and 10.7 mm/yr. A preferred scenario, taking into account an age range of 1200–2200 B.C. for Th6 would correspond to an uplift rate of 8.5 ± 1.5 mm/yr, basically encompassing the three rates above.

Table 3. AMS Radiocarbon (^{14}C) Dates From Detrital Charcoals Collected From Thapatol Trench

Unit[a]	Sample Number	CEA/SacA or SUERC Lab Code[b]	Measured Radiocarbon Age (Years B.P.)[c]	δ^{13}C Value	Calibrated Ages (Calendric, 2σ)[d]
		Trench			
U2	BAR03-08	SacA23045	1770 ± 30	−27.6	A.D.137–345
U2	BAR05-08	SacA23046	2045 ± 30	−27.4	B.C.165–A.D.24
U2	BAR06-08	SacA23047	1590 ± 30	−26.4	A.D.411–543
U4	BAR07-08	SacA23048	3525 ± 30	−30.9	B.C.1935–1756
U4	BAR08-08	SacA23049	3540 ± 35	−21.0	B.C.1965–1754
U4	BAR09-08	SacA23050	3920 ± 30	−31.1	B.C.2480–2297
U4	BAR10-08	SacA23051	3495 ± 40	−24.3	B.C.1923–1695
U5	BAR13-08	SacA23052	4120 ± 30	−31.1	B.C.2866–2578
U5	BAR14-08	SacA23053	8095 ± 35	−27.0	B.C.7181–6862
U5	BAR19-08	SacA23055	8020 ± 30	−28.4	B.C.7061–6826
U5	BAR15-08	Suerc34589	7930 ± 30	−27.8	B.C.7029–6686
U4	BAR18-08	Suerc34593	3535 ± 30	−28.2	B.C.1950–1759
U2	BAR04-08	Suerc34594	2060 ± 30	−28.4	B.C.170–A.D.4
	BAR11-08	Suerc34595	4120 ± 30	−29.2	B.C.2866–2578
U4	BAR12-08	Suerc34596	4100 ± 30	−28.8	B.C.2863–2502
	BAR01-08	Suerc34607	3870 ± 30	−27.8	B.C.2466–2211
U4	BAR08-08	Suerc34606	3480 ± 30	−27.6	B.C.1889–1696

[a]See trench log for stratigraphic unit designations.
[b]Samples have been dated by accelerator mass spectrometry (AMS) measured at CEA/Artemis, France, (samples labeled with laboratory code SacA) or at the Scottish Universities Environmental Research Centre AMS facilities, samples labeled respectively with laboratory code SacA or SUERC. Each number corresponds to the laboratory code for each sample.
[c]Conventional Radiocarbon years B.P. relative to 1950 A.D. (with 1 s confidence level including counting statistics as well as reference standard, blank and random machine errors).
[d]Calendric dates were calibrated using the atmospheric calibration curve IntCal09 for the Northern Hemisphere [*Reimer et al.*, 2009].

At a more detailed level, to be tested by additional dating, an interpretation allowing for the occurrence of large earthquakes might be that the cobbles from the oldest subgroup (3.6 ka) were exposed slightly after an event preceding that responsible for final terrace abandonment (at 2.8 ka). In that case, one interseismic period of ~ 800 years would separate the oldest cobbles from the youngest ones. Note that this value would be in keeping with that (~700 years) separating the last two events on the thrust (A.D. 1255 and 1934), [*Sapkota et al.*, 2013].

The most likely interpretation of the ~ 7 m hanging height of the beheaded Mad Buffalo channel above the present Sir Khola bed (Figures 7, 9f, and 9g), given it was still active from the seventeenth to the twentieth century, is that it resulted from uplift during the 1934 earthquake. Allowing for ~ 1 m of postseismic river incision—~ 2.5 m into F1's footwall minus the river gradient upstream (Figures 7 and 9)—, the net, local 1934

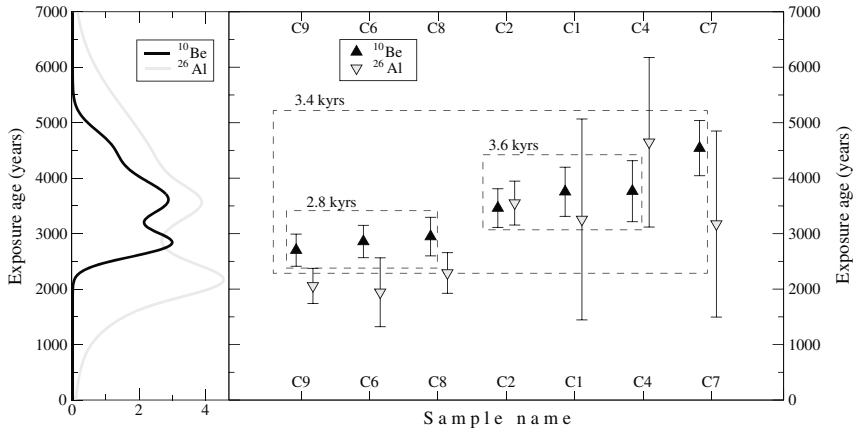

Figure 14. Cosmogenic ^{10}Be and ^{26}Al exposure ages of 7 (out of 11) sandstone cobbles collected on top surface of hanging wall terrace Th6 on Sir Khola east bank, 30 m above river. The boxes delineate the clusters of ages discussed in the text section 6.1.5. (left) Stacked probability distributions of ^{10}Be and ^{26}Al ages, with corresponding uncertainties imply ≈ 3 ka final abandonment age.

coseismic throw on the thrust could have been on the order of ~ 6 m. That there might have been uplift on the stepping, more frontal, Bardibas thrust (Figures 2c and 3) as well as metric, coseismic to postseismic base level subsidence in the Terai foreland [*Bomford*, 1937] (Figure 2b), would be in keeping this estimate. Taking the thrust dip angle at depth to range between 20° and 30°N (19 ± 2°N in Main Trench, 15–30° on river cut, 25° in Auxiliary Trench, and 15°–30° on seismic profile) would imply minimum and maximum 1934 coseismic slip amounts of 12 m and 17.5 m, respectively. Although we found no charcoals in the pebbly deposits capping Th4 and thus still lack definitive age constraints, we strongly suspect that in the wake of the A.D. 1255 earthquake, a scenario comparable to that in 1934, involving similar net coseismic uplift and slip on the thrust, presided to the abandonment of the Th4 remnants now perched ~ 7 m above the Mad Buffalo paleochannel.

Assuming that such coseismic throw and slip amounts are locally characteristic of multiple events in a longer seismic sequence, a total of five such earthquakes would have built the east bank cumulative escarpment, raising the top of Th6 ~ 30 m above the river in ~ 3.6 ± 0.5 ka. This duration includes therefore ~ 4 to 5 interseismic periods and would be consistent with a return period between ~ 720 ± 100 and ~ 900 ± 100 years for characteristic earthquakes, assuming each event of equal interval in between. While this scenario is nonunique and clearly oversimplified, it has the merit to be consistent with all the topographic measurements and ages we have at hand at the Sir Khola outlet, including the last, best defined, and the oldest, more speculative, interseismic periods.

6.2. Patu Meander, Ratu Valley

The results obtained at the Sir Khola outlet are complemented by new findings at another site ~ 5 km eastward, where the Patu thrust crosses a large meander of the Ratu Nadi near the village of Patu (Figures 3 and 5). Here we acquired a high-resolution topographic DEM, based on a detailed Total Station survey (Figure 15). We also dug pits into several abandoned, warped terraces perched at different levels above that larger river. Pit 2, excavated at the top of the highest terrace surface (Th5, 337 m asl), about 47 m higher than the riverbed along the south arm of the meander (Figure 15), exposed uniformly red sand/clays containing large charcoal chunks. Although most of the samples in this humid unit were wet, they provided ages in correct stratigraphic order. The topmost charcoal (PATU12-PIT2-04), only 50 cm below ground, yielded a fairly young, calibrated age of 690–934 A.D. (Table 1 and Figure 15, top right inset (right)). The age of the deepest charcoal (~−1.2 m) was much older (4693–4610 B.C.), while two samples in between had intermediate ages (1882–1610 B.C.). Given that the sands/clays in the 1.5 m thick unit are not high-energy fluvial sediments, it seems likely that their deposition postdates terrace abandonment. Using the oldest, deepest age would yield an uplift rate of ~ 7.1 + 0.1/−0.3 mm/yr, a maximum if the deposits are considered to strictly postdate abandonment, but a value compatible with the lower bound of the rate found in the Sir Khola valley. With the average age (1782 B.C.) of the next sample above, the resulting uplift rate (12.4 mm/yr) would still be no more than 2 mm/yr greater than the upper bound of the Sir Khola uplift rate. Overall therefore, such results corroborate those obtained at the Sir Khola.

To the north, on the left bank of the Ratu River, Pit 4 (2 × 2 × 1.5 m), in terrace Th3′ (322 m asl) 28 to 30 m above the riverbed, exposed a sequence comprising from top to bottom a thick soil, ~ 40 cm of silts, then two thin lenses of pebbles separated by a 10 cm thick sand layer, capping mixed gravel and sands (Figure 15, top right inset (left)). We dated three charcoals (PATU12-PIT4-07/01/08) retrieved 30 to 70 cm below ground, both at the top and base of the silts and beneath the upper pebble lens. The stratigaphically well-ordered ages ranged from 1672–1942 A.D. to 1021–1166 A.D. By comparison with the Sir Khola site, such ages might be taken to be compatible with the occurrence two uplift events, a first one postdating 1021–1166 A.D., leading to terrace abandonment, and a second one following ultimate overbank flood deposition in 1672–1942 A.D. This would fit a scenario involving the great 1255 and 1934 earthquakes. However, given the relative youth of the oldest Th3′ age, its present height above river (29 ± 1 m), even though the 1934 event occurred only 80 years ago, might imply an uplift rate of at least 16.5 mm/yr. While one might interpret such a rate to be the local sum of those on both the Patu and Bardibas thrusts, it would be at least twice that derived from the elevation and minimum age of Th5 on the other bank of the Ratu Nadi or the self consistent range of values at the Sir Khola outlet, and greater than most other extant values along the Himalayan front [e.g., *Burgess et al*., 2012; *Lavé and Avouac*, 2001; *Wesnousky et al*., 1999]. Invoking sharp steepening of the Patu thrust beneath the Patu meander, where the Mid-Siwaliks are strongly folded (Figures 3 and 5) and the terrace treads warped (Figure 15), could provide a solution, but T5h would then be significantly younger,

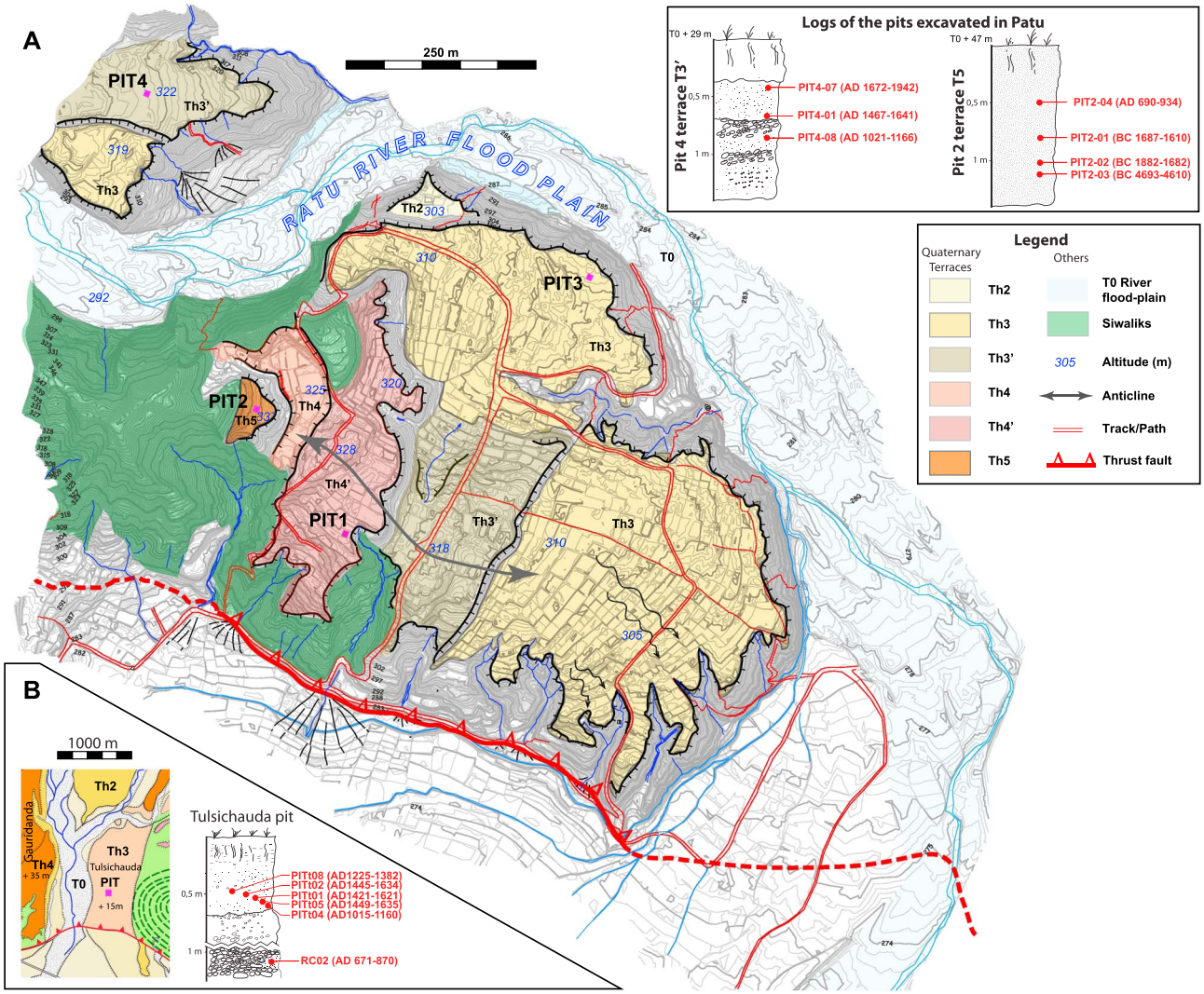

Figure 15. (a) Geomorphic and neotectonic map of Patu meander of Ratu Nadi, based on high-resolution total station DEM (elevation contours spacing, 1 m). See Figure 3 for location. Total height span of inset terrace steps is ≈ 45 m. Top right inset: schematic logs of Pits 2 and 4, excavated on terraces T5 and T'3, respectively. Calibrated ages of detrital charcoals, in red. (b) Location on extract of Figure 5 and schematic log of Tulsichauda terrace pit, ≈ 700 m north of Bardibas strand of MFT (bottom right inset).

which our age data do not rule out. Another possibility might be markedly discontinuous incision by the Ratu Nadi, which was perhaps dammed near the outlet of the meander, where large rockslide scars are observed. Finally, and more simply, even though Pit 4 was excavated where the surface of Th3' is quite flat (Figure 15), it remains possible that the sediments dated in that pit are in large part distal colluvium or alluvium from a perched tributary catchment, which would make using the Ratu Nadi as a base level incorrect.

7. The Bardibas Strand

The Patu Thrust is only one of several "en echelon," closely spaced strands of the MFT along this part of the Siwalik front (Figures 3 and 5). As noted earlier, the many terrace treads uplifted south of the Patu thrust front, all the way to the Bardibas thrust demonstrate that it, too, is an active strand.

7.1. Ratu Terraces: Gauribas, Tulsichauda

That the Bardibas thrust is, in fact, as active as the Patu thrust is particularly clear just west of the Ratu Nadi, where T4, the Gauribas terrace, stands at least 40 m above river, and T5, the regionally highest (~290 m asl) and oldest (~7 ka) fluvial terrace of the piedmont (Figure 5), reaches an elevation of 70 m above the river

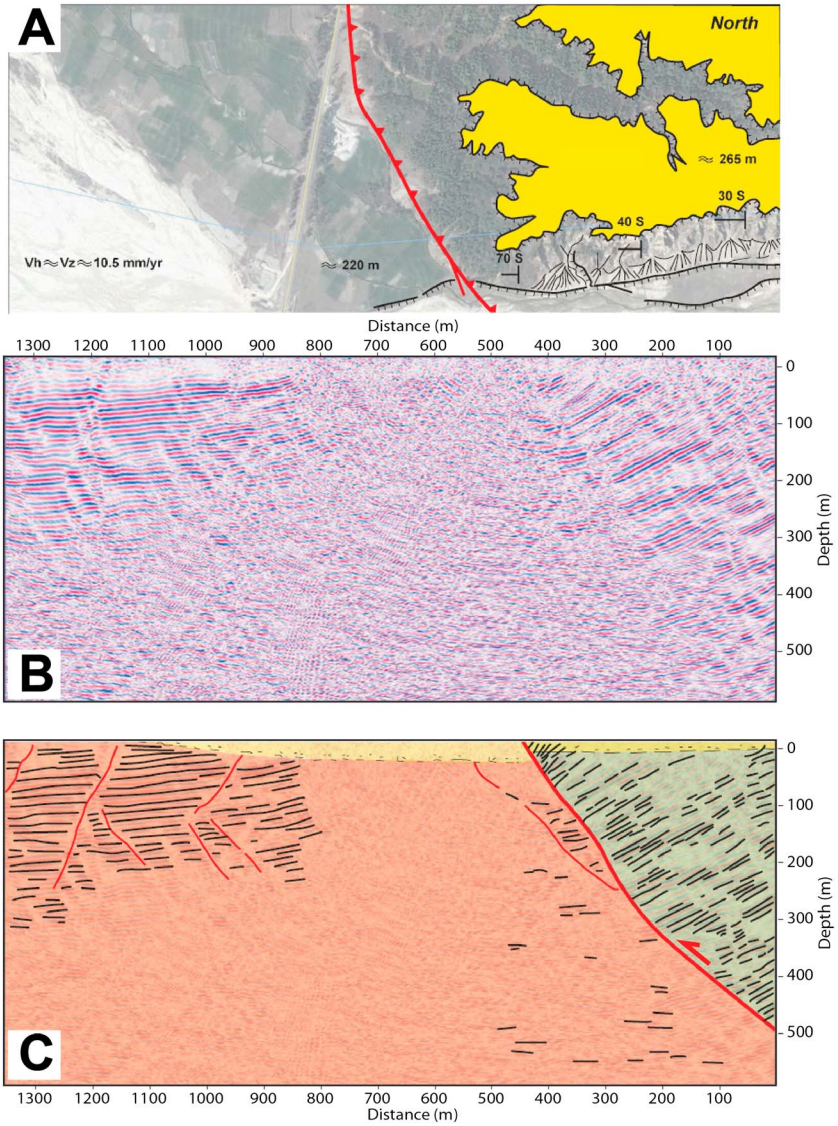

Figure 16. Seismic profile across South branch of MFT, along Ratu River (location in Figure 3). (a) Simplified geomorphology of Ratu west bank. Numbers are elevations Gauribas terrace (yellow) uplifted by Bardibas Thrust (red). Horizontal "T" with numbers are dips toward south. Minimum uplift and shortening rates are indicated in lower left corner. (b) Depth migrated seismic data, at scale 1:1. (c) First-order interpretation of seismic section in Figure 16b, consistent with Figure 16a. Green, hanging wall Siwalik mudstones/sandstones; orange, footwall Pleistocene conglomerates; yellow, late Holocene to modern fluvial gravel and sands. Thrust faults in red.

floodplain (~220 m asl at the thrust cross point, Figure 16). Such height and age are consistent with an apparent uplift rate of ~ 10 mm/yr.

7.1.1. Subsurface Seismic Imaging

The 1300 m long seismic profile we shot along the Ratu riverbed across the Bardibas thrust (Figure 3) shows simpler hanging wall and footwall structures than in the Sir Khola down to ~ 500 m depth. Unlike the Patu thrust, the Bardibas thrust dips more steeply northward (~40–50°) (Figure 16). In the hanging wall, the folded middle Siwalik beds form a 30°–40° south dipping monocline, in keeping with exposures and outcrop measurements along the Gauribas terrace riser along the river (Figure 4). The Pleistocene deposits in the footwall are mostly flat or dip very gently southward (Figure 4). Incipient shortening in these footwall sediments, however, is clear from the presence of small, mostly south dipping thrusts with perhaps small-scale, associated drag folding. That the Bardibas thrust ramp beneath the Ratu Nadi is simpler and steeper than the Patu thrust's beneath the Sir Khola may reflect a much younger localization, age, and growth stage.

7.1.2. Morphotectonics

The cumulative Bardibas thrust escarpment just west of the river exhibits small-scale morphology indicative of recent coseismic faulting. Locally, a free-faced scarp at the top exposes pebble/gravel beds incised by small rills, above a steep, barren, colluvial wedge (Figure 4). Along the base of the escarpment, fans fed by longer gullies that incise more deeply into the hanging wall terrace (T4) also exhibit relatively barren apexes. While man-made degradation or headward erosion could partly cause such rejuvenation, the escarpment orientation makes regressive erosion by lateral cutting during large floods of the Ratu river unlikely (Figures 4, 5, and 16). Additional evidence for very recent coseismic uplift on this southern branch of the MFT is the emergence, inside the Ratu Nadi floodplain, of a thickly grass-covered terrace surface (T1) roughly along the line linking the Bardibas and Tulsichauda escarpments on either side (Figures 4 and 5). Across that line, the width of the active floodplain narrows by more than half from footwall to hanging wall. Such an uplifted terrace, now ~ 1 to ~ 2 m above the riverbed, could not have survived centuries of monsoon floods. This suggests the existence of a primary surface break due to the 1934 earthquake on the Bardibas as well as on the Patu Thrust, as shallow subsurface dating, documented below, further corroborates.

Along the east bank of the Ratu River the Tulsichauda terrace (Th3), on the hanging wall of the Bardibas thrust, stands up to ~ 16 m above the riverbed. One 2 m × 2 m × 1.5 m deep pit we excavated on that terrace ~ 80 m north of the fence of the Lalgadh Leprosy Hospital (Figure 5) exposed 25 cm of soil atop a 50 cm thick silt layer resting on gravel (Figure 15b, lower left inset). Five detrital charcoals sampled near the base of the silts, 48 to 67 cm below ground, were dated. The uppermost four samples (RATU12-PIT1-08, -02, -01, and -05) yielded consistent calibrated ages ranging between A.D. 1225 and 1635 (Table 1 and Figure 15b). The lowest charcoal dated, just on top of the gravel, was distinctly older (1015–1160 A.D.). Excavation of the pit was halted at 1.5 m depth by a resistant, clast-supported layer of pebbles and cobbles. That same layer was found exposed 10–20 m southward in the gully of a small tributary catchment of the Ratu Nadi. Refreshing the gully incision exposed a charcoal-rich sand lens within the pebbles, about 110 cm below ground and a few centimeters above oxydized gravel. One of the large pieces of detrital charcoal sampled in the sand lens provided an age of 671–870 A.D. (Figure 15b).

Such ages are compatible with a simple scenario in which the Tulsichauda fluvial terrace Th3 would have been uplifted by a first earthquake that occurred later than 671–870 A.D. but prior to deposition of the overbank silts in the thirteenth–seventeenth centuries. Coseismic uplift related to a second earthquake would then have brought the terrace surface definitively out of flood reach after the seventeenth century. While nonunique, this scenario would, as elsewhere in the region, be consistent with surface rupture and throw during the two great events of A.D. 1255 and 1934.

Together, the two earthquakes would have lifted Th3 about 16 m above the present Ratu riverbed. Though large, this cumulative uplift is nearly identical to that measured across the MFT 25 km toward the east, in the Charnath Khola valley [*Sapkota*, 2011; *Sapkota et al*., 2013]. Given the 45° N dip of the Bardibas thrust (Figure 16) each earthquake, assumed to be characteristic, would have locally produced 11 to 12 m of coseismic slip, a value compatible with the lower bounds estimated for the same events at the Sir Khola outlet on the Patu thrust. Introducing a few meters of net postseismic incision of the Ratu Nadi into the Terai footwall would slightly diminish these amounts, as at Sir Khola.

7.2. Thapatol Scarp

7.2.1. Morphotectonics

The single thrust that crosses the Ratu Khola divides westward into three smaller splays. West of Bardibas, the southernmost splay, marked by a small scarp across low-level terraces [*Nakata*, 1989] continues to display very youthful relief. Because expansion of the town has altered the natural landscape, the morphotectonics are clearer on the 1964 stereoscopic air photos (Figure 17a) than on the HR satellite images. Our neotectonic/geomorphic map of the area near Thapatol (Figure 17b) was complemented by a Total Station survey of the zone we scouted to select a trenching site. The resulting DEM (400 × 600 m^2) is shown on Figure 18c.

Though small, the Thapatol scarp stands out for its sharpness through cultivated fields and transverse catchments fed by the Siwalik Hills to the north. Across it, there is a clear contrast between active hanging wall incision, with small catchments showing headward retreat (mostly in T2), and deposition on the footwall. South of the scarp, streams were aggrading in 1964, depositing fans of medium size atop the flat surface of T'1, north and east of the Bhabsi Nadi floodplain (Figure 17). Also, the distal edges of the fans, comparable to miniature deltas, were at the time still surrounded by narrow rings of seasonal swamps.

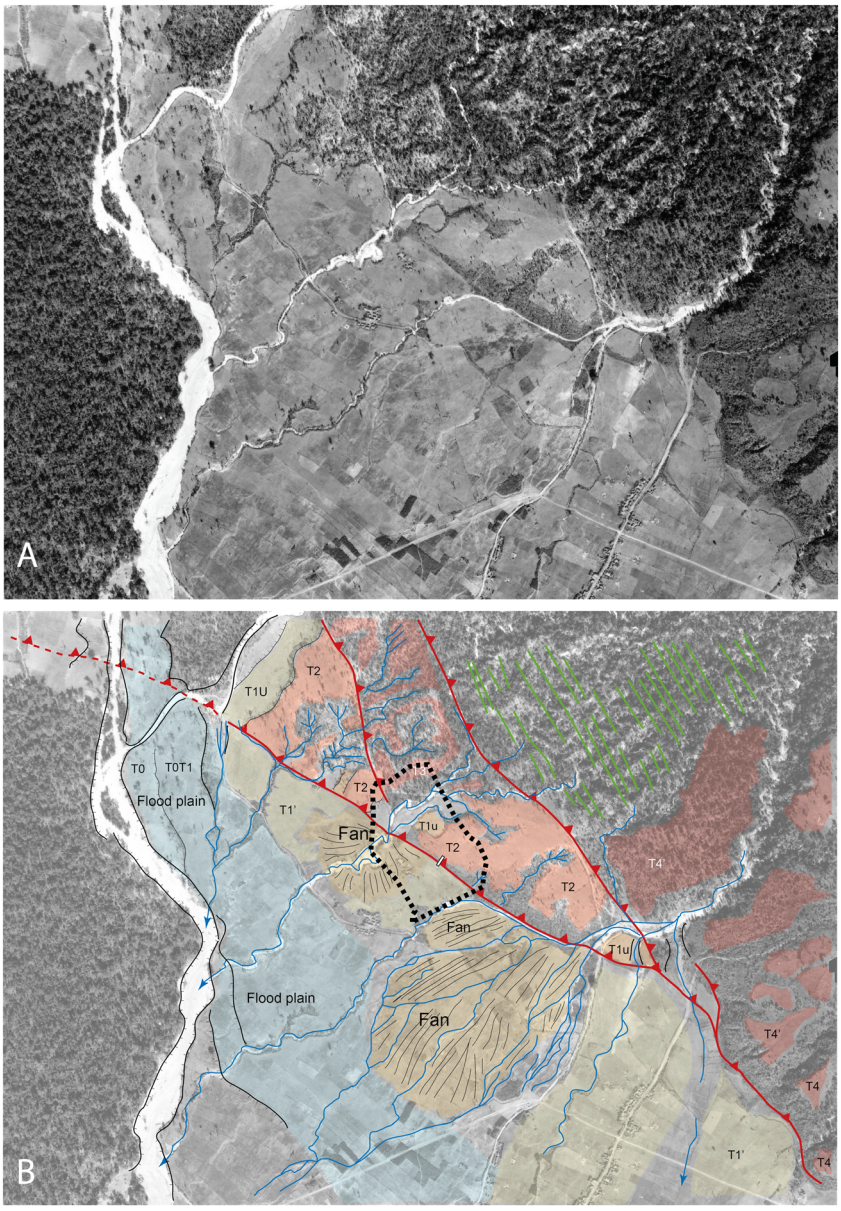

Figure 17. (a) The 1964 air photo of Thapatol branch of Bardibas thrust (location on Figure 3). (b) Schematic morphotectonic interpretation and neotectonic map of area shown in Figure 17a. Main thrust faults are in red. Color shaded surfaces (darker = higher) are main terrace surfaces. Green lines, steep Siwalik beds. Dashed black contour marks limit of total station DEM in Figure 18c.

Despite the now intensive reworking of the cultivated surfaces, the DEM of Figure 18 captures in detail the curved edges and smooth slopes of two fans east and west of the selected trench site and the incision of one stream catchment into small inset terraces on the hanging wall. Given their sharpness and metric height, such fine topographic features may be taken as indicative of recent changes due to coseismic thrusting. The linearity of the scarp and four dogleg stream offsets (Figure 17) also hint at a dextral component slip, consistent with the right-stepping geometry of the thrusts east of the Mahra Khola (Figures 3 and 5). Unfortunately, the clearest 1964 dogleg has now been washed away.

7.2.2. Paleoseismological Trenching

The site selected for trenching (26.997°N, 85.890°E) is located about midway along the morphologically sharpest, ~ 200 m long stretch of the Thapatol scarp. The field view, transverse profiles and DEM of the scarp (Figure 18) show two main levels of terraces in the hanging wall, at heights of 2–3 m and 5–6 m above the

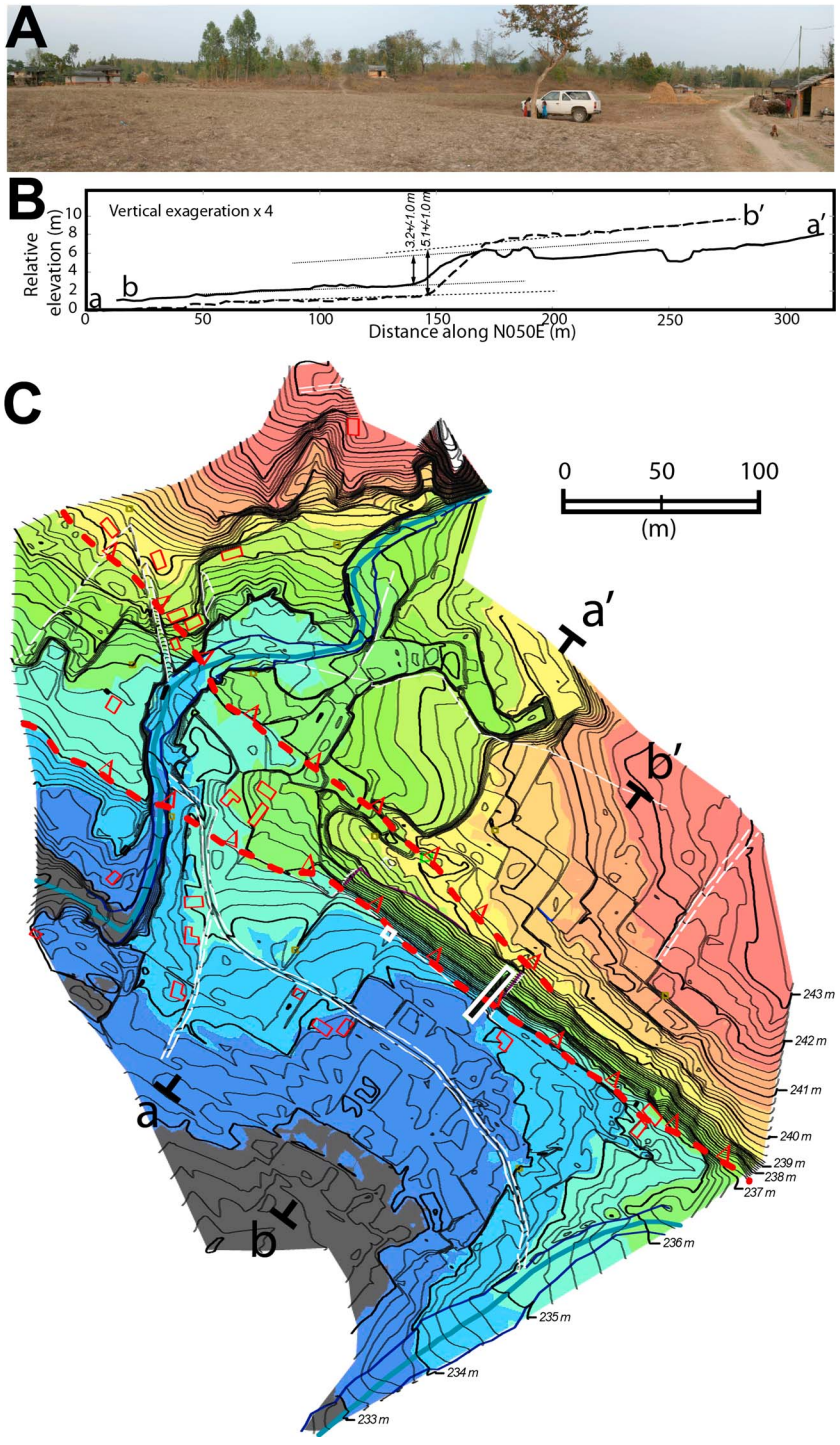

Figure 18. (a) Photograph, looking NE, of main Thapatol thrust scarp. (b) Elevation profiles perpendicular to scarp, a-a′ and b-b′, see location in Figure 18c. (c) Thapatol high-resolution total station DEM (elevation contours spacing, 20 cm). Dashed red lines with teeth are inferred thrust faults underlying southwest facing scarps. White boxes indicate positions of Thapatol trench and pit.

footwall, consistent with perhaps two equal increments in scarp height, hence with the potential occurrence of two uplift events, plausibly in the last 1000 years or so. The trench was excavated across the highest part of the scarp (5 m) where it appeared to be least degraded by man-made beveling. Locally, the maximum scarp slope was on order of 10–15°. The length of the trench, perpendicular to the local N130°E scarp trend, was ~ 31 m, 6 of which in the footwall. It was deepest (~5.2 m) in the footwall, and only 4 to 4.5 m deep in the

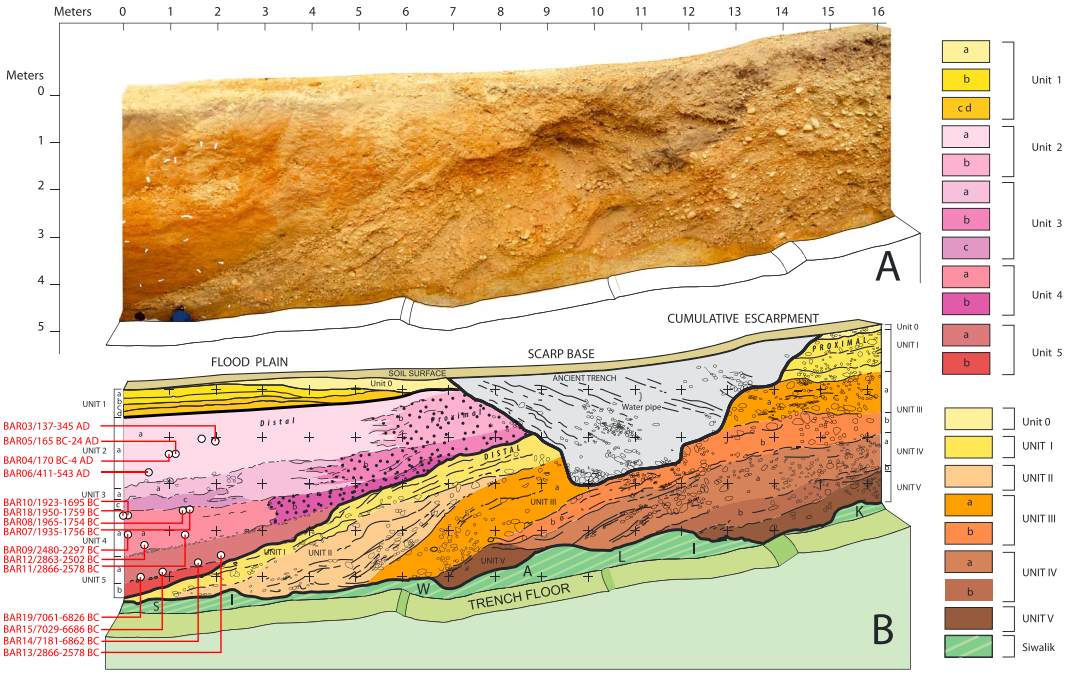

Figure 19. Thapatol trench, across main scarp in Figure 18c. (a) Photomosaic of 16 m long, south part of trench western wall. No fault was found down to ≈ 5 m, implying flexural-folding origin of scarp. Distal, red-brown, sandy/clayey layers with occasional thin pebbly beds at base of scarp onlap coarse, poorly sorted, fluvial fanglomerates dipping ≈ 20°SW on top of scarp. The gravel layers in turn abrade deeper Siwalik beds. (b) Structural and stratigraphic log of wall shown in Figure 19a. Note area (in grey) completely disrupted by digging of older, smaller trench. Calibrated, calendric ^{14}C ages (red) of detrital charcoals within onlapping units of wash deposits at foot of scarp are positioned with white circles. See methodology appendix for calibration details.

hanging wall (Figures 18 and 19). Across the base of the scarp, our excavation exposed an older, smaller, man-made trench about 7 m at its widest and ~ 2.6 m at its deepest. The loose artificial refill of that trench (reworked gravel, pebbles, cobbles, and grey soil), in the middle of which a rubber water pipe was found buried ~ 50 cm deep, unfortunately interrupted logging of shallow units in that key area.

From top to bottom and south to north (west wall, Figure 19) the trench exposed light-colored silts deposited over red, locally clay-rich sands with rare interbedded levels of pebbles (Units 1 to 5) in the footwall, onlapping over warped, buff- to rust-colored conglomerates (Units I to V) flattening northward into the hanging wall. Deeper down, the conglomerates unconformably capped eroded Siwalik beds dipping 20° to 40°SW. The fabric of both sequences of units appeared to shift from proximal to distal from north to south. The conglomerates tended to be coarser, with bigger cobbles up scarp and thinner gravel down under the sands. The sandy units included more gravel and pebbles toward the base of the scarp, with a few pebble layers thinning down into the finer deposits of the footwall (e.g., Units 3a and top of 5b, Figure 19). In general, also, the conglomerates became more consolidated and oxidized with depth. Overall, the two sequences are most simply interpreted to be fluvial terrace deposits on the hanging wall (UI–UV), and colluvium fed by wash from the scarp slope on the footwall (U1–U5), though distal parts of the latter probably include fine flood deposits from adjacent fans (Figures 17 and 18). The deeper units in either sequence have steeper dips, and the whole monoclinal structure is suggestive of progressive flexural folding, although the contact between the Siwaliks and conglomerates suggest that the latter were emplaced as a prograding fan (Figure 19). The modern depositional environment afoot the Thapatol scarp being one of closely spaced fans (Figures 17 and 18), such an environment should have prevailed also at the time of T2 emplacement. While no fault was exhumed in the trench, likely because the excavation did not reach deep enough, we still refer to footwall and hanging wall for simplicity.

In the footwall, Unit 0 is a thin wedge of gravel/pebbles that tapers out away from the base of the scarp. Unit 1, approximately 50 cm thick, is primarily composed of fine silts and may be divided into four subunits,

Table 4. AMS Radiocarbon (^{14}C) Dates From Detrital Charcoals Collected From Thapatol Pit

Sample Number	BETA Laboratory Code[a]	Measured Radiocarbon Age (Years B.P.)[b]	$\delta^{13}C$ Value	Calibrated Ages (Calendric, 2σ)[c]
		Pit		
BR1	336600	810 ± 30	−26.0	A.D.1210–1280
BR2	336601	810 ± 30	−27.3	A.D.1220–1280
BR3	336602	130.5 ± 0.3pMC	−12.5	Postbomb
BR4	336603	690 ± 30	−27.2	A.D.1280–1390
BR5	336604	50 ± 30	−28.1	A.D.1693–1920
BR6	336605	810 ± 30	−27.7	A.D.1220–1280
BR7	336606	970 ± 30	−27.7	A.D.1020–1170

[a]Samples have been dated by accelerator mass spectrometry (AMS) measured at Beta Analytics AMS facility. Each number corresponds to the laboratory code for each sample.
[b]Conventional Radiocarbon years B.P. relative to 1950 A.D. (with 1 s confidence level including counting statistics as well as reference standard, blank and random machine errors).
[c]Calendric dates were calibrated using the atmospheric calibration curve IntCal09 for the Northern Hemisphere [*Reimer et al.*, 2009].

with two shallow, light-colored layers covering two deeper, organic-rich, light and dark grey horizons (subunits c and d, respectively), likely former top soils, now buried. Units 0 and 1, a and b, are thus most simply interpreted to be the most recent, thinnest colluvial wedges fed by wash from the scarp. Unfortunately, we found no charcoals here in these top subunits, the uppermost of which are likely reworked by cultivation or passage.

Below Unit 1 are reddish sand/clay deposits down to a depth of 4.7 m, inclusive of Units 2–5. Unit 2 is chiefly composed of thick, rather homogeneous red sands, becoming interspersed with pebbles northward. We found several detrital charcoals in the sands. This unit caps Unit 3, a buff-colored, silty/sandy layer with an irregular, up to 20 cm thick pebble/cobble bed on top (Unit 3a). At the base of Unit 3b is a very thin layer of small rounded white pebbles, directly overlying Unit 4, a deep red, often mottled, sandy clay layer, rich with fairly big chunks of detrital charcoal. In turn, at the base of Unit 4, one finds again a thin layer of very small round pebbles capping Unit 5. This latter unit, the lowest of the fine colluvial units, closely resembles Unit 4 and is subdivided into two red sands/clays subunits by yet another very thin bed of rounded minipebbles. Several sizable detrital charcoals were found just above this latter thin pebble bed, near the base of Unit 5a.

On the hanging wall, the uppermost units, about half a meter thick (Units 0 and I), are gravel-rich greyish soils, with many roots at the top, that become more pebbly at the base. At the north end of the trench, near the top of the hanging wall, the limit between Units 0 and I, as well as that between Units I and II are indistinct and gradual. The whole package, down to at least a meter, was probably once bioturbated by tree roots, of which we found several remnants on the trench east wall. Unit II is more distinctive under the colluvium of the footwall, where it comprises two subunits of buff-colored, clast-supported conglomerates: the top one (subunit IIa) is weekly stratified roughly parallel to the contact with the footwall colluvium and is made of unsorted, small, flat pebbles and gravel with rare rounded cobbles in a sandy/silty matrix. The bottom subunit (IIb) shows a set of more steeply south dipping layers of the same material, with one thin layer of coarse sand and a few small channels. That these deposits are fluvial is clear from local pebble imbrication indicative of south directed water flow. The relationship between subunits IIa and IIb is reminiscent of a topset/foreset delta fan geometry, corroborating a depositional environment analogous to the present. The footwall part of Unit II appears to form a south tapering wedge between the colluvium base and eroded Siwalik top, the tip of which was not reached in the deepest part of the trench.

Beneath conglomerate Unit II, again with often indistinct transition, is an up to ~ 2 m thick sequence of slightly browner (more oxidized, older) conglomerates (Unit III), with a more dynamic structure showing evidence of inset channels. It is slightly more consolidated than UII and composed of well-rounded to slightly angular sandstone pebbles and gravel in a sandy matrix, with a few grayish sand lenses and irregular accumulations of big cobbles likely marking the bottom of channels.

At the base of Unit III is another similar conglomerate unit (Unit IV), ~ 1 m thick, with well-rounded sandstone pebbles and cobbles and gravel lenses. It is more regularly stratified, consolidated, and oxydized than U II. Both U IV and III rest on top of discontinuous pockets of sandy conglomerates (Unit V) that fill troughs in the irregular surface of the underlying Siwaliks, which is eroded in inverted staircase fashion. This is due to the

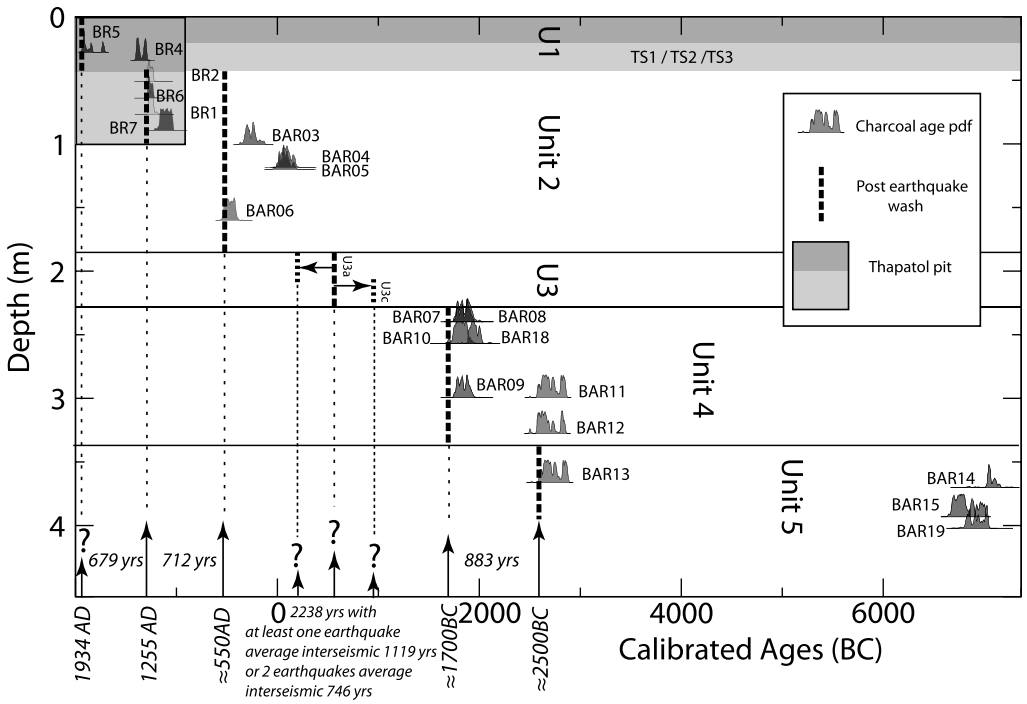

Figure 20. Synthetic plot, as a function of depth, of calibrated calendric ^{14}C ages of detrital charcoals collected within red sand/clay wash deposit units at base of flexural fold scarp, in both (top) Thapatol pit (location on Figure 18) and (bottom) trench (Figure 19). Successive, discrete episodes of wash influx are interpreted to postdate seismic growth increments of flexural fold scarp. Bold, dashed vertical lines mark inferred ages of corresponding events (see discussion in text).

alternance of soft, brown/yellowgreen mudstone beds with indurated ~ 0.5–1 m thick microconglomerates beds, all dipping more steeply than the erosion surface (Figure 19). On the trench floor, the Siwaliks actually strike ~ N130–150°E and dip ~ 30 ± 10°SW. Since no datable charcoal fragment was found in the coarse UI–UV fanglomerates, due to the rarity of fine sand/silt lenses, our interpretation lacks age constraints on the hanging wall.

Fortunately, the 5 m thick, "red sand" footwall sequence yielded more than 15 calibrated detrital charcoal ages, most of them in stratigraphic order (Table 4 and Figures 19 and 20), with two blatant exceptions. The youngest sample in U2, BAR06 (411–543 A.D.) lies stratigraphically ~ 50–70 cm below three older samples (BAR03-BAR04-BAR05). And BAR13 (2866–2576 B.C.), deeper down in U5, lies in the same thin, south dipping level as three ~ 7000 B.C. samples (BAR14-BAR15-BAR19, Figure 19). Colluvial/fluvial reworking accounts best for such out of order chronology, implying that a significant fraction of the ages might be older than the actual time of final redeposition. In keeping with this inference, taking the youngest date at any given depth as a bound on deposition age would imply that U5a, U4, and U2a, ~ 4 m, ~ 3 m, and ~ 1.5 m below surface, were deposited at or slightly after 2500 B.C., 1700 B.C., and 550 A.D., respectively (Figures 19 and 20). The remarkable clustering of ages at 2500 B.C. and 1700 B.C. (Figure 20) suggests essentially episodic, fast depositional influx. That the average sedimentation rate at the foot of the Thapatol scarp (~1 mm/yr) is 1/10 of the uplift rate estimated on the Bardibas thrust (~10 mm/yr) also supports the inference of sporadic, fast and short wash pulses.

The latest such pulses would have led to the emplacement of Units 1a, 1b, and 0 atop the paleosoils of Units 1c and 1d. To compensate for the dearth of datable material in the first meter and a half of the trench footwall, we dug a 2 × 2 × 1 m deep pit ~ 50 m west of the trench (Figure 18) at the very foot of the scarp, near the distal edge of a fan that might have fed fine deposits to Unit 1. Below soil, dark brown fine to coarse sands topped light brown mud containing sparsely distributed pebbles. Seven charcoals were sampled between 37 and 90 cm depth. The calibrated ages obtained (Table 5), in fair stratigraphic order, adequately complemented those obtained deeper in the trench and confirmed that sediments in the top meter below ground are at most 1000 years old. The shallowest samples BR3 and BR5 yielded modern (postbomb) and

Table 5. Summary of Earthquakes and Age Constraints

Calibrated Age/Elevation Above Present-Day River	Sir Khola Outlet	Patu	Thapatol	Bardibas/Tulsishauda
Post EQ1	A.D. 1958/1985			
Pre-EQ1	A.D. 1660–1960	A.D. 1672–1942		
Post EQ2	Sequence of deposit in the rill channel at the foot of the Sir scarp [*Sapkota et al.*, 2013], estimated age: A.D. 1255	A.D. 1467–1641		A.D. 1421–1621 A.D. 1445–1634 A.D. 1449–1635 A.D. 1225–1382 (A.D. 1015–1160 considered as inherited)
Pre-EQ2	A.D. 570–665	A.D. 1021–1166		A.D. 670–870
Pre-EQ3		A.D. 690–934 ?	A.D. 411–543	
EQ4 and possibly EQ5	(B.C. 787–1587)		?	
Pre-EQ5 (or EQ6 previous)			B.C. 1923–1695	
Pre-EQ6 (or EQ7 previous)			B.C. 2866–2578	
Average recurrence interval	Four to five events in 2800 to 3600 years Three to four events before 1934 Taking all models and interpretations (2730/3 and 4; 3530/3 and 4 and 5) we obtain average 873 ± 178 (1σ) ± 356 (2σ)		Hypothesis 1 event in U3: 903 ± 214 (1σ) Hypothesis 2 events in U3: 753 ± 69 (1σ) and 753 ± 139 (2σ)	
Attested surface rupture of historical earthquakes	1255 and 1934	1255 and 1934	1255 and 1934 ?	1255 and 1934

1693–1920 A.D. ages, respectively. The ages of the somewhat deeper sample BR4 (A.D. 1280–1395) and of the two deepest ones (BR 6, A.D. 1188–1282; BR7, A.D. 1025–1169) were distinctly 3 to 4 centuries older. The remarkable clustering of the five stratigraphically lowest sample ages (Table 5) supports the inference of a fast depositional pulse in the thirteenth century, plausibly followed by a more recent (modern?) one (Figure 20).

7.2.3. Coseismic Flexural Fold Growth and the Recording of Past Earthquakes

Since trenching exposed no fault, even at 5 m depth, the Thapatol scarp is not a fault-scarp in a strict sense, at least locally. Yet its sharpness, extent, and linearity transverse to drainage (Figures 17 and 18) imply that it can only be of tectonic origin, ruling out fluvial incision or differential erosion as plausible causative processes. Evidence in map view and section suggests that it formed as a flexural fold scarp above an active, N dipping, though still locally blind thrust buried at shallow depth. The south facing, monoclinal warping of the uplifted terrace fanglomerates abrading the more steeply south dipping Siwaliks in the trench and the shallow geophysical images (Ground-Penetrating Radar radargram and Electrical Resistivity Tomography section presented in *Sapkota* [2011]) are in keeping with this interpretation, implying that west of where the Bardibas thrust divides (Figures 5 and 17), seismic ruptures on individual splays might not emerge. Based on the scales of topographic and structural warping, the depth of the blind Thapatol thrust tip might be only ~ 10–20 m, comparable to that (~13 m) of the Chelungpu thrust beneath the superficial fold scarp that grew coseismically during the M_w 7.6, 1999, Chi-Chi earthquake in Taiwan [*Streig et al.*, 2007].

Even though a climatic origin cannot be ruled out, we tentatively infer that the repetitive, episodic occurrence of depositional pulses afoot the Thapatol fold scarp may be related to incremental growth and steepening of that scarp—and of similar scarps tens to hundreds of meters northward (Figures 5, 17, and 18) during large seismic events. Following this inference, each brief colluvial influx heralded by a cluster of ages in the footwall stratigraphic record would be triggered by, and shortly postdate, coseismic deformation along the scarps.

Such a mechanism is strongly supported by the clustered ages obtained in the pit, given that only 2.5 km eastward at Tulsichauda, there is evidence that the Bardibas thrust ruptured in A.D. 1255 and 1934. The deepest sedimentation pulse, in the thirteenth century A.D., would reflect sediment influx shortly after the A.D. 1255 earthquake, while the shallowest one, postdating A.D. 1693, would be related to the 1934 event (Figure 20).

Similarly, the particularly well defined, oldest age clusters in the trench would mark the occurrence of two great earthquakes, about 800 years apart, around—or slightly after—2500 B.C. and 1700 B.C. Finally, the age group in U2, while less tight, may be interpreted to signal coseismic scarp growth around 550 A.D., attesting to another earthquake about 700 years prior to that in A.D. 1255. This would bring the number

of earthquakes potentially recorded by short colluvial pulses in the footwall of the Thapatol fold scarp to five in the last 4500 years, with three return times ranging between ~680 and ~880 years and a 2250 years long gap corresponding to the lack of charcoals in Unit 3 (Figures 19 and 20). While such lack precludes documenting the existence of other events, the fact that Unit 3 comprises at least two distinct colluvial wash subunits of comparable thickness suggests that at least one more event might have occurred about halfway during this long time gap. If one or two earthquakes had occurred between 1700 B.C. and A.D. 550, their "characteristic" return times, on the order of ~1100 or 750 years, would not have been markedly different from those inferred from the age clusters. Note that the dip of the base of each wash unit, which is an erosion surface, is steeper from top to bottom, from Units 2 to 5b (Figure 19) suggesting that these units were submitted to progressive rotation during the last 4500 years, a rotation that could be due to the incremental growth of the flexural fault scarp.

To recap, short of for now undocumented climatic events, the age clusters observed in the colluvium at the base of the Thapatol fold scarp may be taken to imply—though they fall short of demonstrating—the occurrence of at least five, and perhaps up to seven earthquakes on the Bardibas thrust in the last 4.5 millennia, roughly the second half of the Holocene. The corresponding average return times would be on the order of 750 or 900 years, with a minimum bound of perhaps ~650 years ($<$ 679 years) and a maximum of ~1100 years. These return times are closely comparable to those estimated to characterize the seismic behavior of the Patu Thrust at the Sir Khola outlet (720 ± 100 years to 900 ± 100 years) in the last 3600 years. Even though we cannot fully exclude that climatically driven, exceptional monsoons might return with a similar periodicity—a hitherto unreported cyclical pattern—the observation that in the Thapatol trench, the dips of the erosional bases of footwall wash units steepen from U1 to U5b (top to bottom, ~3.4° to ~23°, Figure 19) is more in keeping with a tectonic process, with each unit rotating increasingly due to incremental, sporadic growth of the flexural scarp since ~4500 years ago.

8. Conclusion

The first, most robust, conclusion to be drawn from the results of our study of the Main Himalayan Frontal Thrust in the Ratu Nadi region is that from consistent observations in at least four distinct sites, both of the shallow, local MFT strands—the Patu and Bardibas thrusts—ruptured coevally in two large slip events in the last millennium. This confirms and expands the findings of *Sapkota et al.* [2013] in the Sir Khola valley, firmly establishing that neither of the last two greatest historical earthquakes in east central Nepal (A.D. 1255 and 1934) were blind.

Another important conclusion is that fluvial terraces in the hanging walls of both thrusts, and colluvial deposits in the footwall of one of them, clearly recorded not only the uplift resulting from these two events, but also that due to several older, comparably large earthquakes. This provided a unique opportunity to constrain, for the first time along the Himalayan front, the average recurrence times of great earthquakes based on 3.6 to 4.5 ka long time sequences of five to seven events (Table 5 and Figures 21 and 22). Furthermore, the timing constraints were accurate enough to attempt correlating the occurrence of such events from strand to strand. Broadly, the average return times at Sir Khola (Patu Thrust) and Thapatol (Bardibas Thrust) appear to be 750 +/− 140 or 870 +/− 350 (2s) years, depending on the interpretation of the sedimentary record (Figure 21).

The dating of the terraces, combined with the quantitative assessment of the morphology and terrace elevations afforded by the TS DEMs, provides constraints on apparent uplift rates on the thrusts, increasing the regional database along the range front [e.g., *Burgess et al*., 2012; *Lavé and Avouac*, 2001; *Wesnousky et al*., 1999]. Such uplift rates appear to be on the order of 8.5 ± 1.5 mm/yr and 10–12 mm/yr on the Patu and Bardibas thrusts, respectively, even though they likely vary along strike, and might possibly exceed 16 mm/yr at one location on the former (near the Patu meander). The surface dips measured in trenches or refreshed outcrops, combined with the shallow dips derived from the interpretation of seismic profiles, may be used to determine bounds on amounts of coseismic slip per event, which, though also likely variable along strike given the overlap between the thrusts, are found to be broadly consistent at two sites, on the order of 11–12 m, and between 12 and 17.5 m.

Such values may be modulated by amounts and rates of net river incision in the thrust footwalls, which are still imprecisely known and appear to be time dependent. For instance, dating of units in the

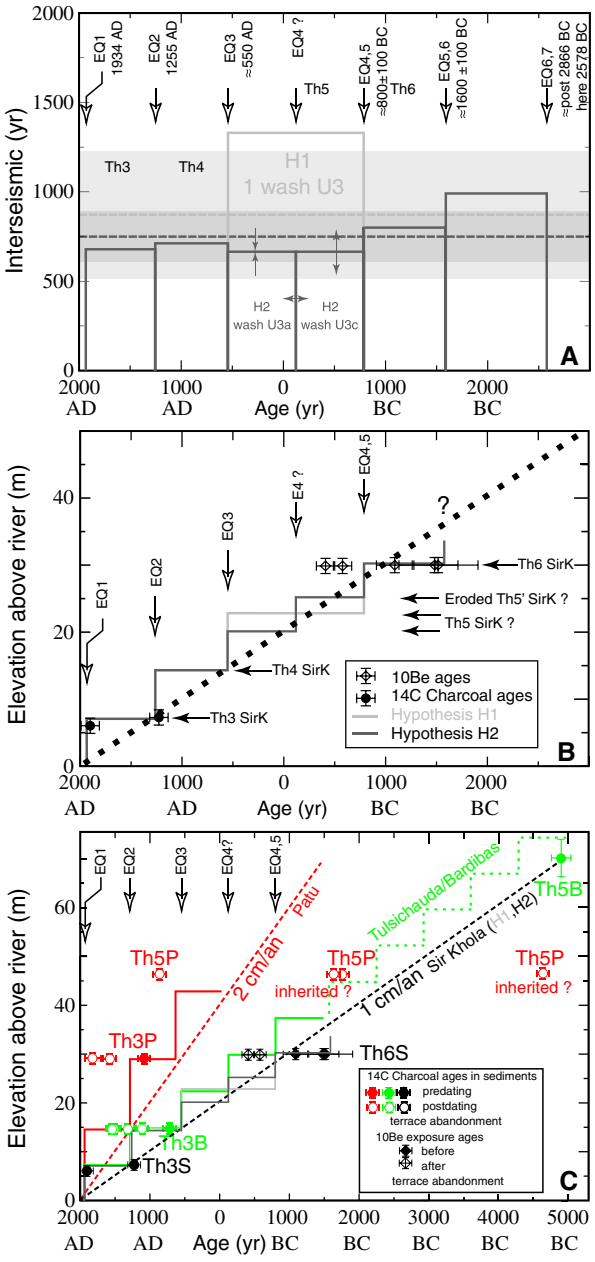

Figure 21. (a) Great earthquake seismic cycles on Patu and Bardibas strands of MFT reconstructed after combining results from Sir Khola and Thapatol, assuming both thrusts always rupture together. Vertical open arrows point to inferred ages of seismic events. H1 scenario (light grey) is based on the hypothesis that only one earthquake occurred between the deposition of U2 and U4 in Thapatol, while one additional earthquake postdating U3c colluvial wash deposition is incorporated in scenario H2 (dark grey). These scenarii are respectively associated with average interseismic periods lasting 870 ± 350 and 750 ± 140 years (dashed dark and light grey lines with bands corresponding to 2σ of the distribution of all simulations within date uncertainties). (b) Composite plot of uplift as a function of terrace ages at Sir Khola, during the period shown in Figure 21a. The data are consistent with a uniform ~ 1 cm/yr uplift rate (dashed line) during the late Holocene period. Given the uplift rate, the return period of the earthquakes implies a characteristic vertical throw of ~ 6 m. (c) Same as Figure 21b but incorporating the mid-Holocene to modern terrace ages at Sir (Black), above the Bardibas thrust along the Ratu River (green), and at Patu (red).

Sir Khola footwall, whether on the east bank river cut or in the west bank trench, implies very small amounts, if any, of net, long-term incision of the river downstream from the thrusts [*Sapkota et al.*, 2013], during in fact most of the Holocene (~8 ka). On the other hand, since 1934, the river has incised at least 2.5 m into terrace Tf2, i.e., in the footwall of thrust F1. This suggests transient, postseismic/interseismic oscillations of the river base level. While such short-term incision likely varies along stream, it should thus definitely be taken into account, at least where submetric topography allows for determination of river gradient, to assess amounts of coseismic throw and slip. Conversely, long-term throw rates and incision rates in the hanging walls should even out to be approximately the same over periods much longer than the seismic cycle.

The coseismic amounts of slip per event estimated at the Sir Khola outlet on the northern thrust strand are compatible with the geodetic shortening deficit accumulated during the time separating the A.D. 1255 and 1934 great earthquakes (~680 years). Indeed, on the locked segment of the Main Himalayan Thrust in eastern Nepal, the most recent cGPS solutions indicate a deficit of ~ 17.8 ± 0.5 mm/yr [*Ader et al.*, 2012], which would correspond to ~ 12.5 ± 1 m of slip in ~ 700 years. At the same rate, 15 ± 3 m of coseismic slip would accrue in ~ 850 ± 170 years, consistent with the longest of our inferred return times, though from data on the southern thrust strand. Whatever the return time, the slip values imply that, at the longitude of Sir Khola, the Patu thrust likely takes up most of the combined shortening on the two strands.

How exactly long-term rates and coseismic slip vary along strike, the way in which slip transfer takes place between the two overlapping MFT thrust strands, and assessing whether events older than the penultimate, A.D. 1255, and 1934 earthquakes were also strictly coeval on both, remain to be fully investigated. The terminations of the active, stepping strands in map view and the offset

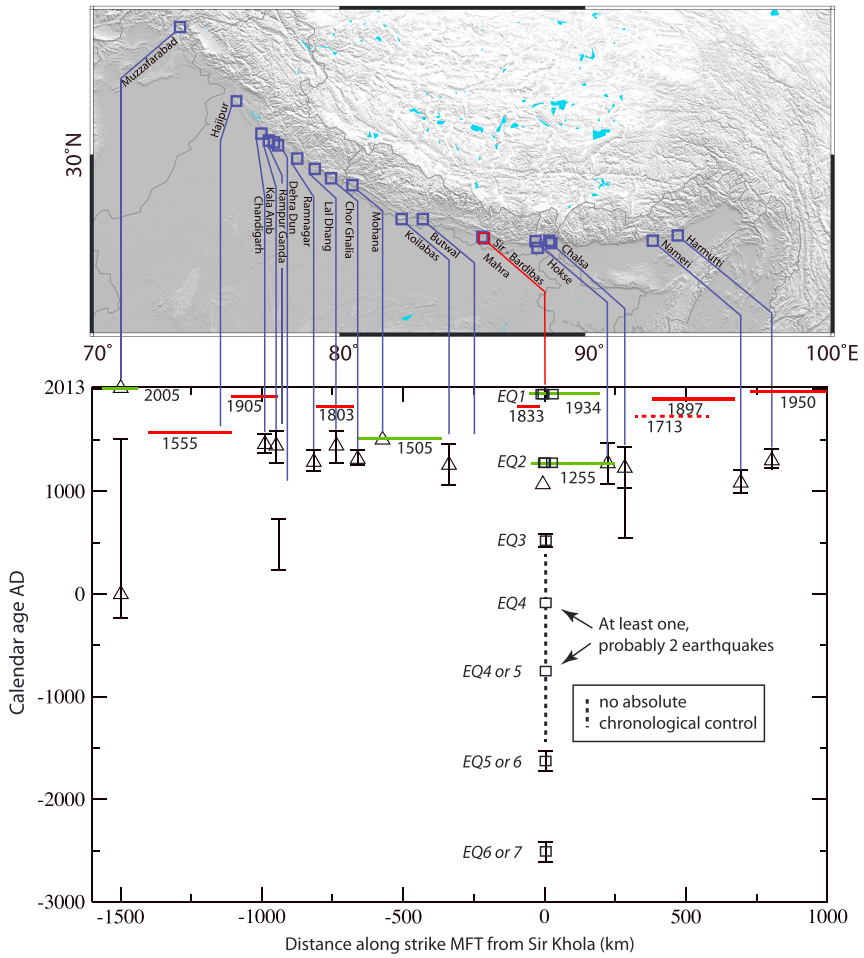

Figure 22. Synoptic calendar and positions of great/large earthquake sources along Himalayan Frontal Thrust (comprising both known instrumental/historical, and inferred paleoseismic events) [from *Kondo et al.*, 2008; *Malik et al.*, 2010; *Kumar et al.*, 2001, 2006; *Yule et al.*, 2006a, 2006b; *Mugnier et al.*, 2012; Kumahara in *Sapkota*, 2011; *Lavé et al.*, 2005; *Upreti et al.*, 2000; *Kumar et al.*, 2010]. Triangles are from latter references. Squares at origin correspond to ≈ 4500 years long time series deduced from our ongoing study of Bardibas and Patu thrusts [*Sapkota et al.*, 2013]. Green and red bars approximate minimum source lengths, with and without observed surface rupture, respectively. EQ1 to EQ7 refer to the earthquake nomenclature from Table 5.

structural periclines of the regional folds (Figure 3) suggest that slip on the Patu strand should decrease abruptly east of the Ratu River. Slip on the main Bardibas strand, by contrast, might decrease more gradually west of the river, not only because of the existence of north oriented splays (Figure 5) but also because it seems to be propagating toward the Mahara Khola across the valleys of the Bhabsi/Jangha/Gadanta and Dungre Khola. Whether slip on both thrusts adds up where they might meet at depth, for instance on the Patu ramp in the middle of the overlap, is as yet unclear, but would be one way to account for potentially faster incision/uplift rates in the narrow and deep canyon of the Ratu River just north of Patu.

At Thapatol, we interpret five dated, footwall wash pulses to reflect transient increases in erosion/sedimentation related to coseismic growth events of the fold scarp on the main, southern splay of the Bardibas thrust (Table 5). One or two more events—EQ4 and EQ5 Table 5—might have occurred in a 2250 year long period during which there is a lack of datable material in one unit (U3). In keeping with that interpretation, great earthquake return times near Bardibas in the last ~ 4500 years might have been as short as 650 years (seven events) or as long as 1100 years (six events) about an average of ~ 875 years (Figures 20 and 21). Figure 21 shows a first attempt at correlating such events with those inferred at the Sir Khola outlet (Figure 21a). It also displays in simplified fashion how the ages and elevations of the terraces would fit cumulative displacements accruing event after event on both thrusts, assuming characteristic slip and return (Figures 21b and 21c).

Our still tentative catalog of a total of five to seven events (including 1934 and A.D. 1255) in the last 3.6 or 4.5 ka on the two MFT strands, illustrated in Figure 22, paves the way toward a better understanding of the seismic behavior of the Himalayan thrust system as a whole. It also affords a first opportunity to compare geologically constrained return times averaged over a long enough period—the latter half of the Holocene—with empirical or theoretical estimates derived either from historical catalogues [e.g., *Bilham et al*., 1998], from the extrapolation of the cumulative frequency-magnitude distribution [*Avouac et al*., 2001], or from refined estimates of the seismic moment deficit [*Ader et al*., 2012]. Previous studies suggested either return times as short as ~ 250–500 years [e.g., *Avouac et al*., 2001], based on the inference that historical events were missing in local chronicles and that many ruptures were overdue, or much longer ones ($>$ 1500 years), implying that the thrust system was capable of generating much greater events [*Ader et al*., 2012; *Feldl and Bilham*, 2006; *Lavé et al*., 2005; *Kumar et al*., 2010]. Very short or very long return times, and the inferred huge event magnitudes associated with the latter, still cannot be completely ruled out, in large part because our study lacks control on the spatial extent of coseismic ruptures, hence on the amount of seismic moment dissipated by each earthquake, and because we cannot demonstrate whether a near characteristic seismic behavior might occur on other stretches of the MFT and thus be a valid working hypothesis along the entire Himalayan front. But the sequence suggested by our observations at the "Ratu-Sir Khola meridian" appears to us to be plausible, and in good agreement with all extant data sources. Certainly, the best path toward fully understanding whether and where great or giant earthquakes are likely to occur along the foothills of the highest mountain range on Earth will be to combine many exhaustive geomorphological and paleoseismological field investigations such as that presented here with extensive, long-term geodetic measurements, capable of narrowing uncertainties in estimates of the full seismic moment deficit.

Acknowledgments

We thank F. Perrier, who organized the framework of Som Nath Sapkota's PhD thesis (from which much of the data presented here are extracted), provided some initial financial support, and invested precious time and energy to kick-start the project. We are also grateful to B.N. Upreti who led us on an introductory field trip along the Main Frontal Thrust in eastern Nepal. Y. Gaudemer (IPGP, Paris, France), M. Etchebes, and E. Kali (EOS, Singapore) for participating in fieldwork. M. Goh (EOS, Singapore) provided essential technical assistance for Lidar data acquisition, and N. Shrestha (Kathmandu), for total station topographic surveying. We acknowledge the crucial contribution of SUERC Glasgow, CEA/Artemis and Beta analytics for ^{14}C dating of numerous charcoal samples. Y. Descatoire (EOS) drew the regional terrace map of Figure 5 and the Thapatol trench log of Figure 19. This study was mainly funded by the Earth Observatory of Singapore (EOS) of Nanyang Technological University (NTU, Singapore) and CEA/DASE (Paris, France), with significant contributions by ANR Paksis (CNRS, Paris, France), and IPG Paris, France. None of the fieldwork would have been possible without the invaluable logistical help and organizational skills of the National Seismological Centre, Department of Mines and Geology (DMG, Kathmandu), and the dedication of many of our Nepali colleagues, among which U. Gautam and I. Siwakoti. Many thanks also to the DMG drivers who worked long hours, day and night, on difficult roads and often off track, to maximize the efficiency of our time in the field. K. Morell and an anonymous reviewer provided constructive comments that helped improve the original manuscript. We dedicate this paper to the memory of M.R. Pandey, whose contribution to demonstrate that the MFT was the source of 1934 earthquake was seminal. This is EOS contribution number 71.

Appendix A: Description of the Great 1934 Bihar-Nepal Earthquake

"It was exactly twenty four minutes and twenty two seconds after 2 PM Nepal time on January 15th, 1934"—Magh 2 1990 in the Bikram Sambat calendar—"when a strange noise, like a rumble coming from the Earth's interior" was perceived by the Kathmandu valley inhabitants. This noise was followed by observations of water in reservoirs, basins, and containers overflowing and spilling out. Observers then felt the ground moving from east to west before describing it as bending. The strong shaking followed immediately, and its arrival induced development of cracks and the collapse of the first houses. These descriptions of the first seconds of the earthquake, as well as many accurate and deeply moving details of the people's reactions during the next several minutes, were reported by Bhrama Shumsher Rana, a military officer responsible for the rescue operation and reconstruction, in his book "Mahabukampa"—The great earthquake—[*Rana*, 1935]. This exceptional testimony of the earthquake and its effects in Nepal are partially translated from Nepali to English in *Sapkota* [2011]. Among the many details provided for a better understanding of the nature of the event and of its effects, B. S. Rana mentions that "The trees were moving as if they were agitated by a storm and it seemed that the tree-tops would touch the ground … Pillars and walls of houses were cracking, doors and windows slamming. With movements up and down, houses collapsed. Statues and decorations placed on top of temples and houses fell to the ground. The noise made by the houses collapsing was reminiscent of canon fire, as…during festivities. Because of the dust, it was darker and no one was able to see at more than a distance of 8 to 10 hands apart. This cloud of dust came from the city itself, invading open areas such as the Thundikhel—a large open and unconstructed space in the centre of Kathmandu—which was such as lost in a fog. People rushed to all these open spaces. Those who could not move themselves were seizing pillars, while others were searching to hide in shelters or ran to the fields. People would run on all fours like animals…"

"Cracks opened in the fields and roads. Water spurted from these cracks. There was flooding in all streams. Rivers like the Bagmati and Bishnumati were invaded by black muddy water. At some places, the water rose 8 to 10 hands above the cracks. Many fields were flooded with water. Warm water and sand spurted from some of the cracks. The roads toward Balaju and Shankhamul were affected by a subsidence as large as one or both hands in height. There were few roads that were not cracked."

References

Abe, K. (1981), Magnitudes of large shallow earthquakes from 1904 to 1980, *Phys. Earth Planet. Inter.*, *27*, 72–92.

Ader, T., et al. (2012), Convergence rate across the Nepal Himalaya and interseismic coupling on the Main Himalayan Thrust: Implications for seismic hazard, *J. Geophys. Res.*, *117*, B04403, doi:10.1029/2011JB009071.

Ambraseys, N. N., and J. Douglas (2004), Magnitude calibration of north Indian earthquakes, *Geophys. J. Int.*, *159*, 165–206.
Avouac, J. P., L. Bollinger, J. Lavé, R. Cattin, and M. Flouzat (2001), Le cycle sismique en Himalaya, *C. R. Acad. Sci.*, *333*, 513–529.
Balco, G., J. Stone, N. Lifton, and T. Dunai (2008), A complete and easily accessible means of calculating surface exposure ages or erosion rates from 10Be and 26Al measurements, *Quat. Geochro.*, *3*, 174–195.
Bashyal, R. P. (1998), Petroleum exploration in Nepal, *J. Nepal Geol. Soc.*, *18*, 19–24.
Bilham, R. (1995), Location and magnitude of the 1833 Nepal earthquake and its relation to the rupture zones of contiguous great Himalayan earthquakes, *Curr. Sci.*, *69*, 101–128.
Bilham, R., and K. Wallace (2005), Future Mw>8 earthquakes in the Himalaya: Implications from the 26 Dec 2004 Mw=9.0 earthquake on India's eastern plate margin, *Geol. Surv. India Spl. Pub.*, *85*, 1–14.
Bilham, R., F. Blume, R. Bendick, and V. K. Gaur (1998), Geodetic constraints on the Translation and Deformation of India: Implications for future great Himalayan earthquakes, *Curr. Sci.*, *74*,(3), 213–229.
Bilham, R., V. K. Gaur, and P. Molnar (2001), Himalayan seismic hazard, *Science*, *293*, 1442–1444.
Bomford, G. (1937), Leveling in Bengal and Bihar, in *Survey of India Geodetic Report 1936*, edited by H. J. Couchman, pp. 93–97, Geodetic branch Survey of India, Dehra Dun.
Boyer, S. E., and D. Elliott (1982), Thrust systems, *Am. Assoc. Petrol. Geol. Bull.*, *66*, 1196–1230.
Bronk Ramsey, C. (2008), Deposition models for chronological records, *Quat. Sci. Rev.*, *27*, 42–60.
Bull, W. (1991), *Geomorphic Response to Climate Change*, 326 pp., Oxford Univ. Press, New York.
Burgess, W. P., A. Yin, C. S. Dubey, Z. K. Shen, and T. K. Kelty (2012), Holocene shortening across the Main Frontal Thrust zone in the eastern Himalaya, *Earth Planet. Sci. Lett.*, *357–358*, 152–167.
Campbell, A. (1833a), Account of the earthquake at Kathmandu, *J. Asiatic Soc. Bengal*, *2*(misc. II), 564–567.
Campbell, A. (1833b), Further particulars of the earthquake in Nepal, *J. Asiatic Soc. Bengal*, *2*(misc. VI), 636–639.
Cattin, R., and J. P. Avouac (2000), Modeling mountain building and the seismic cycle in the Himalaya of Nepal, *J. Geophys. Res.*, *105*, 13,389–13,407, doi:10.1029/2000JB900032.
Chen, W.-P., and P. Molnar (1977), Seismic moments of major earthquakes and the average rate of slip in Central Asia, *J. Geophys. Res.*, *82*, 2945–2969, doi:10.1029/JB082i020p02945.
Chevalier, M.-L., F. J. Ryerson, P. Tapponnier, R. C. Finkel, J. Van der Woerd, L. Haibing, and L. Qing (2005), Slip-rates measurements on the Karakorum Fault may imply secular variations in fault motion, *Science*, *307*, 411–414.
Chmeleff, J., F. von Blanckenburg, K. Kossert, and D. Jakob (2010), Determination of the 10Be half-life by multicollector ICP-MS and liquid scintillation counting, *Nucl. Instrum. Methods Phys. Res. B*, *268*, 192–199.
Corvinus, G. (1987), Patu, a new Stone Age site of a jungle habitat in Nepal, *Quartär*, *37–38*, 135–187.
Corvinus, G. (1989), The Patu industry in its environment in the Siwaliks in eastern Nepal, *Quartär*, *39/40*, 95–123.
Corvinus, G. (2007), Prehistoric cultures in Nepal (from the early Paleolithic to the Neolithic and the Quaternary Geology of the Dang-Deokhuri Dun Valleys), vol. 1. Harrassoeitz Verlag Wiesbaden, 239-286.
Delcaillau, B. (1992), *Les Siwaliks du Népal Oriental*, Presses du CNRS, 1-205, Paris, France.
Dunn, J. A., J. B. Auden, A. M. H. Ghosh, S. C. Roy, and D. N. Wadia (1939), The Bihar-Nepal Earthquake of 1934, *Geol. Surv. India Memoir.*, *73*, 1–391.
Feldl, N., and R. Bilham (2006), Great Himalayan earthquakes and the Tibetan Plateau, *Nature*, *444*, 165–170, doi:10.1038/nature0519.
Gaillard, C., M. Singh, and A. Dambricourt Malassé (2011), Late Pleistocene to early Holocene lithic industries in the southern fringes of the Himalaya, *Quat. Int.*, *229*, 112–122.
Geller, R. J., and H. Kanamori (1977), Magnitudes of great shallow earthquakes from 1904 to 1952, *Bull. Seismo. Soc. Am.*, *67*, 587–598.
Hérail, G., and G. Mascle (1980), Les Siwalik du Népal central: Structure et géomorphologie d'un piémont en cours de déformation, *Bull. Assoc. Geogr. Fr.*, *471*, 259–267.
Hough, S. E., and R. Bilham (2008), Site response of the Ganges basin inferred from re-evaluated macroseismic observations from the 1897 Shillong, 1905 Kangra, and 1934 Nepal earthquakes, *J. Earth Syst. Sci.*, *117*(S2), 773–782.
Hua, Q., and M. Barbetti (2004), Review of tropospheric bomb C-14 data for carbon cycle modeling and age calibration purposes, *Radiocarbon*, *46*, 1273–1298.
Kayal, J. R. (2010), Himalayan tectonic model and the great earthquakes: An appraisal, *Geomatics, Nat. Hazards Risk*, *1*(1), 51–67.
Kohl, C. P., and K. Nishiizumi (1992), Chemical isolation of quartz for measurement of in situ-produced cosmogenic nuclides, *Geochim. Cosmochim. Acta*, *56*(9), 3583–3587.
Kondo, H., T. Nakata, S. S. Akhtar, S. Wesnousky, N. Sugito, H. Kaneda, H. Tsutsumi, A. M. Khan, W. Khattak, and A. B. Kausar (2008), Long recurrence interval of faulting beyond the 2005 Kashmir earthquake around the northwestern margin of the Indo-Asian collision zone, *Geology*, *36*(9), 731–73, doi:10.1130/G25028A.1.
Korschinek, G., et al. (2010), A new value for the half-life of 10Be by heavy-ion elastic recoil detection and liquid scintillation counting, *Nucl. Instrum. Methods Phys. Res. B*, *268*, 187–191.
Kumahara, Y., and R. Jayangondaperumal (2013), Paleoseismic evidence of a surface rupture along the northwestern Himalayan Frontal Thrust (HFT), *Geomorphology*, *180–181*(1), 47–56, doi:10.1016/j.geomorph.2012.09.004.
Kumar, S., S. G. Wesnousky, T. K. Rockwell, D. Ragona, V. C. Thakur, and G. G. Seitz (2001), Earthquake recurrence and rupture dynamics of Himalayan Frontal Thrust, India, *Science*, *294*(5550), 2328–2331, doi:10.1126/science.1066195.
Kumar, S., S. G. Wesnousky, T. K. Rockwell, R. W. Briggs, V. C. Thakur, and R. Jayangondaperumal (2006), Paleoseismic evidence of great surface rupture earthquakes along the Indian Himalaya, *J. Geophys. Res.*, *111*, B03304, doi:10.1029/2004JB003309.
Kumar, S., S. G. Wesnousky, R. Jayangondaperumal, T. Nakata, Y. Kumahara, and V. Singh (2010), Paleoseismological evidence of surface faulting along the northeastern Himalayan front, India: Timing, size, and spatial extent of great earthquakes, *J. Geophys. Res.*, *115*, B12422, doi:10.1029/2009JB006789.
Lal, D. (1991), Cosmic-Ray labeling of erosion surfaces: In situ nuclide production rates and erosion models, *Earth Planet. Sci. Lett.*, *104*(2–4), 424–439.
Lavé, J., and J.-P. Avouac (2001), Active folding of fluvial terraces across the Siwaliks Hills, Himalayas of Central Nepal, *J. Geophys. Res.*, *105*(B3), 5735–5770, doi:10.1029/1999JB900292.
Lavé, J., D. Yule, S. Sapkota, K. Basant, C. Madden, M. Attal, and R. Pandey (2005), Evidence for a Great Medieval Earthquake (~1100 A.D.) in the Central Himalayas of Nepal, *Science*, *307*, 1302–1305.
Liu-Zeng, J., L. Wen, J. Sun, Z. Zhang, G. Hu, X. Xiucheng, L. Zeng, and Q. Xu (2010), Surficial Slip and Rupture Geometry on the Beichuan Fault near Hongkou during the Mw 7.9 Wenchuan Earthquake, China, *Bull. Seismol. Soc. Am.*, *100*, 2615–2650.
Malik, J., A. K. Sahoo, A. A. Shah, D. P. Shinde, N. Juyal, and A. K. Singhvi (2010), Paleoseismic evidence from trench investigation along Hajipur fault, Himalayan Frontal Thrust, NW Himalaya: Implications of the faulting pattern on landscape evolution and seismic hazard, *J. Struct. Geol.*, *32*, 350–361.

Martin, S., and W. Szeliga (2010), A Catalog of felt intensity data for 570 earthquakes in India from 1636 to 2009, *Bull. Seism. Soc. Am.*, *100*(2), 562–569.
Mériaux, A. S., et al. (2005), The Aksay segment of the northern Altyn Tagh fault: Tectonic geomorphology, landscape evolution, and Holocene slip rate, *J. Geophys. Res.*, *110*, B04404, doi:10.1029/2004JB003210.
Mériaux, A.-S., J. Van der Woerd, P. Tapponnier, F. J. Ryerson, R. C. Finkel, C. Lasserre, and X. Xu (2012), The Pingding segment of the Altyn Tagh Fault (91°E): Holocene slip-rate determination from cosmogenic dating of offset fluvial terraces, *J. Geophys. Res.*, *117*, B09406, doi:10.1029/2012JB009289.
Meyer, B., P. Tapponnier, L. Bourjot, F. Métivier, Y. Gaudemer, G. Peltzer, G. Shunmin, and C. Zhitai (1998), Crustal thickening in Gansu-Qinghai, lithospheric mantle subduction, and oblique, strike slip controlled growth of the Tibet Plateau, *Geophys. J. Int.*, *135*, 1–47.
Molnar, P., and M. R. Pandey (1989), Rupture zones of great earthquakes in the Himalayan region, *Proc. Indian Acad. Sci. (Earth Planet. Sci.)*, *98*(1), 61–70.
Molnar, P., and D. Qidong (1984), Faulting associated with large earthquakes and the average rate of deformation in central and eastern Asia, *J. Geophys. Res.*, *89*, 6203–6227, doi:10.1029/JB089iB07p06203.
Monsalve, G., A. Sheehan, V. Schulte-Pelkum, S. Rajaure, M. R. Pandey, and F. Wu (2006), Seismicity and one-dimensional velocity structure of the Himalayan collision zone: Earthquakes in the crust and upper mantle, *J. Geophys. Res.*, *111*(B10), B10301, doi:10.1029/2005JB004062.
Mugnier, J.-L., P. Huyghe, A. P. Gajurel, B. N. Upreti, and F. Jouanne (2011), Seismites in the Kathmandu basin and seismic hazard in central Himalaya, *Tectonophysics*, *509*(1–2), 33–49.
Mugnier, J. L., A. Gajurel, P. Huyghe, R. Jayangondaperumal, F. Jouanne, and B. N. Upreti (2012), Structural interpretation of the great earthquakes of the last millennium in the central Himalaya, *Earth Sci. Rev.*, *127*, 30–47, doi:10.1016/j.earscirev.2013.09.003.
Mugnier, J. L., A. Gajurel, P. Huyghe, R. Jayangondaperumal, F. Jouanne, and B. Upreti (2013), Structural interpretation of the great earthquakes of the last millennium in the central Himalaya, *Earth Sci. Rev.*, *127*, 30–47.
Nakata, T. (1972), Geomorphic history and crustal movements of the foothills of the Himalayas, Sci. Rep. 22, Tohoku Univ., Geogr. Dept., 1-177.
Nakata, T. (1989), Active faults of the Himalaya of India and Nepal, in *Tectonics of the Western Himalayas*, edited by L. L. Malinconico Jr. and R. Lillie, pp. 243–264, Geol. Soc. of Am., Boulder, Colo.
Oldham, T. (1883), A catalogue of Indian earthquakes from the earliest to the end of 1869, *Mem. Geol. Surv. India*, *19*(3), 1–53.
Pandey, M. R., and P. Molnar (1988), The distribution of intensity of the Bihar-Nepal earthquake of 15 January 1934 and bounds on the extent of the rupture zone, *J. Nepal Geol. Soc.*, *5*(1), 22–44.
Pandey, M. R., R. P. Tandukar, J. P. Avouac, J. Lavé, and J. P. Massot (1995), Interseismic strain accumulation on the Himalayan Crustal Ramp (Nepal), *Geophys. Res. Lett.*, *22*, 751–754, doi:10.1029/94GL02971.
Pant, M. R. (2002), *A Step Toward a Historical Seismicity of Nepal*, pp. 29–60, Adarsa 2, Odisha, India.
Peltzer, G., P. Tapponnier, Y. Gaudemer, and B. Meyer (1988), Offsets of late Quaternary morphology, rate of slip and recurrence of large earthquakes on the Chang Ma fault (Gansu, China), *J. Geophys. Res.*, *93*, 7793–7812.
Pradhan, U. M. S., R. B. Shrestha, S. B. KC, D. N. Subedi, S. R. Sharma, and G. N. Tripathi (1996), *Geological Map of Petroleum Exploration Block-8 Janakpur, Central Nepal*, Department of Mines and Geology, Kathmandu, Nepal.
Rana, B. S. (1935), Mahabhukampa, Bahar Mahal BS1992, Kathmandu, 1-250.
Reimer, P. J., et al. (2009), IntCal09 and Marine09 radiocarbon age calibration curves, 0–50,000 years cal BP, *Radiocarbon*, *51*, 1111–1150.
Roy, S. C. (1939), Seismometric study, chapter IV of 'The Bihar-Nepal earthquake of 1934', *Mem. Geol. Surv. India*, 49–75.
Sapkota, S. N. (2011), Surface rupture of 1934 Bihar-Nepal earthquake: Implications for Seismic Hazard in Nepal Himalaya, *Unpublished thesis, IPGP*, 1–292.
Sapkota, S. N., L. Bollinger, Y. Klinger, P. Tapponnier, Y. Gaudemer, and D. Tiwari (2013), Primary surface rupture of the great Himalayan earthquakes of 1934 and 1255, *Nat. Geosci.*, *6*, 71–76, doi:10.1038/ngeo1669.
Schiffman, C., B. S. Bali, W. Szeliga, and R. Bilham (2013), Seismic slip deficit in the Kashmir Himalaya from GPS observations, *Geophys. Res. Lett.*, *40*, 5642–5645, doi:10.1002/2013GL057700.
Seeber, L., and J. G. Armbruster (1981), Great detachment earthquakes along the Himalayan arc and long-term forecasting, in *Earthquake Prediction: An International Review*, *Maurice Ewing Series 4*, edited by D. E. Simpson and P. G. Richards, AGU, Washington, D. C.
Srivastava, H. N., B. K. Bansal, and M. Verma (2013), Largest earthquake in Himalaya: An appraisal, *J. Geol. Soc. India*, *82*(1), 15–22.
Stone, J. O. (2000), Air pressure and cosmogenic isotope production, *J. Geophys. Res.*, *105*, 23,753–23,759.
Streig, A. R., C. M. Rubin, W. Chen, Y. Chen, L. Lee, S. C. Thompson, C. Madden, and S. Lu (2007), Evidence for prehistoric coseismic folding along the Tsaotun segment of the Chelungpu fault near Nan-Tou, Taiwan, *J. Geophys. Res.*, *112*, B03S06, doi:10.1029/2006JB004493.
Szeliga, W., S. Hough, S. Martin, and R. Bilham (2010), Intensity, magnitude, location, and attenuation in India for felt earthquakes since 1762, *Bull. Seismol. Soc. Am.*, *100*(2), 570–584.
Upreti, B. N. (1999), An overview of the stratigraphy and tectonics of the Nepal Himalaya, *J. Asian Earth Sci.*, *17*, 577–606.
Upreti, B. N., T. Nakata, Y. Kumahara, H. Yagi, K. Okumura, T. K. Rockwell, N. S. Virdi, and H. Maemoku (2000), The latest active faulting in southeast Nepal, Proceedings of the Kohudan International Symposium and School in Active Faulting, 17–26 January, 2000, 533–536.
Van Der Woerd, J., F. J. Ryerson, P. Tapponnier, Y. Gaudemer, R. Finkel, A. S. Mériaux, M. Caffee, Z. Guoguang, and H. Qunlu (1998), Holocene left-slip rate determined by cosmogenic surface dating on the Xidatan segment of the Kunlun Fault (Qinghai, China), *Geology*, *26*, 695–698.
Van Der Woerd, J., X. Xiwei, H. Li, P. Tapponnier, B. Meyer, F. J. Ryerson, A. S. Meriaux, and X. Zhiqin (2001), Rapid active thrusting along the northwestern range front of the Tanghe Nan Shan (western Gansu, China), *J. Geophys. Res.*, *106*(B12), 30,475–30,504.
Wesnousky, S. G., S. Kumar, R. Mohindra, and V. C. Thakur (1999), Uplift and convergence along the Himalayan Frontal Thrust, *Tectonics*, *18*(6), 967–976, doi:10.1029/1999TC900026.
Wesnousky, S. G. (2008), Displacement and geometrical characteristics of earthquake surface ruptures: Issues and implications for seismic hazard analysis and the process of earthquake rupture, *Bull. Seismol. Soc. Am.*, *98*, 1609–1632.
Xu, X., X. Wen, G. Yu, G. Chen, Y. Klinger, J. Hubbard, and J. Shaw (2009), Coseismic reverse- and oblique-slip surface faulting generated by the 2008 Mw 7.9 Wenchuan earthquake, China, *Geology*, *37*, 515–518, doi:10.1130/G25462A.1.
Yule, D., J. Lave, S. N. Sapkota, D. Tiwari, B. Kafle, M. R. Pandey, S. Dawson, C. Madden, and M. Attal (2006a), Large surface rupture of the Main Frontal Thrust in east-central and western Nepal—Evidence for an unprecedented type of Himalayan earthquake, Proceedings on the International Workshop on Seismology, seismotectonics and seismic hazard in the Himalayan region, Kathmandu, 28–29 November, 2006, 13–14.
Yule, D., S. Dawson, J. Lave, S. Sapkota, and D. Tiwari (2006b), Possible evidence for surface rupture of the Main Frontal Thrust during the great 1505 Himalayan earthquake, far-western Nepal, in AGU Fall Meeting Abstracts, S33C-05, 1, 5.